ARCHIVES OF ACOUSTICS
21, 1, 3–13 (1996)

# USEFULNESS OF THE ACOUSTIC SPEECH SIGNAL INFORMATION IN THE NERVOUS SYSTEM EVALUATION

CZ. BASZTURA* AND R. PODEMSKI**

* Institute of Telecommunication and Acoustics
Wrocław Technical University I-28
(50-370 Wrocław, Wyspiańskiego 27)
** Department and Clinic of Neurology
Wrocław Medical University

In the paper a preliminary analysis of the possibilities of using a speech signal for the objective diagnostics assistance, as well as for monitoring the process of the reconvalescence from the nervous system diseases, was presented. This paper presents also a conception of the acoustic speech signal computer analysis for some nervous pathological states. The possibilities of making acoustic patterns for the dysarthria disease states from distinctive acoustic parameters compared to the physiological standards, are also described in the papers. The paper presents conditions required for making speech pathology that can determine the kind, and in some cases, even the localization of the nervous system changes. The examples of the acoustic pictures of different types of dysartrhia compared to the psychological standards, were also described in the papers. The examples of the acoustic patterns of different types of dysartrhia compared to the psychological standards were described, and future research directions are set.

## 1. Introduction

Human speech is a set of the specific sound signals that result from a transformation taking place on different levels:

a) intellectual, connected with the process of thinking and initial verbalization of the information perceived reversibly and creating the so called inner speech [25],

b) semantic, where the verbal elements (words, phonemes) acquire certain meaning,

c) linguistic, connected with the phonetical and grammatical form of a statement,

d) articulatory, connected with the process of making and forming of speech sounds characteristic of a given language and conditioned by the correct function of a certain nervous system, speech and structures of the breathing organs [21, 23, 26],

e) acoustic, i.e. the physical representation of speech.

Signals of speech sound, set in order according to the rules of the given language, are the conveyors of the substance that we want to transmit the complex

process of communication with other people. They include personal information (e.g. development level, sex) and are certain reflections of the emotional conditon as well as complex functions of the central and peripheral nervous systems and the speech organ of the speaker. All these elements, along with the transformations mentioned above, have an influence on and are built in the speech signal's acoustic structure [4, 24]. Thus, except for the information connected directly with the communicative function (the substance of the statement), the speech sound signals include nonverbal elements seemingly redundant or useless in the process of verbal communication. However, a number of these elements is closely connected with the pronounced substance giving an appropriate emotional tone to it and to the sound characteristic of the given language (the prosody of speech) [20, 25]. To sum up, it may be stated that the acoustic signal of speech includes two essential information categories:

a) the verbal-semantic category that determines substance of the statement and makes the ground for communication by means of speech (It has to be observed that this category refers not only to the acoustic speech signal but also to the "soundless" written or gesture speech),

b) the nonverbal categories, that penetrates — so to say — all the elements of the pronounced speech and determines the physical structure of speech as an acoustic signal.

The first of the given above categories of information (a) is fundamental for the process of communication between men or between man and computer, while the other one (b) is a database which, after performing a computer acoustic analysis, can be used e.g. for voice identification and verification of the speech disturbances diagnostics [19, 20]. The range of instantaneous value changes of the pressure level of the sound signal of speech is of tens of decibels, the frequency ranges to 10 000 Hz, which in effect gives an information efficiency estimated to about 250 000 bits per second.

## 2. Basic acoustic properties of the speech signal

Speech being a complex acoustic phenomenon is the result of functions of particular central and peripheral nervous systems, articulation muscles and the breathing system [21]. Individual perception of the phenomena contributing to the picture of speech is impossible by means of the sens of hearing. The application of a precise computer analysis with graphic and digital description makes it possible to acquire many data that are not available by direct auditory perception connected with the function of anatomical structures initiating the speech process, stimulating it and giving the speech sounds their ultimate acoustic shape [5, 6, 7, 9, 13, 19, 20]. The possibility of exploration of these structures by means of conventional research methods is often limited and is mostly based on a personal view of the researcher.

In order to utilize the speech signal for objective diagnostic assistance as well as for monitoring the course of convalescence from diseases related to the nerve system one has to take into consideration the definitions of particular pathological states and characteristic recurrent features of the speech signal of people in good health (physiological acoustic standard of speech signal). The computer analysis of the acoustic signal in the defined pathological states will make it possible to distinguish the features typical of a particular syndrome by comparison with the physiological standard [7, 8, 11, 12, 22]. Then the conditions are made for the creation of acoustic speech pathology models which would indicate the kind and, in some cases, even the localization of the nerve system's changes [19, 20].

The task to determine a connection between pathological states and certain acoustic symptoms included in the speech signal that have a diagnostic significance is very complex because, among others, of the fact that the described transformations that take place on different levels of the nervous system (cortex, sub-cortex structures, brain stem, nerves, neuro-muscular connections i.e. synapses, articulation muscles) [1, 2, 14, 21]. This requires the introduction of an acoustic comparative survey on every stage of the signal analysis. This survey may be based, in the initial phase of research, on spectrograms, time parameters as the course of envelope or energy, the density of zero crossings etc. [19, 20]. The essential method task before the beginning of an acoustic speech research is to determine the optimal set of "key entries" i.e. the forms of speech (test tasks) that would deliver information concerning the changes within the widely recognized speech organ (central and peripheral elements of the nervous system, executive structures — voice apparatus), showing at the same time the least possible sensibility to other features (as the personal or social-linguistic ones etc.). The starting point for the sound speech signal characteristics is the thesis that perceptible acoustic features are primarily connected to the voice descriptions that take into consideration the following elements:

1) the elementary pitch period of the vocal cords vibration tone,
2) laryngeal tone peak amplitudes,
3) the frequency spectrum ranges of the speech signal,
4) the frequency ranges of noise components in the speech signal,
5) the amplitude envelope decrease or increase,
6) the time of duration (abbreviation, elongation) of the speech sequence.

Objective acoustic diagnostic methods are now widely applied in phoniatrics. They are based on the speech signal information value analysis as natural and ultimate product of the speech organ operation [3, 10, 15, 16]. These methods support conventional phoniatric studies. Sometimes they show their advantages as they:

a) are varried out in normal physiological conditions of phonation and articulation,

b) do not need any introduction of auxiliary instruments or foreign matters to the patient's body and therefore are not traumatizing,

c) enable the real time visualization of chosen speech signal acoustic parameters on a TV monitor or any other peripheral device of a computer system,

d) the results of the research can be recorded, e.g. as a computer printout. This enables an objective comparative estimation of the course of the therapy disease and the course efficiency.

The functions of the speech organ, being a matter of interest for the phoniatrists, are determined by stimulation and cooperation of some structures in the nervous system. The elimination of the executive speech organ primary disesase e.g. inflammatory or tumorous process within larynx as well as the determination of physiological and pathological models of the acoustic speech signal makes it possible to apply the computer speech analysis in noninvasive, sensitive and objective diagnostics of nervous system function disturbances [8, 11].

### 3. Acoustic analysis of speech disturbances of nervous origin

Cortex systems controlling the speech process are located in the dominating (mostly the left one) cerebral half. Impairement or handicap of these systems functions leads to a complex speech disturbance called aphasia which is the subject of interdisciplinary neurological, neuropsychological, linguistic research [18]. Dysarthria is the other crucial category of speech disturbances. Its acoustic expression is a speech signal's deformation taking — in extreme cases — the form of anarthria that makes it impossible do identify speech sounds [17]. Dysarthria results from an incorrect transfer of impulses from the cortex of the dominating cerebral half to the articulation muscles through nerve pathways (central part), nerves and neuro-muscular synapses (peripheral part). It is also the result of sufficiency of the articulation muscles as well as of the systems modulating the movement functions connected with the speech process cerebellar and extrapyramidal systems [21, 23]. Dysarthria of the cortex origin is a very rare phenomenon. Selective damage of certain movement areas of the dominating cerebral half is the reason for this speech disturbance. The individual types of dysarthria have a series of characteristic features that enable their identification by means of audition:

1) cerebral dysarthria — faint, "neglectful" articulation, the pace of prononunciation gives it a scanning nature. The damage concerns cerebellum or nerve pathways connecting the cerebellum with other structures of the nervous system [1],

2) bulbar dysarthria — speech is "blurred", with a distinct nasal sound. The damage may concern central nervous paths transmitting impulses from the movement cortex of both cerebral halves to the medulla oblongata, i.e. bulbous, concentrations of nerve cells (nuclei) in the bulbous, nerves supplying the articulation muscles, neuro-muscular synapses and the muscles [14],

3) extrapyramidal dysarthria — the speech is low, "shivering" often accelerated and faint (in Parkinson's disease) or less frequently it has "burtsting" character (in Huntington's disease). The damage concerns under-cortex nuclei and/or the extrapyramidal system's nerve pathways,

4) dysarthria in myasthenia — in the course of speaking the voice lowers, articulation aggravates as in bulbous dysarthria. This state is originated by weakness

of the articulation muscles caused by the impulse transmission from nerve to muscle capability exhaustion within synapse.

Considering the acoustic phenomena appearing in different types of dysarthria, this kind of speech disturbances seems to be richest source of diagnostic information. It is possible to obtain these information by a properly programmed computer speech signal analysis.

The initial stage of research includes the preparation of test tasks taking into consideration the widest possible range of articulation schemes having a suitable, for the given language, difficulty level (noise, voiced, fricative, plosive sounds put together into sequences that realization requires full articulation proficiency). During the research carried out at the Department and Clinic of Neurology of the Medical University of Wrocław and the Institute of Telecommunication and Acoustics of the Wrocław Technical University a basic sentence: "The maintenance technician tightens radiator" (in Polish: "Konserwator uszczelnia kaloryfer" — [*konserwator uʃtʃelnɲa kalorƎferƎ*]) was used [19, 20]. It was a kind of a key entry which, after recording it on a magnetic tape, was subject to computer analysis. The construction of the test sequence, apart from articulation possibilities of a man, should take into account the diagnostic purpose that one wants to achieve.

The spectrograms of a test statement in case of the cerebellar dysarthria show characteristic phenomenon of "jitter" demanding further analyses (Fig. 1). The acoustic pattern of bulbar dysarthria is characterized by "disorganisation" of the sound spectrum; selectivity of each element of a statement deteriorates, the energy of the voice diminishes, the time to perform subsequent stages of the test task elongates. An increase of the formants having higher frequency can also be observed (Fig. 2).

In the extrapyramidal speech disturbances the main element is the loss of amplitude (decrease of voice energy), particularly clearly visible when compared to the test pronouncement of a healthy man (Fig. 3).

The sentence which is captious in the sense of articulation "Konserwator uszczelnia kaloryfer" ("The maintenance technician tightens radiator"), can cause difficulties to the people with cerebellar or bulbar dysarthria, while for those with myasthenia, where it is essential to discover or evidence of muscle weakness, the oral test should include repeating (therefore provoking the fatigue of certain group of muscles) articulation structures. A series of pronounced digits may be a good example of it "jeden i jeden" ("one and one"), "jeden i dwa" ("one and two"), "jeden i trzy" ("one and three"), "jeden i cztery" ("one and four") etc. Owing to miasthenic weakness of muscles, the "tired" articulation structure refuses to work properly. This in turn leads to disorganisation of the speech signal which, in the acoustic picture of speech, is characterized by increasing abbreviation of the unit pronouncement time and loss of amplitude. After intravenous injection of a drug causing a fast but brief improvement of the neuro-muscular conductivity (Tensilon), one can register renewed gain of amplitude, the change of the structure of particular phonemes and elongation of the test speech pronouncement time taking the form similar to that one of healthy people (Fig. 4) [19, 20].

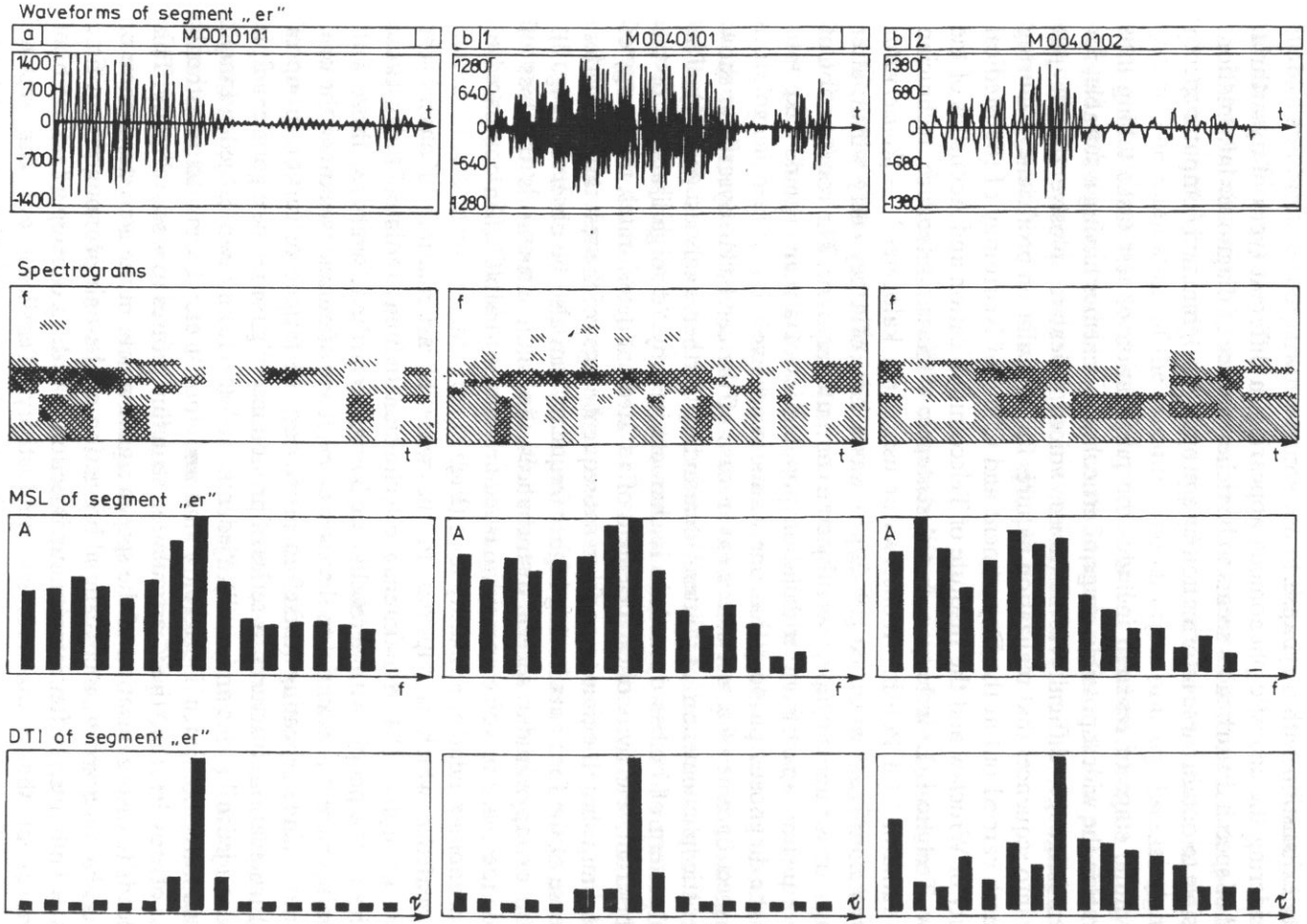


Fig. 1. The waveforms, spectrograms, mean spectrum levels (MSL), and distribution of time intervals between zero-crossings of the speech signal (DTI) of diade "er" of "konserwator", spoken by male voice; a — normal voice, b1 — patient with middle form of cerebellar dysarthria, b2 — patient with severe form of cerebellar dysarthria.

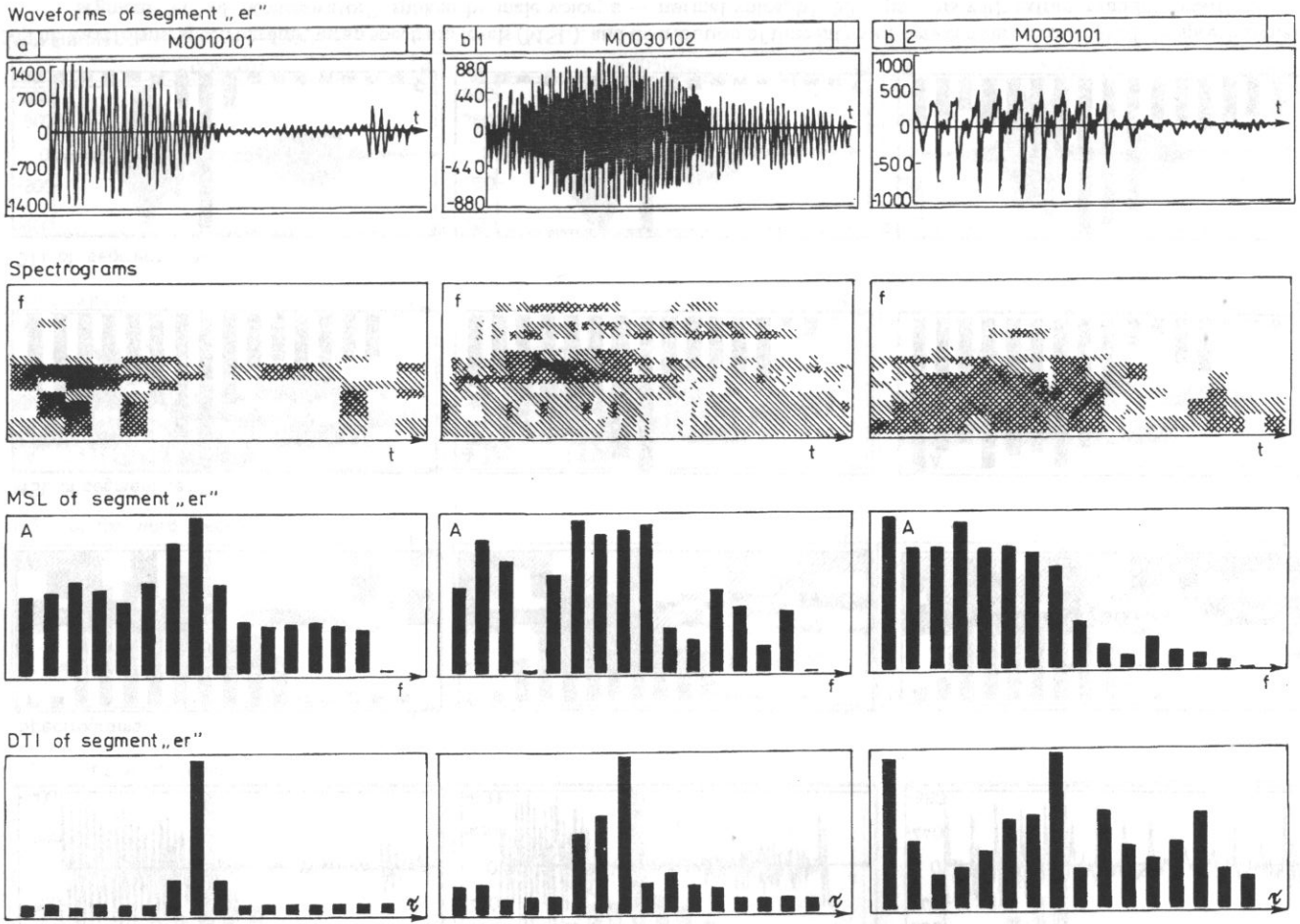


Fig. 2. The waveforms, spectrograms, mean spectrum levels (MSL), and distribution of time intervals between zero-crossings of the speech signal (DTI) of segment "er" of "konserwator", spoken by male voice; a — normal voice, b1 — patient with middle form of bulbar dysarthria, b2 — patient with severe form of bulbar dysarthria.

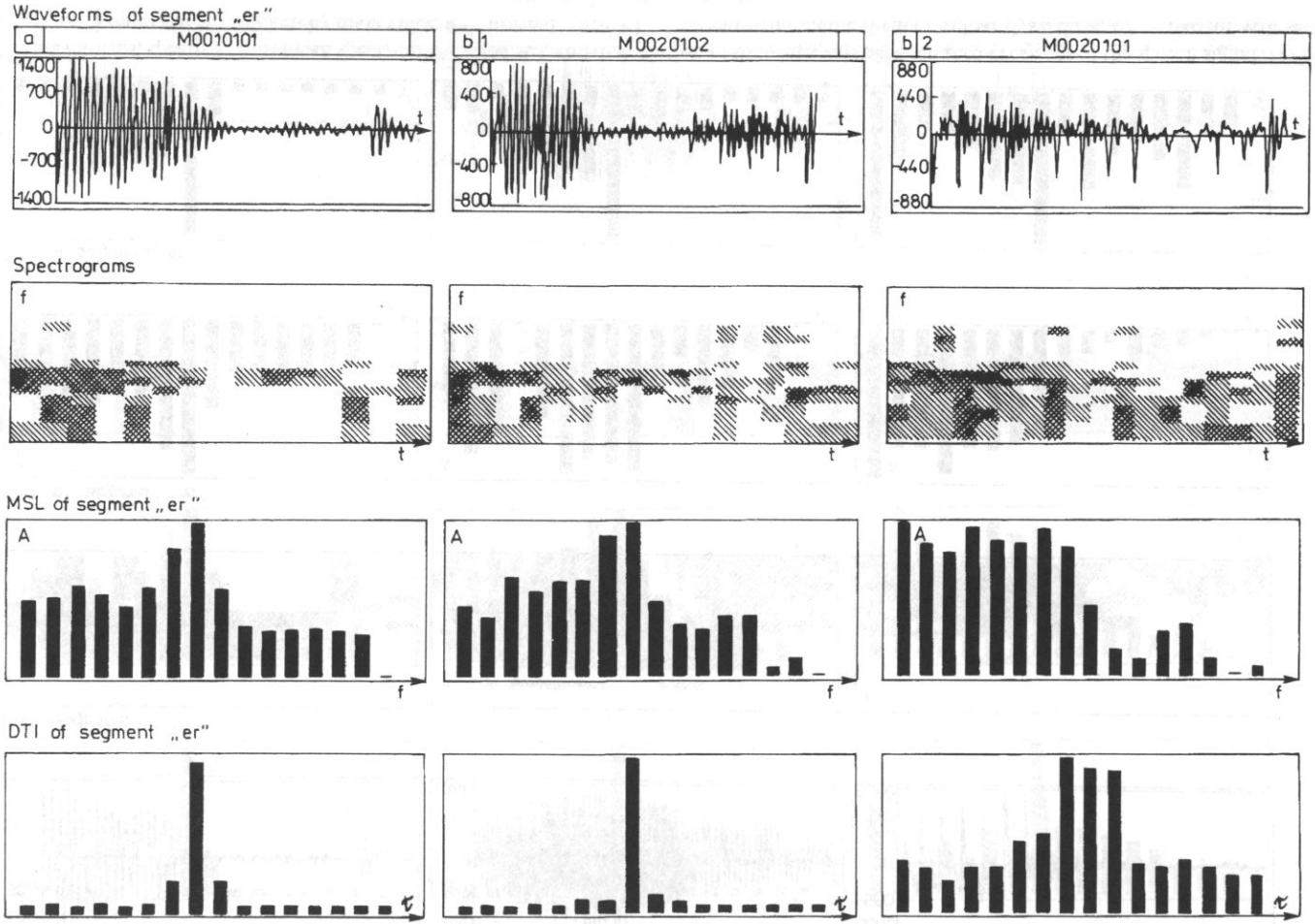


Fig. 3. The waveforms, spectrograms, mean spectrum levels (MSL), and distribution of time intervals between zero-crossings of the speech signal (DTI) of segment "er" of "konserwator", spoken by male voice; a — normal voice, b1, b2— patients with extrapyramidal dysarthria.

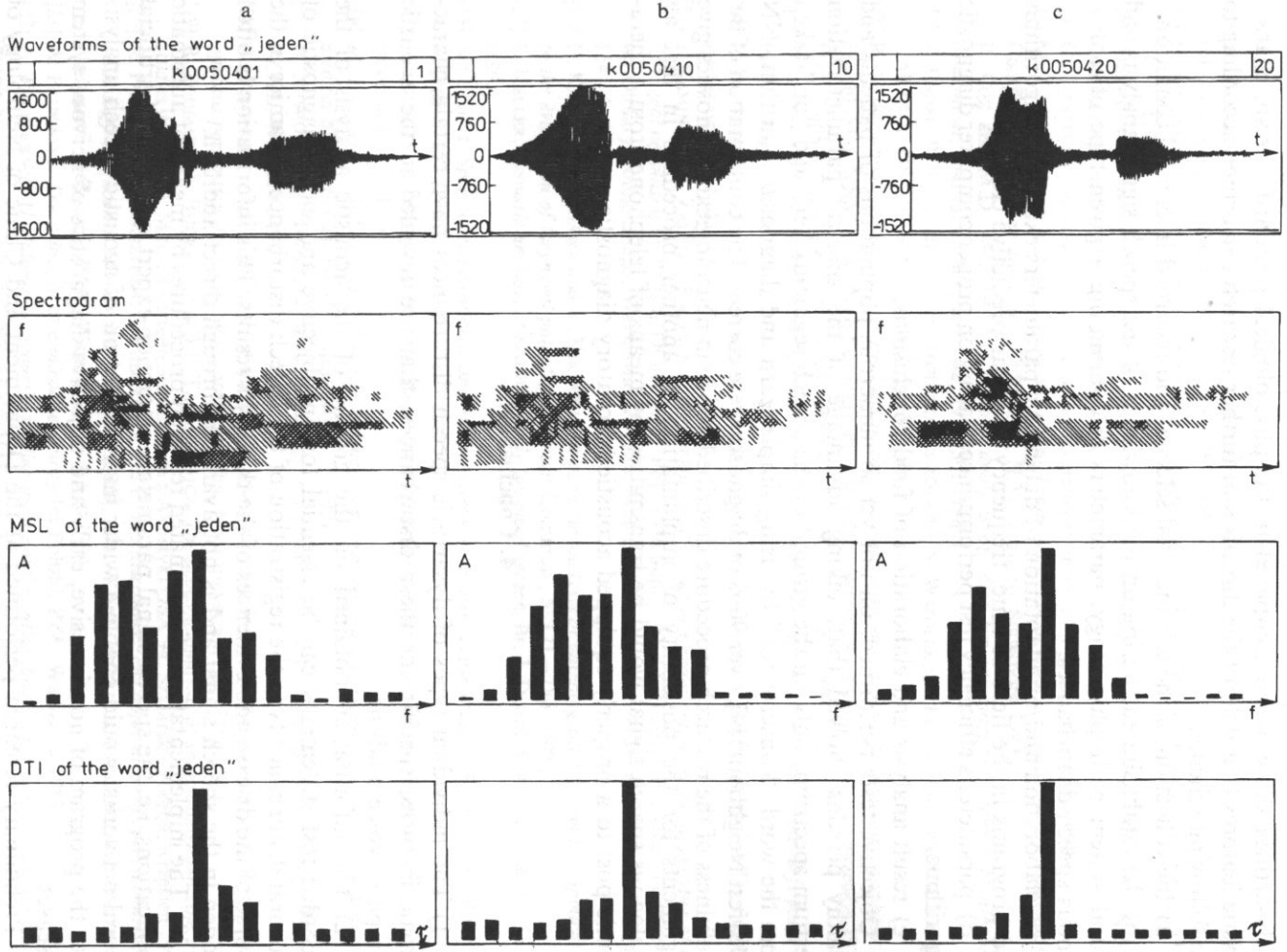


Fig. 4. The waveforms, spectrograms, mean spectrum levels (MSL), and distribution of time intervals between zero-crossings of the speech signal (DTI) of word "jeden" [*jeden*]; a, b, c — patient (woman) with dysarthria in myasthenia — successive 1-th, 10-th and 20-th repetitions.

The described examples of the speech acoustic patterns evidencing different types of dysarthria show, when compared to the physiological standard, certain characteristic features that delimit the direction of further research performed according to the following scheme:

a) the collection of the test material selected and recorded in clinical conditions,

b) the establishment basing on the knowledge of the speech signal analysis and neural system pathophysiology, parameters discriminating a given type of neurogenous speech disturbances,

c) elaboration and/or adaptation of diagnostic parameters extraction algorithms and programs in the field of time, frequency or linear predictive coding,

d) parameter's efficiency test performances basing on proper computer diagnostic algorithms,

e) result analysis and elaboration of final conclusions.

Objective tests performed, on not yet so numerous populations of patients and healthy persons showed that, taking advantage of the spectral parametrization (tertium spectrum) only on the ground of the speech segments "er" and "on" taken from the word "konserwator" by using simple learn and diagnosis algorithms NN (Nearest Neighbour) [4], over 90% of diagnoses were correct. The confirmation of the usefulness of the research procedure described above in neurological diagnostics give arguments for the possibility of implantation of another procedure in that an analogous speech signal would be transmitted by means of telephone from a therapeutic post to a properly equipped acoustic laboratory diagnostic center.

## 4. Conclusions

1) The individual types of dysarthric speech disturbances have certain characteristic features, specific for these disturbances, that are revealed in the acoustic computer voice analysis.

2) The information obtained on the ground of the acoustic analysis of the recorded test statements can be essential for an objective and early diagnostic of a neural disturbance type the registration of the speech disturbance dynamics in the course of the disease and evidences of the therapy's results. This information is often hidden in the speech signal and is not available through direct audition.

3) The implementation of automated research procedures by means of automatic applications, i.e. the speech signal parameters extraction expert systems and artificial neural networks, would enable a wider implementation of acoustic speech analysis into the program of non-invasive, early and objective diagnostics of nervous system diseases.

Preliminary research performed at the Department and Clinic of Neurology of Medical University of Wrocław and at the Institute of Telecommunication and Acoustics of Wrocław Technical University give every reason to believe that this program is perfectly real.

## References


[1] H. ACKERMANN, *Articulatory deficits in parkinsonian dysarthria: an acoustic analysis*, J. Neurol.-Neurosurg.-Psychiatry, **54**, 12, 1093–1098 (1991).

[2] H. ACKERMANN, *Cerebellar voice tremor: an acoustic analysis*, J. Neurol.-Neurosurg.-Psychiatry, **54**, 1, 74–76 (1991).

[3] ALKU-PAAVO, *Glotal wave analysis with synchronous iterative adaptive inverse filtering*, Speech Communication, **11**, 109–118, (1992).

[4] Cz. BASZTURA, *Sources, signals and acoustics patterns* [in Polish], WKL, Warszawa 1988.

[5] M. COOKE, S. BEET and M. CRAWFORD, *Visual representation of speech signals*, Willey Professional Computing, J. Willey and Sons, Chichester, N.Y., Toronto, Singapore 1993.

[6] B. COX and M.D. MORRISON, *Acoustical analysis of voice for computerized laryngeal pathology assessment*, Journal Otolaryngol., **12**, 295–301 (1983).

[7] Z. ENGEL, R. TADEUSIEWICZ, H. TOSIŃSKA-OKRÓJ and W. WSZOŁEK, [in Polish], Otwarte Seminarium z Akustyki OSA-92, Kraków 1992, pp. 95–98.

[8] R. GUBRYNOWICZ, *The acoustic analysis of the substitutive speech in patients after laryngectomy* [in Polish], Mat. XXVI Otwartego Seminarium z Akustyki, Wrocław–Oleśnica, 17–19 wrzesień 1979, Prac. Nauk. Inst. Telek. Pol. Wrocławskiej 43, Ser. Konf. 11, pp. 189–192.

[9] J. KACPROWSKI, W. MIKIEL and A. SZEWCZYK, *The acoustic model investigations of the cleft palat* [in Polish], Arch. Akust., **11**, 2, 167–187 (1976).

[10] J. KACPROWSKI, *The objective acoustic methods in the diagnostics of organ of speech* [in Polish], Archiwum Akustyki, **14**, 4, 287–304 (1979).

[11] J. KAMIŃSKI, M. ZALESKA-KRECICKA, *The technique of the speech examination in the diagnostics of the laryngeal neoplasms* [in Polish], Otolaryngol. Pol., 1986 Supl. — XXXIII Zjazd Polskiego Towarzystwa Otolaryngologicznego, Warszawa 29, 1986, Materiały Naukowe, v. 1, Leczenie raka krtani, pp. 164–1.

[12] H. KASUYA, Sh. OGAWA and Y. KIKUCHI, *An acoustic analysis of pathological voice and its application to the evaluation of laryngeal pathology*, Speech Commun., **5**, 171–186 (1986).

[13] E. KELLER, *Acoustic analysis of neurologically impaired speech*, Br. J. Distrd. Commun., **26**, 1, 75–94 (1991).

[14] R.D. KENT, *Speech deterioration in amyotropic lateral sclerotsis; a case study*, J. Speech Hear. Res., **34**, 6, 1269–1275 (1991).

[15] J. KULIKOWSKI, *The computer analysis of the pictures in biology and medical diagnostics* [in Polish], Informatyka, 1, 1–4 (1991).

[16] M. KURZYŃSKI, J. SAS and E. PUCHAŁA, *Unconventional methods of recognition in the computer aid medical diagnostics* [in Polish], Informatyka, 7, 1991.

[17] A. MITRONOWICZ-MODRZEJEWSKA, *Physiology and pathology of voice, hearing and speech* [in Polish], PZWL, Warszawa 1963.

[18] R. PODEMSKI *et al.*, *Character of the middle and late components of the acoustic evoced potenti in aphasus perception disorders*, Electrocephal. Clin. Neurophysical., **52**, 21P (1981).

[19] R. PODEMSKI, S. BUDREWICZ and P. TARANTOWICZ, *The acoustic analysis of speech diagnostic the pilot studies* [in Polish], Mat. Otwartego Seminarium z Akustyki OSA'94, Szklarska Poręba, wrzesień 1994.

[20] R. PODEMSKI, Cz. BASZTURA, S. BUDREWICZ and P. TARANTOWICZ, *The application of speech analysis in pathology diagnostics of nerves system* [in Polish], Mat. Konf. Naukowa Komitetu Biocybernetyki i Inżynierii Medycznej PAN, Warszawa 12–13.10.1994.

[21] A. PRUSIŃSKI, *The principle of clinical neurology* [in Polish], PZŁ, Warszawa 1989.

[22] A. PRUSZEWICZ, *Usefulness of acoustic studies on the differential diagnostics organic and functional dysphonia*, Acta Otolaryngol. Stockholm, **111**, 2, 414–419 (1991).

[23] R. TADEUSIEWICZ, *The speech signal* [in Polish], WKiL, Warszawa 1988.

[24] L.S. WYGODSKI, *The thinking and speech* [in Polish], PWN, Warszawa 1981.

[25] A. ZAKRZEWSKI, *The clinical otholaryngology* [in Polish], PZWL, Warszawa 1982.

ARCHIVES OF ACOUSTICS
21, 1, 15–28 (1996)

# MEASURING DIRECTIONAL MASKING IN A SOUND FIELD USING ADAPTIVE THRESHOLD PROCEDURES

K.S. ABOUCHACRA, J.T. KALB* and T.R. ŁĘTOWSKI**

* The U.S. Army Research Laboratory,
Human Research and Engineering Directorate,
Aberdeen Proving Ground, MD 21005-5425
** The Pennsylvania State University
110 Moore Building, University Park, PA 16802

The accuracy of three adaptive threshold procedures for measuring directional masking was assessed in two experiments. For each experiment, detection of a target signal, located at either 0°, 90°, 180° or 270° azimuth was measured in the presence of a masker located at 0°, 90° or 180° azimuth. In Experiment 1, masked thresholds for ten normal hearing subjects were measured using the Bekesy Procedure and an Ascending Up-and-Down Procedure. In Experiment 2, masked thresholds for another group of ten normal hearing subjects were measured using the Bekesy Procedure and a Maximum Likelihood Procedure. Results confirmed the dependence of detection thresholds on the angular separation between the target and masker. In addition, threshold reliability depended on the location of the signal and the masker. No statistically significant differences were found in detection thresholds over repeated trials or between threshold procedures in Experiment 1 or 2.

## 1. Introduction

Within the last ten years, new technologies and techniques have been used to externalize earphone-presented sounds. Externalization is successful if the earphone-presented sounds appear to originate from locations outside of the head (i.e., at azimuths, elevations, and distances from the listener), similar to natural everyday listening. An externalized acoustic environment, which includes stationary or moving phantom sources, is commonly referred to as a three-dimensional (3D) audio display.

One new and exciting application of 3D audio displays is for enhancing multi-channel communication systems [8, 27, 28]. In traditional communication systems, operators may have the challenging assignment of monitoring many simultaneous auditory messages (sometimes up to six communications at one time) presented diotically through earphones. In diotic presentation, messages presented equally to both ears are perceived as originating within the operator's head. This type of presentation acoustically mixes the messages, making message extraction difficult.

If the messages are misunderstood, the resulting errors may cost time, equipment and even loss of life.

It the same multi-channel communication task is performed using a 3D audio display, the operator will perceive the messages as originating in the surrounding acoustic environment, at locations outside of the earphones. A 3D audio display spatially separates messages from one another, thereby making it easier for the operator to attend to any selected message. It is well documented that as a noise source is moved away from the location of a speech message, listeners can better detect, recognize or understand the message [e.g., 4, 6, 9, 10, 11, 13, 16, 18, 20, 23, 24, 29, 30, 34]. Similarly, researchers using more traditional signals (e.g., pure tones or narrow bands of noise) have reported that, as the angular separation between the masker and a target signal increases, detection performance improves [e.g., 11, 17, 32]. Given the advantages of spatially separated messages, strategic positioning of message directions in a 3D audio display may improve operator and system performance with multi-channel communications.

Proper positioning of message sources in a 3D audio display requires, however, an understanding of how multiple auditory signals interact in the environment. A typical listening environment is not only filled with many signals, but also with noises that interfere with our ability to monitor them. With a 3D audio display, messages have an apparent spatial location. Thus, messages that are not attended to can be though of as spatially-located maskers. Such maskers can singly, or in combination with background noise, mask sounds that carry information to the listener. Background noise differs from a spatially-located masker in that it appears to originate from no particular location, changes only occasionally in level and frequency, and is constantly present. Given that desired sounds, interfering messages, and background noise are present in a 3D audio display, the optimization of message spatial location, level, and content, under such conditions should be evaluated.

How should a 3D audio display be optimized? As a first approximation, the masking effect of a spatially-located masker on a target message could be established using some measure of detection. Frequently, detection of signals in noise is measured using adaptive procedures. An adaptive procedure is one in which the stimulus level on any one trial is determined by the response to the preceding stimulus level. Although adaptive procedures are known to be reliable and appropriate in threshold related studies, some adaptive procedures are time-consuming and inefficient. The purpose of the present study was to determine which adaptive threshold procedure should be used in evaluating multi-channel 3D audio displays. Specifically, the primary objective of the study was to determine which of three adaptive procedures (i.e., Bekesy Procedure, Ascending UP-and-Down Procedure, and Maximum Likelihood Procedure) was best for measuring the amount of masking by spatially-located directional masking in 3D audio displays. An ideal procedure should yield sufficiently repeatable detection thresholds in the shortest amount of time.

## 2. Methodology

### *2.1. Subjects*

Twenty adults (aged 21 – 35) voluntered to participate in this study. Ten subjects participated in Experiment 1 and a different group of ten subject's participated in Experiment 2. All subjects had normal hearing (i.e., hearing thresholds 15 dB HL [1] or better in each ear from 250 through 8000 Hz, in octave steps), and bilaterally symmetrical hearing sensitivity (i.e., inter-aural sensitivity differences did not exceed 5 dB at any test frequency).

### *2.2. Instrumentation*

A target signal and spatially-located masker were simultaneously presented to the subject by two independent loudspeakers representing signal (S) and noise (N). The different combinations of azimuth are shown in Fig. 1, where a letter-symbol directly in front of the head icon corresponds to a loudspeaker positioned at 0° azimuth. Letter symbols to the right and left correspond to a loudspeaker located at 90° and 270° azimuth, respectively. For example, in the second spatial configuration, the target signal was located directly in front of the subject at 0° azimuth, and the noise directly behind at 180° azimuth. Whenever the first spacial configuration was evaluated, both the target signal and the noise were presented through one loudspeaker located at 0° azimuth.

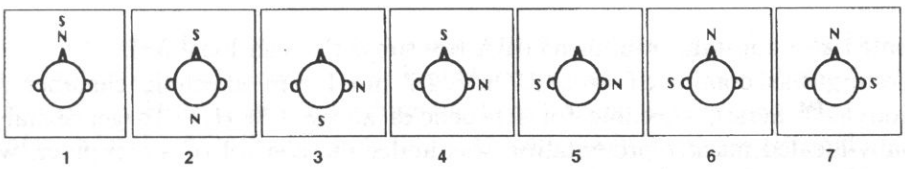


Fig. 1. The spatial configurations of the target signal and the spatially-located masker source. The first five configurations were used in experiment 1. All seven configurations were used in experiment 2.

The target was a single spondaic word (two-syllable compound words having equal stress on each syllable) from the CID W-1 standardized word list. Initially, a tape recording of the word was played from a cassette deck (Nakamichi, MR-1) through a graphic equalizer (General Radio, Model 1925) and digitally recorded and stored in a computer (Zenith 248, AT class, DSP-16, Ariel Corporation). The target word, 'Northwest', was selected for the following reasons. First, it is a simple representation of the target signal of interest in communication systems (i.e., speech). Second, the word is included in standardized recordings of word lists and can be easily available for use by any researcher. Third, of all the spondaic words in standardized recordings, OLSEN and MATKIN [25] reported that the two syllables in

'Northwest' are the most similar with respect to audibility. In summary, the major consideration in target signal selection was to identify a word that would reduce variability in test results, produce highly reliable threshold data, in require minimal training.

The spatially-located masker was a broadband signal approximating the long-term average speech spectrum [2]. The output from a noise generator (General Radio, Model 1825) was filtered to obtain the desired spectrum (Fig. 2) and always

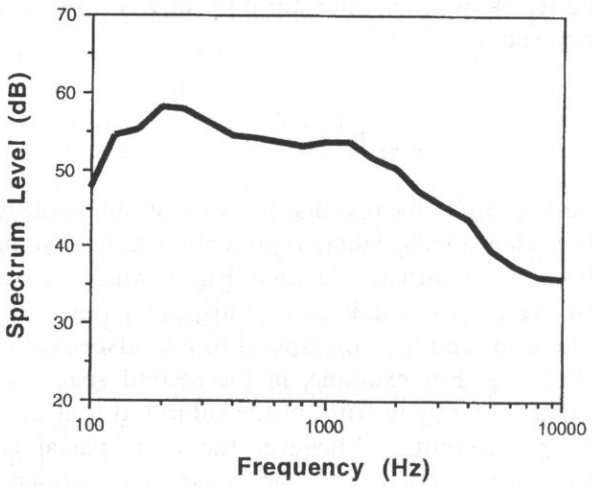


Fig. 2. The one-third octave sound pressure level spectrum of the masking noise used in this study.

presented at a constant level of 65 dBA (re: subject's head location).

Testing was conducted in a 2.7 m × 2.7 m × 1.9 m anechoic chamber (IAC Microdyne™ Series; anechoic for frequencies above 170 Hz). Target signal and spatially-located masker presentation was under the control of a computer, which directed the stimuli to two boom-mounted loudspeakers (Bose, 1180385A). The booms were suspended from the ceiling of the chamber and pivoted on the same axis, holding the loudspeakers at a uniform 1 m from the subject's head at ear level. Its design permitted independent movement of both loudspeakers anywhere on the circumference of the circle, in 1° steps, via computer-controlled stepper-motors (Arrick Robotics™). Four additional Bose loudspeakers were placed at fixed locations in the chamber and presented speech spectrum noise (65 dBA) to mask any audible motor or gear sounds that existed while the booms were in motion (Fig. 4). The output from all six loudspeakers was examined daily, using a 75 dBA pink noise signal that was presented sequentially through each louspeaker. Spectral outputs from the loudspeakers were compared in 1/3 octave bands and adjusted to be equal (within 2 dB) in the 200 to 9000 Hz range.

An acoustically-transparent cylindrical curtain (inside diameter of 1.75 m) kept the listeners from seeing any of the loudspeakers in the test chamber or the boom

system overhead. A two-light display was located within the curtain at 0° azimuth and 1.2 m from the grated floor of the chamber. A white light was on continuously throughout the experiment to provide illumination inside the curtain (the chamber lights were turned off throughout testing). To mark listening intervals, a green light was illuminated by the control computer. Subjects provided threshold responses using either a hand switch or a response board, depending on the adaptive threshold procedure.

### *2.3. Adaptive Threshold Procedures*

*2.3.1. Bekesy Procedure.* During the Bekesy tracking procedure, subjects used a hand-held resonse button to track their own detection thresholds. For each threshold measure, the green display light marked a 65 second listening interval. The target signal was initially presented at a level approximately 20 dB below the subject's actual masked threshold. With the presentation level changing at a rate of 5 dB/sec in 0.5 dB steps (this rate was found in a pilot experiment as optimal for the task), the intensity of the target signal was increased until the subject pressed the response button. Pressing the button caused the signal level to be attenuated. When the subject released the response button, the level of the target signal increased. Tracking of the target signal continued for 60 seconds beyond the first reversal on the tracing. Detection threshold was defined as the mean midpoint of several excursions during a 60 second tracking period [3, 5, 31]. The first reversal was excluded from the calculation of threshold because it increases the overall error of the threshold estimate [21, 36].

*2.3.2. Ascending Up-and-Down Procedure.* The Ascending Up-and-Down Procedure was adapted from the clinical methods of HUGHSON and WESTLAKE [19] and CARHART and JERGER [7]. During this procedure the target signal was played once at each presentation level, rather than in a continuous manner as in the Bekesy Procedure. The initial presentation level of the target signal was at an intensity of about 10 dB below the subject's estimated masked threshold. Following this presentation, the target signal was presented in ascending 1-dB steps, until the subject responded. Once detected, its level was decreased by 10 dB and presented again in ascending 1-dB steps until the subject responded. Again, the green light marked listening intervals for subjects. Specifically, while the light was on (5 sec), a single presentation of the target signal occurred following a random time delay. Subjects were instructed to listen for the target signal and, when the light turned off, subjects were to press the response button if they heard something in addition to the spatially-located masker. The procedure continued until six ascending threshold responses were obtained. Detection thresholds was defined as the mean of the six ascending response levels [15].

*2.3.3. Maximum Likelihood Procedure.* The maximum likelihood procedure selected for this experiment was a PEST (Parameter Estimation by Sequential

Testing) Procedure incorporating maximum-likelihood principles [14, 22, 26, 33]. In all versions of PEST the results of previous trials are used to adjust the target signal level. However, the added maximum-likelihood principles determine the spread and threshold midpoint values that have the highest probability of being the best threshold estimate. Detection threshold can be chosen arbitrarily and in this case was chosen as the 50% detection point on a psychometric function.

To establish a detection threshold using this procedure, the target signal was presented to the subject 17 times, with the first two presentations defining the presentation level range (i.e., the first and second presentation of the target signal was at the highest and lowest level in the range of possible spread values, respectively. These presentations were not included in threshold calculation). Step sizes for the last 15 presentations of the target signal were determined by Maximum Likelihood Procedure rules [26], with the maximum step size limited to 20 dB, and a minimum of 1 dB.

During threshold determination, the green light on the display was used to indicate a listening interval. The "light on" condition marked an observation interval. The "light off" condition indicated a response interval. Subjects were instructed to respond by pressing either the left or right push-button on the response pad, indicating "No, I did not hear the target signal" or "Yes, I did hear the target signal", respectively. The masked detection threshold was established following the final 15 presentations of the target signal, with the last presentation level taken as the subject's detection threshold.

### *2.4. Procedure*

*2.4.1. General.* Across all experiments the following procedure was used. The subject was seated on a custom-made, height-adjustable chair, which was bolted ot the floor of the anechoic chamber. While in a seated position, the chair was adjusted so that the ears of the subject were aligned with the centers of the boom-mounted loudspeakers. This arrangement allowed for the same center position to be used as a reference during the experiment. No restraints were used to keep the subject's head from moving during trials. Instead, two plomb-bobs were dropped from the roof of the curtain, 50 cm apart, directly in front of the subject. Subjects were instructed to visually align the two plomb-bobs during testing. In addition, head orientation was monitored by a head tracking electromagnetic device (Polhemus, 3-SPACE ISOTRAK). The device was mounted to the back of the subject's head using a Velcro™ strap that was wrapped around the subject's head at forehead level. Any target signal presentations that occurred during excessive head movement ($\geqslant 3°$) were discarded and repeated [12].

After the subject was positioned in the chamber, room lights were turned off and the white display light remained on for testing. The boom-mounted loudspeakers were rotated to one of the randomly selected spatial configurations (Fig. 1). Once the loudspeakers were in position, the spatially-located masker (65 dBA, measured at the

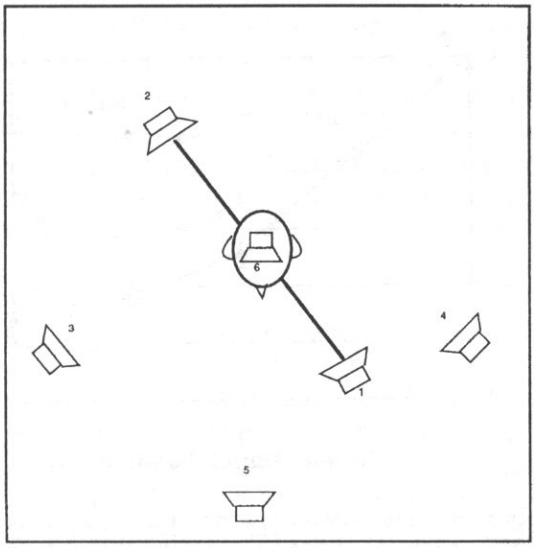


Fig. 3. Schematic of the experimental equipment and test chamber. Boom-loudspeakers are numbered *1* and *2*. Stationary loudspeakers are numbered *3*, *4*, *5* and *6*. Loudspeaker *6* was directly overhead.

subject's head position) was introduced and remained on until a detection threshold was established. The boom-mounted loudspeakers moved to the next randomly selected spatial configuration. To mask any apparatus-related noises, a 65 dBA speech-spectrum noise was delivered through the four stationary loudspeakers while the booms were in motion (Fig. 3).

In Experiment 1, threshold estimates for a group of ten subjects were obtained using the Bekesy Procedure and the Ascending Up-and-Down Procedure for the first five spatial configurations shown in Fig. 1. Thresholds were repeated six times at each spatial configuration. One adaptive threshold procedure was used during one, 45-minute session while the other was used during a second 45-minute session. The order of adaptive threshold procedures was counterbalanced across subjects.

In Experiment 2, threshold estimates for the second group of ten subjects were obtained using the Bekesy Procedure and the Maximum Likelihood Procedure. All seven configurations shown in Fig. 1 were used. Two additional configurations were added to explore other masking possibilities. As in the first experiment, thresholds were obtained six times at each spatial configuration and for each test procedure, in two, 45-minute sessions. Again, the order of adaptive procedures was counterbalanced.

## 3. Results and Discussion

### *3.1. Experiment 1*

Figure 4 presents the mean thresholds and standard error bars for the thresholds obtained in Experiment 1, using the Bekesy Procedure and the Ascending

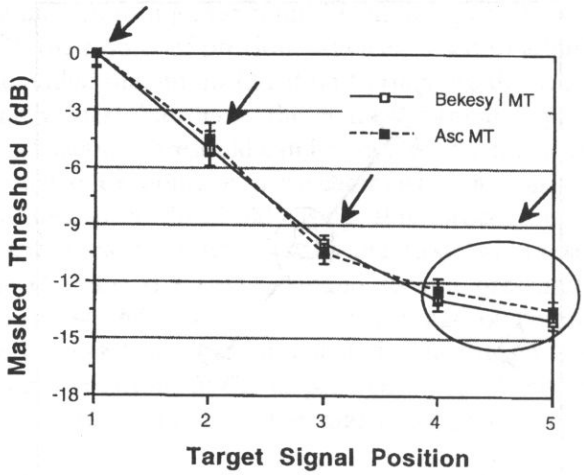


zFig. 4. Experiment 1. Mean detection thresholds and standard error bars for both the Bekesy Procedure (Bekesy I MT) and the Ascending Up-and-Down Procedure (Asc MT).

Up-and-Down Procedure. The spatial configurations (Fig. 1) for the target signal and noise are presented along the abscissa. Masked threshold levels are represented along the ordinate, with 0 dB representing the threshold obtained when both the signal and noise were presented directly in front of the subject (spatial configuration 1). Since detection thresholds were always the poorest (highest) in this loudspeaker arrangement, spatial configuration 1 was used as a reference for which to compare the data obtained in other configurations. Error bars in Fig. 4 represent standard error of the mean.

Collected threshold data were analyzed using a three-way analysis of variance (ANOVA) with repeated measures [35]. The main effects included: adaptive procedure (Bekesy Procedure versus Ascending Up-and-Down Procedure), spatial configuration (1, 2, 3, 4, and 5), and trial (1, 2, 3, 4, 5, 6). A statistically significant difference was found for spatial configuration ([$F(4, 36) = 1670.86$, $\mathbf{p} < 0.0001$]). No statistically significant differences in threshold measures were found for the main effects of adaptive procedure and trial, and for any of the interactions ($\mathbf{p} > 0.05$).

The Schéffè *post hoc* multiple comparison test was performed using appropriate error terms, to examine mean thresholds for each spatial configuration. At an alpha level of 0.05, four Schéffè groupings were found, as depicted by the arrows in Fig. 4 (mean thresholds within the circled area did not differe statistically),. The poorest detection thresholds occurred when the target and spatially-located masker occupied the same spatial position; that is, both S and N were presented at 0° azimuth (spatial configuration 1). In spatial configuration 2, a slight improvement was found in detection. The changes in perceived spectra of the target signal and spatially-located masker resulted in a 4–5 dB improvement in the detection threshold. When *both* the target signal and masker were located to the left or right of the median plane,

improvements of as much as 10 to 14 dB in detection threshold were seen (spatial configuration 5). In these conditions, subjects were able to take advantage of all auditory spatial cues; changes to the pinna cues and interaural difference cues, together, provided listeners with information that significantly improved detection of the target. In summary, if the threshold obtained in the first spatial configuration is used as a reference, the maximum improvement in the mean detection threshold amounted to approximately 14 dB.

### *3.2. Experiment 2*

To compare the Bekesy and Maximum Likelihood Procedures, a repeated measures ANOVA was conducted. The main effects included: adaptive procedure (Bekesy Procedure versus Maximum Likelihood Procedure), spatial configuration (1, 2, 3, 4, 5, 6 and 7), and trial (1, 2, 3, 4, 5, 6). A statistically significant difference was found for spatial configuration ([$F(9, 54)=46037.73$, $\mathbf{p}<0.0036$]). No statistically significant differences in mean detection thresholds were found for the main effects of adaptive procedure and trial, and for any interactions ($\mathbf{p}>0.05$).

Figure 5 presents the mean thresholds and standard error bars obtained using the Bekesy Procedure and Maximum Likelihood Procedure. The spatial configurations for the target signal and spatially-located masker are numbered along the abscissa. Masked threshold level is represented along the ordinate of the figure. Error bars represent the standard error of the mean. The reported results are very similar to those found in the first experiment. The poorest detection performance occurred when the target and spatially-located masker were at the same position in space (i.e.,

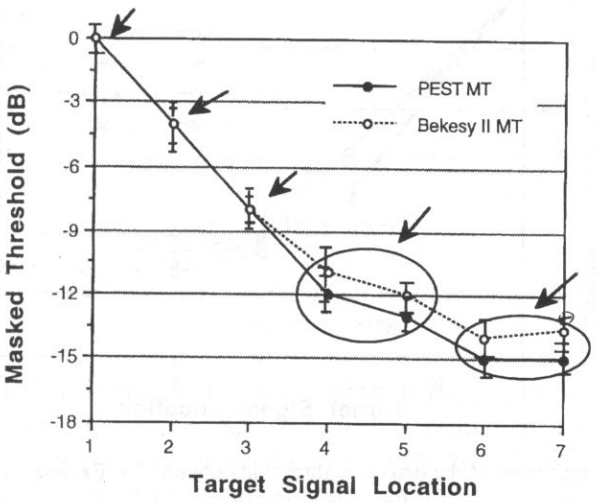


Fig. 5. Experiment 2. Mean detection thresholds and standard error bars for both the Bekesy Procedure (Bekesy II MT) and the Maximum Likelihood Procedure (Maximum Likelihood MT).

both S and N presented at 0° azimuth) and best performance resulted when one or both sound sources were off of the median plane, with the target being directed down the ear canal (i.e., positioned at either 90° azimuth of 270° azimuth).

To determine if statistically significant differences occurred between the mean thresholds at each spatial configuration, the Schéffè *post hoc* multiple comparison method was used. At an alpha level of 0.05, five Schéffè groupings were found, which are depicted by arrows in Fig. 5 (no statistically significant differences existed between mean thresholds within circled areas). Again, if the threshold obtained in the first spatial configuration is used as a reference, the maximum improvement in the detection threshold amounts to approximately 14–15 dB.

### *3.3. Comparison of Adaptive Threshold Procedures*

The mean detection thresholds found in Experiment 1 and Experiment 2 using the Bekesy, Ascending UP-and-Down and Maximum Likelihood Procedure are illustrated in Fig. 6. Threshold means obtained using the Bekesy Procedure for Experiments 1 and 2 are represented in this figure as Bekesy I and Bekesy II, respectively. Using a mixed design structure, where one independent variable (Experiment) was a between-subject factor and one independent variable (spatial configuration) was a within-subject factor, an ANOVA with repeated measures was conducted. No systematic differences in threshold were found across adaptive threshold procedures ($\mathbf{p} < 0.05$). Thus, for this particular task, no statistical or practical difference in detection threshold occurred between the Bekesy, Ascending Up-and-Down, or Maximum Likelihood Procedure.

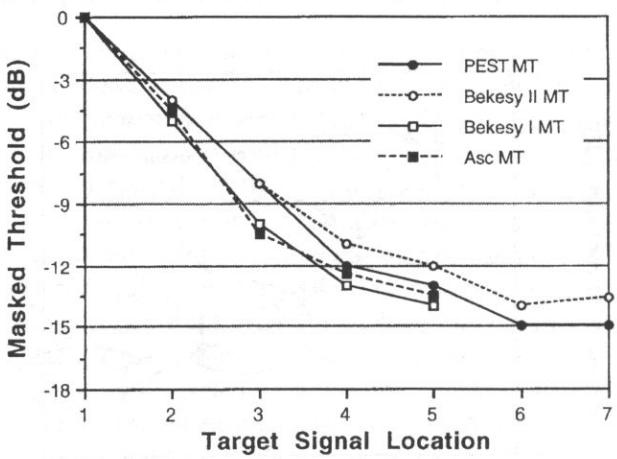


Fig. 6. Comparison of the detection thresholds obtained in Experiments 1 and 2.

At the end of each experiment, subjects were asked to comment on the adaptive threshold procedures. All subjects preferred the Bekesy Procedure for obtaining

a detection threshold. The Ascending UP-and-Down and Maximum Likelihood Procedures were described as being taxing and stress producing. Moreover, all three procedures were reported as being time consuming. To evaluate this last comment, the Bekesy and Maximum Likelihood threshold data were studied in more detail. Specifically, detection thresholds were examined after 15, 30 and 60 seconds for the Bekesy Procedure, and after 3, 6, 8, 10, 12 and 15 trials for the Maximum Likelihood Procedure. (Data collection techniques would not allow for a break-down of the data from the Ascending Up-and-Down Procedure).

When Bekesy threshold data over time (i.e., after 15, 30 and 60 seconds) were subjected to an ANOVA with repeated measures, a statistically significant difference was found for the main effect of time [$F(2, 18) = 12.57$, $\mathbf{p} < 0.0112$)]. The Schéffè *post hoc* multiple comparison technique revealed that a detection threshold after 15 seconds was significantly different than thresholds after either 30 or 60 seconds. No significant difference in mean thresholds occurred between 30 and 60 seconds of tracking ($\mathbf{p} < 0.05$). Mean thresholds are shown in Fig. 7 for the three time periods. The results suggest that, for the directional masking experiment reported, a detection threshold after 30 seconds would not be statistically different from a threshold reported after 60 seconds; thus, the same detection threshold results could be found in half the amount of time.

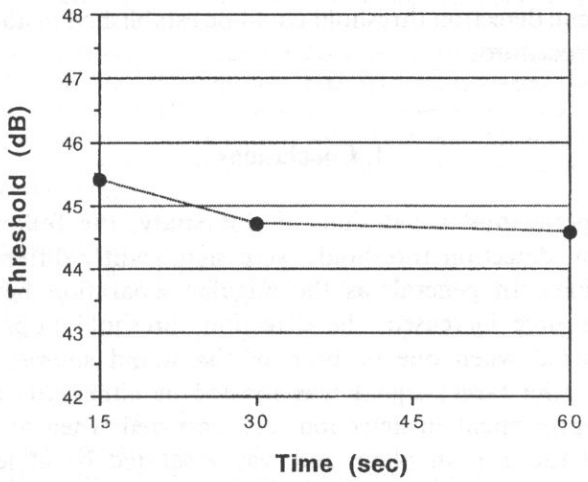


Fig. 7. Mean detection thresholds obtained using the Bekesy Procedure after 15 seconds, 30 seconds and 60 seconds of tracking.

Maximum Likelihood threshold data over trials (i.e., after 3, 6, 8, 10, 12, and 15 trials) were also subjected to an ANOVA with repeated measures. A statistically significant difference was found between number of trials [$F(5, 45) = 16.49$, $\mathbf{p} < 0.001$]. The Schéffè *post hoc* multiple comparison technique revealed that a detection threshold after 3 trials was significantly different than a detection threshold after 6, 8, 10, 12 or 15 trials. Mean threshold data are shown in Fig. 8. The results suggest that,

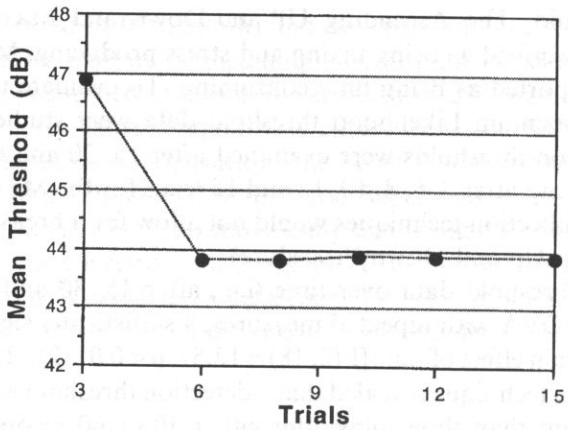


Fig. 8. Mean detection thresholds obtained with the Maximum Likelihood Procedure after 3, 6, 9, 12 and 15 trials.

for the directional masking experiment reported, a detection threshold obtained with the Maximum Likelihood Procedure after 6 trials would not be statistically different from a threshold reported after 15 trials, for this data. Given that each trial requires five seconds, the same detection threshold could be established in about half the time, as in the Bekesy Procedure.

## 4. Conclusions

Within the experimental constraints of this study, the following conclusions were reached. First, detection thresholds were significantly different at almost all spatial configurations. In general, as the angular separation between the target signal and noise source increased, the detection threshold improved. Maximum improvement occurred when one or both of the sound sources were off of the median plane, and the target signal was located at either 90° azimuth or 270° azimuth. Some improvement in detection also occurred when at least one source was located off of the median plane and was separated by at least 90° azimuth from the other source. Second, the results of this study support previous findings that, for a complex target presented together with a spatially-located masker, the changes in detection threshold can be as high as 15 dB depending on the spatial configuration of both sources [4, 7, 9, 10, 11, 13, 16, 18, 20, 23, 24, 29, 30, 35]. Third, although all three adaptive procedures yielded reasonably accurate results and render similar mean thresholds, subject satisfaction, and differences in administration time suggest that advantages might accrue from choosing the Bekesy Procedure for obtaining directional masking thresholds.

The measurement of directional masking should provide designers of multi-channel communication systems with a valuable tool for positioning messages in

3D audio displays. Specifically, the measurement of directional masking will help designers optimize the spatial locations and presentation levels of the messages so that background noise and directional maskers minimally affect message detection.

## Acknowledgments

This research was supported by the U.S. Army Research Laboratory. We wish to thank Dr. G. Richard Price for his helpful comments and suggestions throughout this research project. All the subjects are thanked for volunteering their time.

## References

[1] American National Standards Institute, *Specifications for audiometers*, S3.6-1989 (1989).

[2] American National Standards Institute, *Testing hearing aids with a broad-band noise signal*, S3.42-1992 (1992).

[3] G.V. Bekesy, *A new audiometer*, Acta Otolaryngol., **35**, 411–422 (1947).

[4] A.W. Bronkhorst, R. Plomp, *Binaural speech intelligibility for simulated cocktail-party conditions*, In: Binaural aspects of speech perception in noise, A.W. Bronkhorst, [Ed.], Netherlands: TNO Institute for Perception 1990.

[5] M.A. Brunt, *Bekesy audiometry and loudness balance testing*, In: *Handbook of clinical audiology*, 3rd Ed., In: J. Katz, Ed., pp. 273–291. Baltimore, MD: Williams & Wilkins 1984.

[6] G.L. Calhoun, G. Valencia and T.A. Furness, *Three-dimensional auditory cue simulation for crew station design/evaluation*, Proc. Human Factors Soc., 31st Annual Meeting, 1398–1402 (1987).

[7] R. Carhart, J.F. Jerger, *Preferred method for clinical determination of pure-tone thresholds*, J. Speech Hear Disord., **24**, 330–345 (1959).

[8] T.J. Doll, T.E. Hanna, J.S. Russotti, *Masking in three-dimensional auditory displays*, Human Factors, **34** (3), 255–265 (1992).

[9] D.D. Dirks, R.H. Wilson, *Binaural hearing of speech for aided and unaided conditions*, J. Speech Hear. Res., **12**, 650–664 (1969).

[10] A.J. Duquesnoy and R. Plomp, *The intelligibility of sentences in quiet and in noise in aged listeners*, J. Acoust. Soc. Am., **74**, 1136–1144 (1983).

[11] M. Ebata, T. Sone and T. Nimura, *Improvement of hearing ability by directional information*, J. Acoust. Soc. Am., **43**, 289–297 (1968).

[12] M. Ericson, *Personal communication* (1992).

[13] J.M. Festen and R. Plomp, *Effects of fluctuating noise and interfering speech on the speech-reception threshold for impaired and normal hearing*, J. Acoust. Soc. Am., **88**, 1725–1737 (1990).

[14] J.M. Findlay, *Estimates on probability functions: A more virulent PEST*, Perception & Psychophysics, **23**, 181–185 (1978).

[15] T.A. Frank, *High-frequency hearing threshold levels using a Beltone 2000 audiometer and Sennheiser HD 250 earphones*, Ear Hear., **11**, 450–454 (1990).

[16] S.A. Gelfand, L. Ross and S. Miller, *Sentence receptionn in noise from one versus two sources: Effects of aging and hearing loss*, J. Acoust. Soc. Am., **83**, 248–256 (1988).

[17] M. Good, R.H. Gilkey, *Masking between spatially separated sounds*, Proc. Human Factors Soc., 36th Annual Meeting, 253–257 (1992).

[18] I.J. Hirsh, *The relation between localization and intelligibility*, J. Acoust. Soc. Am., **22**, 196–200 (1950).

[19] W. HUGHSON and H. WESTLAKE, *Manual for program outline for rehabilitation of aural casualties both military and civilian*, Trans. Am. Acad. Ophthal. Otolaryngol., (Suppl) **48**, 1–15 (1944).
[20] W.E. KOCK, *Binaural localization and masking*, J. Acoust. Soc. Am., **22**, 801–804 (1950).
[21] R.J. LEZAK, B.M. SIEGENTHALER and A.J. DAVIS, *Bekesy-type audiometry for speech reception threshold*, J. Aud. Res., **4**, 181–189 (1964).
[22] H.R. LIEBERMAN and A.P. PENTLAND, *Microcomputer-based estimation of psychophysical thresholds: The Best PEST*, Beh. Res. Methods & Instr., **14**, 21–25 (1982).
[23] N.W. MACKEITH and R.R.A. COLES, *Binaural advantages in hearing of speech*, J. Laryngol. Otol., **85**, 213–232 (1971).
[24] B. NORLUND and B. FITZELL, *Physical factors in angular localization*, Acta Otolaryngol., **54**, 75–93 (1967).
[25] W.O. OLSEN and N.D. MATKIN, *Speech audiometry* [In:] Hearing assessment (second edition), W.F. Rintelmann, [Ed.] Baltimore: University Park Press (1991).
[26] A. PENTLAND, *Maximum likelihood estimation: The best PEST*, Perception & Psychophysics, **28**, 377–379 (1980).
[27] D.R. PERROTT, *Auditory and visual localization: Two modalities and one world*, Audio Eng. Soc., 12th International Conference, Snekkersten, Copenhagen, Denmark (1993).
[28] D.R. PERROTT, T. SADRALODABAI, K. SABERI, T.Z. STRYBEL, *Aurally aided visual search in the central visual field: Effects if visual loaded and visual enhancement of the target*, Human Factors, **33**, 389–400 (1991).
[29] R. PLOMP, *Binaural and monaural speech intelligibility of connected discourse in reverberation as a function of azimuth of a single competing sound source (speech or noise)*, Acoustica, **34**, 200–211 (1976).
[30] R. PLOMP and A.M. MIMPEN, *Effect of the orientation of the speaker's head and the azimuth of a noise source on the speech-reception threshold for sentences*, Acoustica, **48**, 325–328 (1981).
[31] S. RREGER, *A clinical and research version of the Bekesy audiometer*, Laryngoscope, **62**, 1333–1351 (1952).
[32] K. SABERI and L. DOSTAL, T. SADRALADABAI, V. BULL, *Free-field release from masking*, J. Acoust. Soc. Am., **90**, 1355–1370 (1992).
[33] M.M. TAYLOR and C.D. CEELMAN, *PEST: Efficient estimates on probability functions*, J. Acoust. Soc. Am., **41**, 782–787 (1967).
[34] F.M. TONNING, *Directional audiometry. II: The influence of azimuth on the perception of speech*, Acta Otolaryngol., **72**, 352–357 (1971).
[35] M.W. VASEY and J.F. THAYER, *The continuing problem of false positives in repeated measures ANOVA in psychophysiology: A multivariate solution*, Psychophysiol., **24**, 479–486 (1987).
[36] J. ZWISLOCKI, M.F. FELDMAN and H. RUBIN, *On the effects of practice and motivation on the threshold of audibility*, J. Acoust. Soc. Am., **30**, 254–262 (1958).

ARCHIVES OF ACOUSTICS
21, 1, 29–36 (1996)

# HARMONIC COMPONENTS OF FINITE AMPLITUDE SOUND WAVES REFLECTED AT A SURFACE

MOSAAD A. FODA

Department of Mechanical Engineering,
King Saud University
(Riyadh, P.O. Box 800, 11421 Saudia Arabia)

The current analysis addresses the reflection of finite amplitude sound waves at a stationary surface. The analysis develops a two-orders perturbation solution for the nonlinear wave equation governing the velocity potential. The expression for the acoustic pressure derived from the potential lacked uniform validity. Hence it was corrected by employing coordinate straining transformations and thereby a uniformly accurate expression was obtained. Then, the strained coordinate transformations are eliminated by a Fourier analysis and a series representation solution is derived.

## 1. Introduction

It has been known for some time that finite amplitude acoustic waves will distort as it propagates [1–2]. This means that many harmonics are progressively generated even if the initial wave is purely monochromatic. The analysis of nonlinear propagation and distortion of finite amplitude acoustic waves has been given much attention in the literature. This is because the role of nonlinearities in generation and propagation of acoustical waves has many practical applications in addition to theoretical interest [3].

The present paper aims at studying the reflection of finite amplitude plane sound waves at a stationary plane target for which the nonlinearities of the medium are sufficient to alter the linear propagation of the waves. These alterations may play an important role in the processes employing acoustic devices using purposely intense sound waves such as devices used in ultrasonic measurements and in medical diagnostics.

If a finite amplitude wave travelling in a homogeneous medium reaches an interface where the properties of the medium change abruptly, various frequency components generated before incidence on the interface might be in part reflected and transmitted. The finite amplitude sound beam generated by a piston source and reflected at a pressure-release surface was investigated experimentally by MELLEN and BROWNING [4]. A pulse technique was used by VAN BUREN and BREAZEALE [5–6] to

measure the propagation and the phase shift reflection. Experimental evidence of the nonlinear effects in the reflection of parametric radiation from a finite planar targets was reported by MUIR *et al.* [7] and by KARABUTOVA *et al.* [8]. GARRETT *et al.* [9] studied theoretically and experimentally the difference frequency wave that generated by the interaction of two finite amplitude primary waves and reflected from finite size planar targets at normal incidence. The propagation of a thin finite amplitude acoustic beam generated by an oscillating piston and its reflection from a plane pressure-release surface was considered by HAMILTON *et al.* [10]. Their analysis used The Kuzentosv' equation in sound pressure, which is the parabolic approximation of the wave equation. The reflected waveform was shown to be different from that of the incident signal.

In this paper we investigate the behaviour of finite amplitude plane sound waves reflected at a stationary surface. This problem has previously been treated by QUAIN [11]. The method applied by him was straight perturbation expansion of Heap's wave equation and, as a consequence, his solution contained secular terms. Apart from this shortcoming, the solution fails to satisfy the boundary condition at a pressure-release surface.

The current investigation treats the reflection of finite amplitude waves at a stationary surface. A regular perturbation expansion is employed to obtain the velocity potential as a solution of the nonlinear wave equation that satisfies the boundary conditions at rigid or pressure-release surface. Only the first two orders of the velocity potential are derived. The first order terms correspond to the linearized field. The terms that represent the cumulative distortional effects of nonlinearities and represent the significant part of the potential are included in the second order terms. The expression for the acoustic pressure that derived from the potential contains secular terms. The method of renormalization is invoked to correct the nonuniform validity by introducing two independent near identity coordinate straining transformations. Further, these transformations are eliminated with the aid of Fourier analysis. Thus a simple expression for the acoustic pressure in terms of the original coordinates is obtained.

## 2. Basic equations

Consider a monochromatic finite amplitude acoustic plane wave impinges on a stationary surface with an impedance possibly depending on the angle of incidence $\theta$ $(0 \leqslant \theta < \pi/2)$. The amplitude of the wave is characterized by a small parameter $\varepsilon$ where $|\varepsilon| \ll 1$ in most practical situations. The subsequent analysis is confined for simplicity to two dimensional waves. The $x$-axis coincides with the surface that is located a t $y=0$-plane. The unit normal $\mathbf{n}_s$, which is pointing outward the surface, is in the direction $\mathbf{e}_y$.

The nonlinear wave equation governing the velocity potential under isentropic conditions in invicid and irrotational fluid motion is [12]

$$c_0^2 \nabla^2 \phi - \frac{\partial^2 \phi}{\partial t^2} = \frac{\partial}{\partial t}\left[\frac{1}{c_0^2}(\beta_0 - 1)\left(\frac{\partial \phi}{\partial t}\right)^2 + \nabla \phi \cdot \nabla \phi\right] + O(\varepsilon^3), \tag{2.1}$$

where $\beta_0$ is the coefficient of nonlinearity and $c_0$ is the small signal speed of sound in linear theory. The fluid velocity is defined such that $\mathbf{v} = \nabla \phi$. Whilst the acoustic pressure is obtained from the Bernoulli equation using the binomial expansion and the fact that $\phi$ is $O(\varepsilon)$. It can be written, valid to the second order, as

$$p = -\rho_0\left[\frac{\partial \phi}{\partial t} + \frac{1}{2}\nabla \phi \cdot \nabla \phi - \frac{1}{2c_0^2}\left(\frac{\partial \phi}{\partial t}\right)^2\right] + O(\varepsilon^3). \tag{2.2}$$

The response must satisfy the appropriate boundary conditions, which depend on the reflectivity of the surface. For a rigid surface, the magnitude of its specific acoustic impedance $|z| \to \infty$ which corresponds to the reflection coefficient $R = 1$. This requires that the component of the fluid velocity normal to the surface vanishes ($\mathbf{v} \cdot \mathbf{n}_s = 0$ at $y = 0$). For the ideal pressure-release reflector $|z| \to 0$, corresponding to $R = -1$. This condition is satisfied when the amplitude of the acoustic pressure vanishes at the surface regardless of the value of the fluid velocity [13].

The velocity potential is expanded in a perturbation series

$$\phi = \varepsilon \phi_1 + \varepsilon^2 \phi_2 + \ldots \tag{2.3}$$

The equation governing $\phi_1$ and $\phi_2$ are obtained by collecting like powers of $\varepsilon$ in Eq. (2.1)

$$c_0^2 \nabla^2 \phi_1 - \frac{\partial^2 \phi_1}{\partial t^2} = 0, \tag{2.4}$$

$$c_0^2 \nabla^2 \phi_2 - \frac{\partial^2 \phi_2}{\partial t^2} = \frac{\partial}{\partial t}\left[\frac{1}{c_0^2}(\beta_0 - 1)\left(\frac{\partial \phi_1}{\partial t}\right)^2 + \nabla \phi_1 \cdot \nabla \phi_1\right]. \tag{2.5}$$

The solution of the first order equation, Eq. (2.4), that satisfies the boundary conditions on either solid or pressure-release surfaces can be written as

$$\phi_1 = \frac{c_0^2}{2\omega}\left[e^{i(\omega t - k_x x + k_y y)} + R e^{i(\omega t - k_x x - k_y y)}\right] + \text{c.c}, \tag{2.6}$$

where $R$ is the pressure amplitude reflection coefficient in linear theory. It can depend on the incident angle $\theta$ as well as the angular frequency $\omega$. Without loss of generality, $R$ is considered to be real. Here c.c denotes the complex conjugate of all preceding terms. The wavenumber components $k_x$ and $k_y$ are found from satisfying the linear wave equation to be

$$k = \frac{\omega}{c_0}, \quad k_x = (k^2 - k_y^2)^{1/2} \equiv k \sin\theta, \quad k_y = k \cos\theta. \tag{2.7}$$

### 3. Description of the second order potential

The substitution of the first order solution $\phi_1$ given by Eq. (2.6) into the right hand side of Eq. (2.5) yields the inhomogeneous equation for $\phi_2$

$$\nabla^2\phi_2-\frac{1}{c_0^2}\frac{\partial^2\phi_2}{\partial t^2}=-\frac{i\omega}{2}\left[\beta_0 e^{2i(\omega t-\psi_1)}+\beta_0 R^2 e^{2i(\omega t-\psi_2)}+\right.$$
$$\left.+\frac{4k_y^2 R}{k^2}\left(\frac{\beta_0 k^2}{2k_y^2}-1\right)e^{i(2\omega t-\psi_1-\psi_2)}\right]+\text{c.c}, \tag{3.1}$$

where

$$\psi_1=k_x x-k_y y\,,$$
$$\psi_2=k_x x+k_y y\,. \tag{3.2}$$

The first two inhomogeneous terms on the right hand side of Eq. (3.1) are the result of self-action of the incident and of the reflected waves respectively. They excite the second harmonics of the corresponding waves. Such signals propagate parallel to the corresponding waves forming $\phi_1$. The third inhomogeneous term is due to the nonlinear interaction of the incident and the reflected waves. It is independent of $y$ since $\psi_1+\psi_2=2k_x x$. Therefore it excites a second harmonic wave whose propagation direction is parallel to the surface.

The solution of Eq. (3.1) consists of the complementary solution and the particular solution. The form of the right hand side of Eq. (3.1) suggests that the later solution is the superposition of the solutions associated with each of these inhomogeneous terms. These solutions may be found by the aid of the variation of parameters method. To this end one lets

$$\phi_2^p=C_1(y)e^{2i(\omega t-\psi_1)}+C_2(y)\,e^{2i(\omega t-\psi_2)}+C_3(x)\,e^{i(2\omega t-\psi_1-\psi_2)}+\text{c.c.} \tag{3.3}$$

The result of requiring that Eq. (3.3) satisfies Eq. (3.1) is a set of uncoupled differential equations for the unknown amplitude functions $C_j$. Making use of Eq. (3.2) these equations are found to be

$$C_1''+4ik_y C_1'=-\frac{i}{2}\omega\beta_0\,,$$
$$C_2''-4ik_y C_2'=-\frac{i}{2}\omega\beta_0 R^2\,, \tag{3.4}$$
$$C_3''-4k_y^2 C_3=-2i\omega R\frac{k_y^2}{k^2}\left(\frac{k^2\beta_0}{2k_y^2}-1\right),$$

The prime identifies differentiation with respect to the argument.

Without much analysis, one may solve Eqs. (3.4) and form the particular solution according to Eq. (3.3). Then, of course, one adds the complementary solution and requires that the total solution must satisfy the boundary conditions for a solid surface as well as for a pressure-release surface, and thereby chooses the arbitrary constants contained in the complementary solution. After performing these steps, one thus combines the resulting expression for $\phi_2$ with the linearized solution given by Eq. (2.6) to arrive at the following expression for the potential

$$\phi=\varepsilon\frac{c_0^2}{2\omega}\left[e^{i(\omega t-\psi_1)}+Re^{i(\omega t-\psi_2)}\right]-$$

$$-\varepsilon^2\frac{c_0^2}{8\omega}\left\{\frac{k^2\beta_0 y}{k_y}\left[e^{2i(\omega t-\psi_1)}-R^2e^{2i(\omega t-\psi_2)}\right]+\right.$$

$$\left.+\frac{iRk_y^2}{k^2}\left[2(\mu-1)\,e^{i(2\omega t-\psi_1-\psi_2)}-\mu e^{2i(\omega t-\psi_1)}-\mu e^{2i(\omega t-\psi_2)}+2i\omega t\right]\right\}+\text{c.c}+O(\varepsilon^3), \tag{3.5}$$

where

$$\mu=\frac{2k^2}{k_y^2}\left(\frac{\beta_0 k^2}{2k_y^2}-1\right)+1. \tag{3.6}$$

The potential functions given by Eq. (3.5) contain secular terms and, consequently, the resulting expressions for the acoustic pressure and the velocity components will not be uniform. NAYFEH and KLUWICK [14] and GINSBERG [15] have proved that the secular terms should be removed from the physical response variables such as acoustic pressure and velocity components, because the potential does indeed contain growing terms and an analysis that removes such terms is therefore conceptually in error. Accordingly, the method of renormalization will be applied to the acoustic pressure.

## 4. Application of the renormalization method

The acoustic pressure is linked to the potential by Eq. (2.2). The quadratic products in that relation will introduce non-secular terms. Thus differentiating Eq. (3.5) yields

$$\frac{p}{\rho_0 c_0^2}=\frac{\varepsilon}{2i}\left[e^{i(\omega t-\psi_1)}+Re^{i(\omega t-\psi_2)}\right]-$$

$$-\frac{\varepsilon^2}{4}\left\{\frac{\beta_0 k^2 y}{ik_y}\left[e^{2i(\omega t-\psi_1)}-R^2e^{2i(\omega t-\psi_2)}\right]-\right. \tag{4.1}$$

$$-\frac{k_y^2 R\mu}{k^2}\left[e^{2i(\omega t-\psi_1)}+e^{2i(\omega t-\psi_2)}-2e^{i(2\omega t-\psi_1-\psi_2)}+\right.$$
$$\left.+\frac{2}{\mu}(e^{i(\psi_1-\psi_2)}-1]\right\}+\text{c.c}+O(\varepsilon^3)\,. \tag{4.1}$$
[cont.]

Inspection of Eq. (4.1) shows that at $O(\varepsilon^3)$ the first set of terms represents the sound in the second harmonics of the incident and of the reflected signals, respectively. The amplitude of each signal grows linearly with increasing $y$ (secular behaviour). In contrast, the amplitude of the last set of terms remains bounded at all locations and these terms represent local effects. This means that the cumulative distortion only originates from the self-action of the incident and of the reflected waves.

In order to eliminate the secular terms which produce the nonuniformity in the expansion given by Eq. (4.1) the renormalization version of the method of strained coordinates is employed [16]. Different transformation is introduced for each of the wave variable $\psi_j$, $j=1, 2$. Further examination of Eq. (4.1) suggests that the trial transformations are

$$\psi_j=\alpha_j+\varepsilon[F_j e^{i(\omega_j t-\alpha_j)}+\text{c.c}], \quad j=1, 2, \tag{4.2}$$

where the complex conjugate term is introduced to ensure that each transformation is real.

The aforementioned transformations are substituted into Eq. (4.1) and the result is expanded in a Taylor series in ascending powers of $\varepsilon$. Then the functions $F_j$ are selected on the basis of removing the second order secular terms. This procedure yields the following expression for the acoustic pressure in real functional forms after accounting for the complex conjugate of each term

$$\frac{p}{\rho_0 c_0^2}=\varepsilon[\sin(\omega t-\alpha_1)+R\sin(\omega t-\alpha_2)]+p_{Ns}+O(\varepsilon^3)\,, \tag{4.3}$$

where

$$p_{Ns}=-\varepsilon^2\frac{k_y^2 R}{k^2}\{\mu[1-\cos(2k_y y)]\cos(2\omega t-2k_x x)+1\}\,. \tag{4.4}$$

The coordinate transformation are given by

$$\psi_1=\alpha_1-\varepsilon c\sin(\omega t-\alpha_1)\,,$$
$$\psi_2=\alpha_2+\varepsilon R c\sin(\omega t-\alpha_2)\,, \tag{4.5}$$

where

$$c=\frac{\beta_0 k^2 y}{k_y}\,.$$

Equations (4.3) and (4.5) reveal that the response consists of two non-interactive waves, each is reminiscent of that for a planar wave with an important exception. The linear effect is measured by the difference between the nonlinear and linear spatial phases $\alpha_j - \psi_j$. In an isolated planar wave, this difference is proportional to the propagation distance which would be $(k_x x \pm k_y y)/k$ for the oblique wave. Instead, the distance parameter for each wave in Eq. (4.3) is $ky/k_y$. Therefore, it is to be concluded that although Eq. (4.3) specify a superposition of two waves, the response of one affects the other by altering the spatial dependence for the difference $\alpha_j - \psi_j$.

To this end, calculating the acoustic pressure at set of values $(x, y, t)$ requires solution of each of the transcendental equations for the coordinate straining transformations, given by Eqs. (4.5). This can be accomplished by using a numerical procedure such as the Newton-Raphson's method. The frequency content of the temporal pressure waveform may be evaluated from its spectral analysis. However, with the aid of Fourier analysis, the acoustic pressure can be expressed in terms of the physical coordinates to avoide the solution of the transcendental equations for the coordinate transformations. The procedures are similar to that used in [17–18] and will not be repeated here. Specifically, the series representations for the acoustic pressure is

$$\frac{p}{\rho_0 c_0^2} = \frac{2}{c} \sum_{m=1}^{\infty} \left\{ \frac{(-1)^{m-1}}{m} J_m(\varepsilon mc) \sin[m(\omega t - \psi_1)] + \right.$$
$$\left. + \frac{1}{m} J_m(\varepsilon Rmc) \sin[m(\omega t - \psi_2)] \right\} + p_{Ns} + O(\varepsilon^3), \tag{4.6}$$

where $J_m$ are the Bessel functions of first kind of order $m$.

The Fourier series solution given by Eq. (4.6) is analogous to the FUBINI-GHIRON [19] representation of a planar wave. It is valid if no shock forms. This occurs at distances less than the first location where multivaluedness of the waveform occurs. From Eq. (4.6) it is seen that each of the individual Fourier harmonics will undergo the same phase shift. This was noted experimentally by previous investigators [4–6].

## 5. Conclusion

The reflection of finite amplitude planar waves at a rigid or a pressure-release surface is investigated. The reflection takes place as though there were no coupling among harmonics. The nonlinear interaction between the incident and the reflected waves results in a wave with propagation direction that is parallel to the plane surface no matter what the incident angle is. It represents a local effect. In other words, it has no contribution to the distortion process. As a corollary, the cumulative distortion originates only from the self-action of the incident and of the reflected waves.

## References


[1] D.T. BLACKSTOCK, *On plane, spherical and cylindrical waves of finite amplitude in lossles fluid*, J. Acoust. Soc. Amer., **36**, 1, 217–219 (1964).

[2] D.T. BLACKSTOCK, *Propagation of plane sound waves of finite amplitude in nondissipative fluids*, J. Acoust. Soc. Amer., **34**, 1, 9–30 (1962).

[3] L. BJORNO, *Undewater applications of nonlinear ultrasound*, [in:] Ultrasonics Int. 1975 conf. Proc., IPC Science and Technlogy, London (1975).

[4] R.H. MELLEN and D.G. BROWNING, *Reflection from a plane pressure-release surface*, J. Acoust. Soc. Amer., **44**, 2, 646–647 (1968).

[5] A.L. VAN BUREN and M.A. BREAZEALE, *Reflection of finite-amplitude ultrasonic waves. I. Phase shift*, J. Acoust. Soc. Amer., **44**, 4, 1014–1020 (1968).

[6] A.L. VAN BUREN and M.A. BREAZEALE, *Reflection of finite-amplitude ultrasonic waves. II. Propagation*, J. Acoust. Soc. Amer., **44**, 4, 1021–1027 (1968).

[7] T.G. MUIR, L.L. MELLENBRUCH and J.C. LOCKWOOD, *Reflection of finite amplitude waves in a parametri array*, J. Acoust. Soc. Amer., **62**, 5, 271–276 (1977).

[8] N.E. KARABUTOVA, B.K. NOVIKOV and S.P. TARASOV, *Behaviour of the characteristics of a parametric radiator in the presence of a reflecting boundary*, Sov. Phys. Acoust. **27**, 223–226 (1981).

[9] G.S. GARRETT, J.N. TJOTTA, R.L. ROLLEIGH and S. TJOTTA, *Reflection of parametric radiation from a finite target*, J. Acoust. Soc. Amer., **75**, 5, 1462–1072 (1984).

[10] M.F. HAMILTON, J.N. TJOTTA and S. TJOTTA, *Propagation and reflection of finite amplitude sound beams*, Proceedings, 12th International Congress on Acoustics, Vol. 3, Toronto, Canada, 1986, p. 12–4.

[11] Z.W. QIAN, *Reflection of finite amplitude sound wave on a plane boundary of half space* (II), Fortschritte. der Akustik FASE/DAGA'82, 1982, pp. 821–824.

[12] S. GOLDSTEIN, *Lectures in fluid mechanics*, Wiley-Interscience, New York 1960, ch. 4.

[13] A.D. PIERCE, *Acoustics: An introduction to its physical principles and applieations*, McGraw Hill, New York 1981, Ch. 3.

[14] A.H. NAYFEH and A. KLUWICK, *A comparison of three perturbation methods for non-linear waves*, J. Sound. Vig. **48**, 2, 293–299 (1976).

[15] J.H. GINSBERG, *A re-examination of non-linear interaction between an acoustic fluid and a flat plate undergoing harmonic excitation*, J. Sound. Vig. **60**, 3, 449–458 (1978).

[16] A.H. NAYFEH, *Introduction to perturbation techniques*, Wiley-Interscience, New York 1981.

[17] M.A. FODA, *Uniformly accurate expressions for sound waves induced by a vibrating planar boundary*, Acoustica, **73**, 254–263 (1991).

[18] M.A. FODA, *Analysis of nonlinear propagation of waves induced by a vibrating flat plate*, Acoustica, **72**, 118–130 (1990).

[19] E. FUBINI-GHIRON, *Anomalies in acoustic wave propagation of large amplitude*, Alta. Freq. **4**, 530–581 (1935).

ARCHIVES OF ACOUSTICS
21, 1, 37–51 (1996)

# MEASUREMENT TECHNIQUE OF SHOCK WAVE PULSES AT EXTREMELY HIGH PRESSURES

L. FILIPCZYŃSKI, J. ETIENNE, G. ŁYPACEWICZ, T. WASZCZUK

Department of Ultrasound, Institute of Fundamental Technological Research,
Polish Academy of Sciences
(00-049 Warsaw, 21 Świętokrzyska Street)

Two methods were developed for measuring the pressure of shock wave pulses generated by lithotriptors: with a piezoelectric foil transducer and a capacitance one. In the study, the properties of a PVDF type foil transducer working in water were analysed. Its sensitivity was determined as a function of frequency. Compliance was gained between measurements and theory. The impacts of fixed metal electrodes, an additional back plastic load and an electric load on the frequency responses were shown. The principle and various design alternatives of a capacitance transducer designed for measuring the extremely high pressure of shock wave pulses in water were presented. A transducer of this type makes it possible to perform absolute measurements. After implementation, the two transducer types were applied for measuring purposes. Their advantages and disadvantages were shown. The pressure of shock wave pulses measured on this basis in a domestic and a foreign lithotriptors were found to be very close to each other. The pulse rise times were approximately the same for the two devices compared.

## 1. Introduction

The lithotriptor model designed for noninvasive disintegration of renal calculi required above all the development of methods for measuring shock wave pulses the peak pressure of which in amplitude may reach values of about 100 MPa ($\cong$ 100 atm.) and the rise times are a fraction of a microsecond. Because, for obvious reasons, measurements of these pulses are impossible "in situ", they are made in water the acoustic impedance of which is practically the same as that of soft human tissues, although attenuation is different [6].

As studies began on the subject there was no system anywhere permitting measurements of this type to be carried out. Conventional hydrophones applied in underwater acoustics are not suitable for measuring such high pressures, for they disintegrate immediately, just as do renal calculi. At present, expensive piezoelectric foil hydrophones sporadically used for this purpose are quickly destroyed even after a few minutes of work.

In this situation, a decision was taken by the authors to develop their own methods for measuring the extremely high pressures of shock wave pulses based on two transducer types: piezoelectric foil and capacitance transducers.

## 2. Piezoelectric foil transducers

In lithotripsy problems, it is necessary to carry out measurements over a high ultrasound frequency range caused by very short rise times of shock wave pulses. Piezoelectric plastic foil transducers, e.g., of PVDF (polyvinyldifluoride), provide such a possibility [11], although they show small nonlinearity of about 5% for high pressures of 80 MPa [12]. The basic parameters of such a transducer are shown in Table 1 as compared with those of a quartz one.

**Table 1.** A comparison of the properties of PVDF and quartz transducers

| Material | Multiplier | | Quartz, $x$-cut, [3], [8] | PVDF transducer [12] |
|---|---|---|---|---|
| 1. Density | $\rho$ | $10^3$ kg/m$^3$ | 2.65 | 1.8 |
| 2. Dielectric constant | $\varepsilon$ | 1 | $\varepsilon_1^T=4.5$ | $\varepsilon_1^T=5.2$ |
| 3. Longitudinal wave velocity | $c$ | $10^3$ m/s | $c^E=5.74$ | $c=2.15$ |
| 4. Acoustic impedance | $\rho c$ | $10^6$ kg/m$^2$s | $\rho c^E=15.4$ | $\rho c=3.86$ |
| 5. Piezoelectric coefficient | $h$ | $10^9$ N/C | $h_{11}=4.2$ | $h_{11}=2.08$ |
| 6. Electromechanical coupling coefficient for thickness vibration | $k$ | 1 | 0.1 | 0.15* |

* Determined by authors after [12]

The frequency response of a PVDF transducer developed in cooperation with the Limburg University in Maastricht may now be considered. It has an active diameter of 0.5 mm and the piezoelectric foils is 25 μm thick. Electrodes were fixed using a very thin gold layer. The electroacoustic properties of the transducer can be determined from Mason's equivalent circuit [10], [7], derived for one-dimensional, longitudinal vibrations and an electric field with the same direction (Fig. 1). This scheme will be expanded in an appropriate way so as to account for the impact of metal electrodes [9] and that of internal foil damping [1]. It is assumed that this transducer is a linear element. The wave source is adopted in the form of the generator of the force $2F$ with internal impedance such as for water, i.e. $R_A=\rho_A c_A A=0.294$ kgs$^{-1}$. Here, $F$ is the force and $A=19.6\times10^{-8}$ m$^2$ is the active surface area of the transducer. The value of the generator force results from THEVENIN's theorem [13], [14], according to which in a linear system the electromotor force of the source is equal to the voltage at open output clamps, whereas the internal resistance of the source is equal to the resistance measured at clamps at a shorted source.

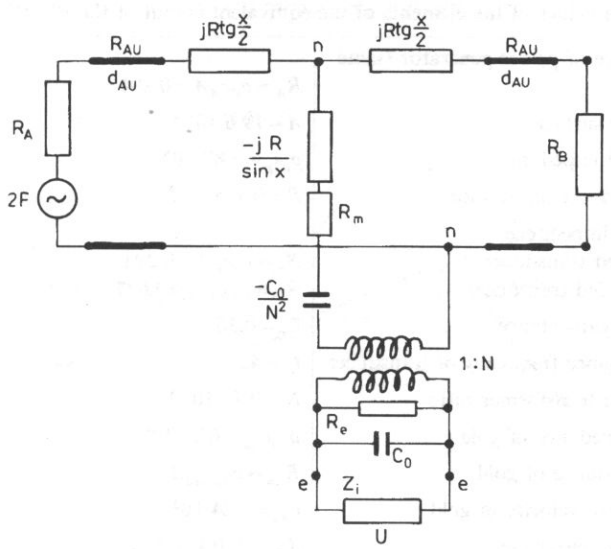


Fig. 1. The equivalent circuit of a transducer, according to Mason, expanded with metal electrode layers in the form of long lines and the internal foil damping in the form of the resistances $R_m$ and $R_e$. The source of the incident wave has the form of a generator of the electromotor force 2 F with the internal resistance $R_A$.

The mechanical impedance $R$ and the electrical impedance $Z$ can can be transformed by an electromechanical transformer (Fig. 1), according to the relation

$$R\,[\mathrm{kg\,s^{-1}}] = N^2 Z\,[\mathrm{m^2 kg\,s^{-3}\,A}], \tag{2.1}$$

where A is amper.

On the other hand, the force $F$, the electrical voltage $U$, the velocity $V$ and the current $I$ are transformed according to the relation

$$\begin{aligned} F\,[\mathrm{kg\,m\,s^{-2}}] &= N\,U\,[\mathrm{m^2 kg\,s^{-3}}\,I\,\mathrm{A^{-1}}], \\ V\,[\mathrm{m\,s^{-1}}] &= N^{-1}\,[\mathrm{A}], \end{aligned} \tag{2.2}$$

where electromechanical transformer ratio has the form

$$N = h\,C_0\,[\mathrm{s\,A\,m^{-1}}]. \tag{2.3}$$

By solving the circuit in Fig. 1 and applying dependencies (2.1), (2.2) and (2.3), the following relation can be obtained between the output voltage signal $U$ at the electrical clamps of the transducer and the force $F$

$$U/F = \frac{2bNZ}{a\left[R_B + jR\left(\operatorname{tg}\frac{x}{2} - \frac{1}{\sin x}\right) + \frac{jN^2}{2xf_m C_0} + ZN^2\right] + b\left[\frac{jN^2}{2xf_m C_0} - \frac{R}{\sin x} + ZN^2\right]}, \tag{2.4}$$

**Table 2.** The values of the elements of the equivalent circuit of the PVDF transducer

| | | |
|---|---|---|
| 1. Internal impedance of power generator (same as for water) | $R_A=\rho_A c_A A=0.294$ | kg/s |
| 2. Active transducer surface | $A=19.6\ 10^{-8}$ | $m^2$ |
| 3. Characteristic foil impedance | $\rho_p c_p=3.87\ 10^6$ | $kg/m^2s$ |
| 4. Mechanical transducer impedance | $R=0.758$ | kg/s |
| 5. Mechanical back impedance | | |
| — of water loaded transducer | $R_B=\rho_B c_B A=0.294$ | kg/s |
| — of plastics loaded transducer | $R_{B'}=\rho_{B'} c_{B'} A=0.627$ | kg/s |
| 6. Static transducer capacitance | $C_0=0.36$ | pF |
| 7. Mechanical resonance frequency of transducer | $f_m=43$ | MHz |
| 8. Electromechanical transformer ratio | $N=0.75\ 10^{-3}$ | sA/m |
| 9. Characteristic impedance of gold | $\rho_{Au} c_{Au}=62.5\ 10^6$ | $kg/m^2s$ |
| 10 Mechanical impedance of gold | $R_{Au}=\rho_{Au} c_{Au} A$ | kg/s |
| 11. Longitudinal wave velocity in gold | $c_{Au}=3.24\ 10^3$ | m/s |
| 12. Thickness of gold electrodes | $d_{Au}=0,\ 0.1,\ 0.5,\ 1$ | μm |
| 13. Resistance of mechanical losses inside foil $R_m=W_m R\tan\delta_m$ (see [1] and [9] formula (11)) | $\mathrm{tg}\delta_m=0.1$ | |
| 14. Resistance of dielectric losses inside foil $R_e=(\omega C_0)^{-1}\tan\delta_e$ | $\mathrm{tg}\delta_e=0.1$ | |

where $a=R_A+jR\tan x/2$, $b=R_B+jR\tan x/2$ (see Table 2), $Z=Z_i/(1+jZ_i 2xf_m C_0)$, $Z_i$ is the electrical impedance loading the transducer, $C_0$ is the static capacitance of the transducer, $x=nf/f_m$, $f$ is the current frequency, $f_m$ is the mechanical resonance frequency of the transducer. When on both sides of the transducer there is the same medium ($R_A=R_B$), formula (2.4) becomes greatly simplified.

In the further calculations for the PVDF transducer, Mason's equivalent circuit will be expanded to include thin gold layers in the form of two long lines with the impedance $R_{Au}$ and the thickness $d_{Au}$, and the mechanical and dielectric losses inside the foil, represented by the resistances $R_m$ and $R_e$. The values of the parameters of the expanded circuit in Fig. 1 are listed in Table 2.

In numerical calculations, purpose-built programmes were applied in calculations for piezoelectric transducers used to generate and receive ultrasound pulses [9].

Figure 2 shows the calculated sensitivity of the PVDF transducer for different electric loads, based on the equivalent circuit in Fig. 1, accounting for the thin bilateral gold electrode layers with different thickness. For all the cases demonstrated, the load at electrical clamps was adopted in the form of capacitance of 130 pF.

A lossless transducer, bilaterally loaded by water, with a thin gold layer of zero thickness ($H_2O$, 0 μm) and with no internal losses (dashed curve), shows electrical resonance at a frequency of $\cong$ 40 MHz. In keeping with theory, this frequency is lower than the mechanical frequency of 43 MHz [7].

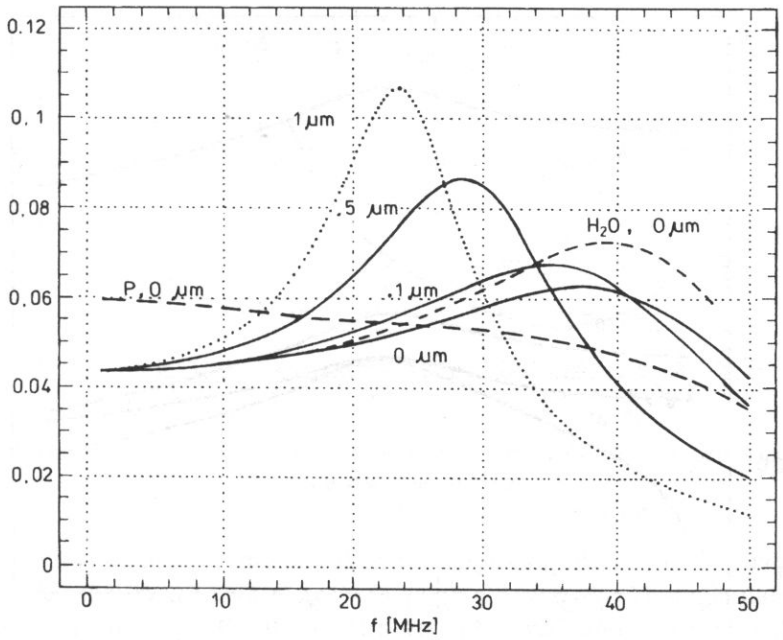


Fig. 2. The sensitivity characteristics of a PVDF transducer loaded by 130 pF capacitance, calculated without internal losses (dashed curves) in the case of bilateral water ($H_2O$) loading and additional plastic back load (*P*). The solid curve denotes the characteristics, taking into account internal damping. The thicknesses of gold electrodes are given along all the curves.

When the back surface of the transducer is loaded by plastics (P, 0 μm), its resonance peak becomes blurred and the 3 dB transmission band expands by a factor of about 1.5. When internal losses in foil are introduced (solid curves), the curve ($H_2O$, 0 μm) turns into the curve (0 μm) which is lower only by about 0.7 dB at the resonance frequency, it does not change at the lowest frequency.

It is interesting to observe the response as the thickness of the gold electrodes grows. In this case, the frequency of the electrical resonance distinctly decreases, by as much as a factor of 0.65 for 1 μm layer thickness. It is a very important conclusion from the point of view of the design of the PVDF transducer, to which no attention has been paid to date in the literature.

Figure 3 shows the frequency responses of the PVDF transducer calculated for different electrical load types in the case of 1 μm thick gold electrodes. The real load with 50 Ω resistance fully distorts the response, making the transducer useless for measuring purposes. The capacitance load, on the other hand, makes is possible to obtain a plane response, ensuring high-fidelity representation of the measured shape of the shock wave pulse. In the present experimental study, electrical clamps were connected with an amplifier with 30 dB amplification. The capacitance of the cable was 130 pF. When it is cut down to, e.g., 50 pF, the sensitivity of the transducer grows

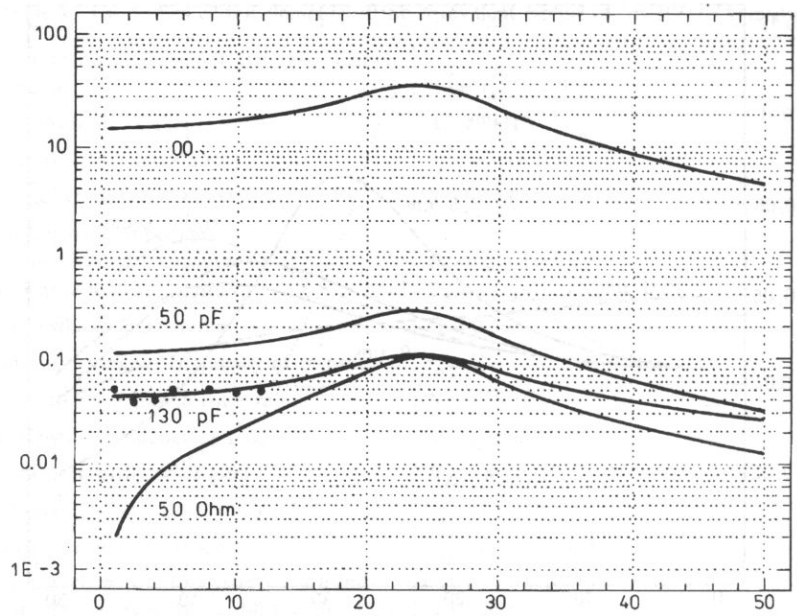


Fig. 3. The sensitivity characteristics of a PVDF transducer calculated for bilateral loading with water, with gold electrode thickness of 1 μm. The electrical loads were 50 Ω, 130 pF and 50 pF, and was equal to ∞.

2.5 times. In the extreme case of opening electrical clamps ($z_i = \infty$), the sensitivity grows by another 125 times. Such a case is, however, practicaly impossible to implement.

The experimental results (the points in Fig. 3), obtained by calibration using a hydrophone manufactures by Marconi Company [11], showed good compliance with the theoretical curve. The capacitance $C_k = 130$ pF was used in the measurements, providing the mean sensitivity of the transducer in question of 0.018 μV/Pa. In this case, the upper cut-off frequency (within the 3 dB limits) was 15 MHz. The lower one was, on the other hand, limited by the plane nature of the wave.

The experimentally confirmed flat sensitivity curve over the range up to 12 MHz is completely sufficient for high-fidelity representation of the shape of the shock wave pressure pulse (see the pulse spectrum in Fig. 6).

Figure 4 shows the shape of a shock wave pulse with a pressure peak of 20 MPa, measured in water, using a PVDF transducer. This pulse was obtained using an electromagnetic generator involving the use of a plastic shock wave focussing lens [4]. The pulse rise time was about 100 ns.

A further increase in the upper cut-off frequency of the PVDF transducer can be obtained by applying an additional acoustic load of its back surface with plastics (Fig. 2, curve *P*). Because of the thickness of the material loading the back surface of the transducer, however, the duration of the measured pluse is limited up to 7 μs in the case of a 1 cm thick plastic layer.

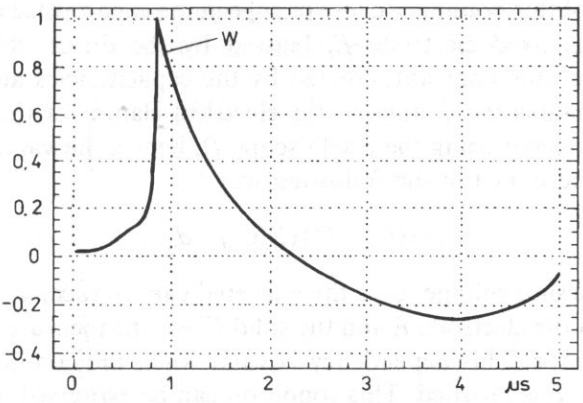


Fig. 4. The shock wave pulse shape obtained by the authors using a PVDF transducer with the positive peak pressure of 20 MPa.

In the course of measurements taken for large-amplitude shock wave pulses, it was found that the PVDF transducer was quickly destroyed. These damages were of the cavitation-incited type. Point pinholes were observed, and so were breakdowns in the gold electrodes and in the PVDF foil itself.

Given this, a decision was made to use a transducer of this type only in single, most important measurements. A capacitance transducer was developed for "mass" measurements. For, an advantage of an PVDF transducer is the accurate representation of the shape of the acoustic pressure; both in its rise phase and its drop as a function of time. In this range, a capacitance transducer shows some limitations.

### 3. The capacitance method for measuring shock wave pressures

Figure 5 shows the idea of a transducer which measures the absolute value of plane wave displacement in water [2]. The plane wave pulse $P$ penetrates the water-solid, $W-F$, boundary. Then, it is totally reflected from the solid-air boundary

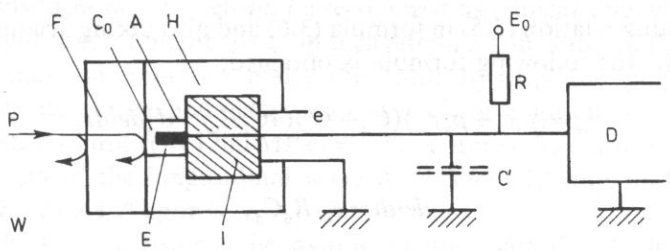


Fig. 5. The principle of the measuring capacitance transducer. $P$— incident wave pulse, $F$— solid, $W$ — water, $A$ — air, $I$ — insulator, $C_0$ — electrode capacitance, $C'$ — scattered capacitances, $E_0$ — biassing voltage, $R$ — resistor, $D$ — calibrated digital oscilloscope.

*A*. The vibrations of this boundary cause change in the capacitance $C_0$, created by this boundary, and the fixed electrode $E$, biassed by the direct voltage $E_0$. For an appropriately large time constant, created by the capacitancies and resistance $R$ in this circuit, one obtains the voltage at the electrical clamps of the transducer. This voltage is then measured using the oscilloscope $D$, hence, the value of the measured displacement is determined in the following way:

$$\zeta=(C_0+C')(E_0C_0)^{-1}d_0e, \tag{3.1}$$

where $E_0$ is the biassing voltage, $C'$ is the scattered capacitance, $d_0$ is the thickness of the air slit between the electrode $E$ and the solid $F$, $e$ is the measured voltage signal at the transducer clamps. This dependency is valid when the condition that $\zeta$ is very much smaller than $d_0$ is satisfied. This condition can be expressed in a different way:

$$e(C_0+C')(E_0C_0)^{-1}\ll 1. \tag{3.2}$$

After differentiation relative to time, the partial velocity can be obtained from formula (3.1):

$$u_g=d\zeta/dt. \tag{3.3}$$

on the solid-air boundary. There is the following relation between the pressure $p_w$ of the measured plane wave, incident perpendicularly onto the water-solid boundary and the wave pressure $p_s$ penetrating this boundary and going on:

$$p_s/p_w=2\rho_sc_s/(\rho_wc_w+\rho_sc_s), \tag{3.4}$$

where $\rho_sc_s$ and $\rho_wc_w$ are, respectively, the acoustic impedances of the solid and water.

Therefore, using dependence (3.4), the partial wave velocity in a solid medium is

$$u_s=p_s/\rho_sc_s=2(\rho_wc_w+\rho_sc_s)^{-1}p_w. \tag{3.5}$$

In turn, on the solid-air boundary there is perfect backscattering of a wave pulse and the partial velocity $u_s$ at this boundary doubles. Thus,

$$u_g=2u_s. \tag{3.6}$$

By substituting relation (3.5) in formula (3.6) and also taking account of (3.3) and (3.1), ultimately, the following formula is obtained:

$$p_w=(\rho_sc_s+\rho_wc_w)(C_0+C')(4C_0E_0)^{-1}d_0de/dt, \tag{3.7}$$

where

$$de/dt=e_d/R_dC_d, \tag{3.8}$$

$e_d$ is the electrical voltage measured at the output of an additional differentiating system with the time constant $R_dC_d\ll 1/\omega$, where $\omega$ is the maximum angular frequency in the spectrum of the measured pulse.

The shape of the shock wave pulse measured in water using a PVDF transducer is shown in Fig. 4, whereas the spectrum of this pulse is demonstrated in Fig. 6.

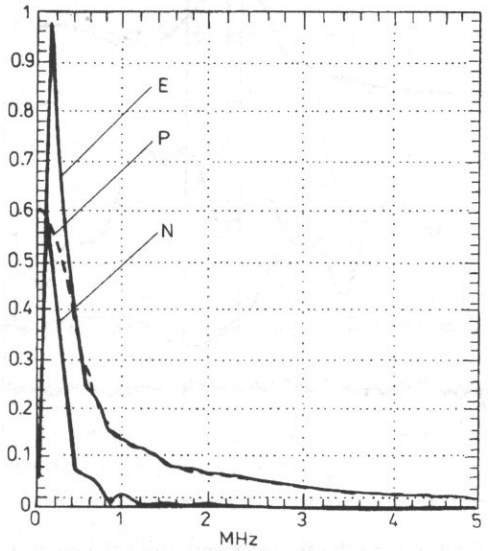


Fig. 6. The amplitude spectrum of a shock wave pulse measured using a PVDF transducer (see Fig. 4). $E$ — spectrum of the whole pulse, $P$ — of its positive part, $N$ — of its negative part.

In deriving formula (3.7) a linear dependency was assumed between the acoustic pressure and the partial velocity, which is satisfied with appropriate approximation. Moreover, it is necessary to account for the fact that water is a medium which is more nonlinear than a solid out of which the front plate is made.

The ratio between the acoustic pressure and the partial plane wave velocity as well as its deviation from the acoustic impedance for a given value of the acoustic pressure may be regarded as a measure of medium linearity. These deviations for water and soft tissues are, for $p=100$ MPa, respectively, smaller than 7% and 12%, on the other hand, for steel and aluminium they are smaller by three orders of magnitude [5]. A capitance transducer can, therefore, be recognized as a linear one, which does not introduce any additional nonlinearities in measurements in water and soft tissues.

Following many attempts to make the front hydrophone plate from such materials as steel, aluminium and plastics, it was made of titanium and showed a high value of the elasticity limit $R_r=1200$ MPa ($\cong 120$ kg/mm$^2$). Its density is $\rho=4.5\times10^3$ kg/m$^3$, the velocity of the longitudinal wave is $c=5.99\times10^3$ m/s and the acoustic impedance is $\rho c=27\times10^6$ kg/m$^2$s.

Figure 7 shows a registered behaviour of the partial velocity $u$ and the displacement $\gamma$ as a function of time for a shock wave with an amplitude of about 20 MPa ($\cong 200$ atm.). What is most important here is the 3 μs time interval after a cross-shaped marker. After this time there emerge multiple wave reflections within

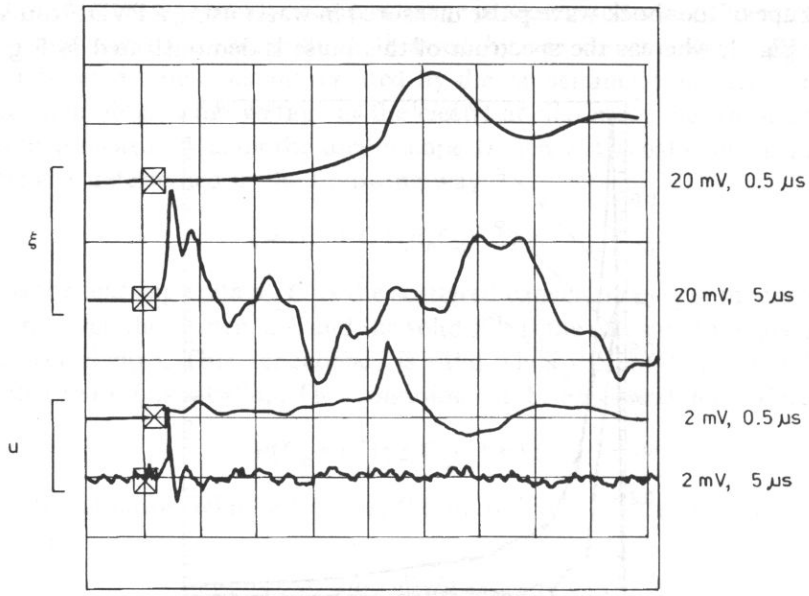


Fig. 7. The partial velocity $u$ (bottom) and the displacement $\gamma$ (top) of a shock wave pulse with an amplitude of 20 MPa, registered using a capacitance transducer in two time scales. The horizontal scale corresponds to time intervals of 5 μs and 0.5 μs; and the vertical scale corresponds to voltages of 2 mV and 20 mV.

the transducer which interfere with one another. The upper course which represents the partial velocity has been obtained by electronic differentiation of the lower curve denoting the displacement.

The same figure shows the partial velocity pluse $u$ extended in time by a factor of ten and detected in conditions close to those in Fig. 4. Here, the rise gain time is 50 ns. Probably, this time is shorter, however, the sampling interval of the applied digital oscilloscope Tektronix 2230, 50 ns, limits the possibilities of measuring shorter rise times.

In the case of a focussed wave, the use of the transducer in the form represented in Fig. 5 may lead to distortions as a result of the refraction of the wave on the water-solid body boundary because of the different wave velocities in these media. In the case of a focussed beam, this may cause a change in the position of the focus and its defocussing (Fig. 8a). Therefore, it would be desirable to use a solid with a possibly lowest velocity of the longitudinal wave so as to minimize the refraction.

A semicircular front surface (Fig. 8b) may also be used. Then, however, the transducer cannot be used for absolute measurements. For in its front plate there emergies a focus with a greater longitudinal dimension than in water because of the longer wavelength in solid media. Therefore, there occur a different beam concentration and a lower maximum pressure than in water. Hence, a practical conclusion follows. The wave refraction may be avoided by taking measurements in the focus of

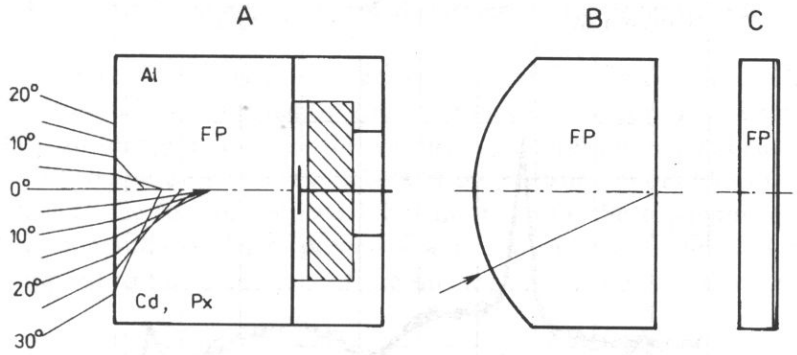


Fig. 8. Different versions of capacitance transducers. A — with a thick front plate (*FP*), from aluminium (Al), cadmium (Cd) or plastics (Px). The refraction of acoustic rays on the water-front plate boundary is shown. The critical angle for Al is 15° and for Cd or Px it is 33°. B — semicircular front plate, C — thin, flat front plate from Al, Cd or Px, coated with the conducting layer (*L*).

the shock wave, where the beam is practically plane, using at the same time a 1 cm thick front plate (Fig. 8c). In the present case, the plane range of this wave in the focus is much longer, considering the measured pressure drop relative to the maximum pressure in the focus itself (cf. Fig. 9).

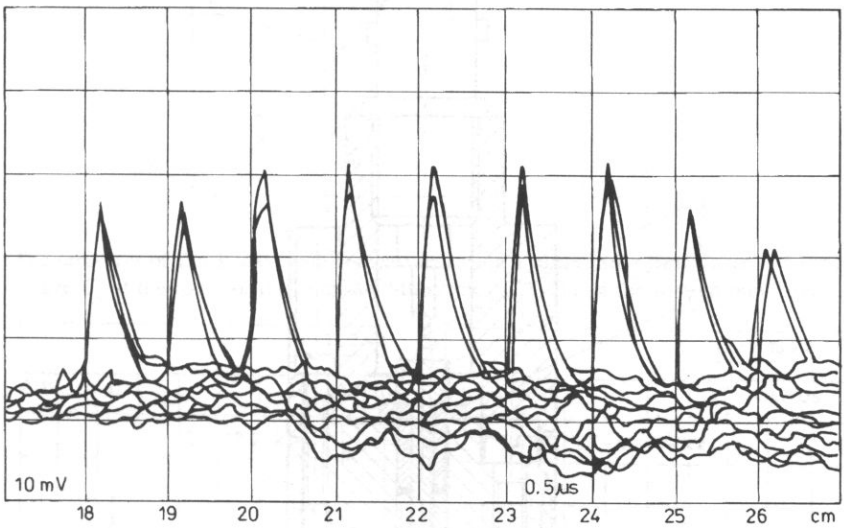


Fig. 9. The acoustic pressure distribution along the beam axis of the authors' lithotriptor, measured within the focal area.

Figure 10 indicates the repeatibility of the measured results gained using the present capacitance transducer. It shows the results of ten measurements of the same shock wave pulse registered on the oscilloscope screen.

Then, Fig. 11 shows the design drawing of the capacitance transducer in question, used for measuring the pressure of shock wave pulses.

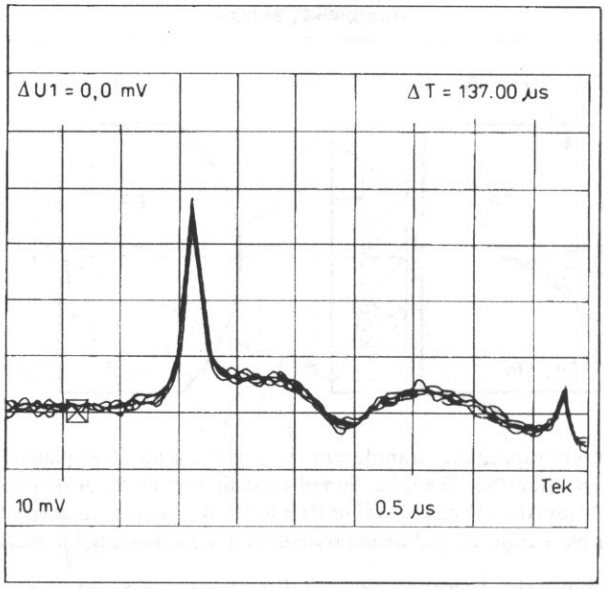


Fig. 10. The recordings of ten shock wave pulses using the capacitance transducer, on the same oscilloscope image.

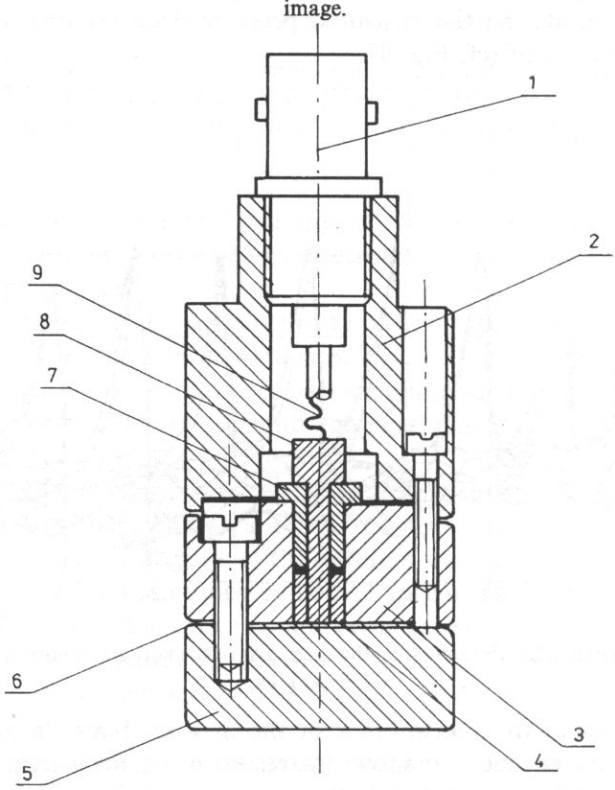


Fig. 11. The design assembly drawing of the capacitance transducer. *1* — signal connector, *2* — metal housing, *3* — electrode holder, *4* — electrode reductor, *5* — metal front plate, *6*— metal foil 50 μm thick, *7* — isolating tube, *8* — brass electrode, *9* — connecting wire.

## 4. The results of application of the designed measuring transducers

The transducers were used for measuring acoustic pressures in the lithotriptor designed by the authors team and the Lithostar type lithotriptor from Siemens used at the Medical Academy in Warsaw for routine disintegration of renal calculi.

Figure 12 compares the measurements of the pressure amplitudes of shock wave pulses taken at the foci of the two lithotriptors using the capacitance transducer designed by the authors. These pressures were measured as a function of the high voltage supplied to the generators of the shock heads of the two devices.

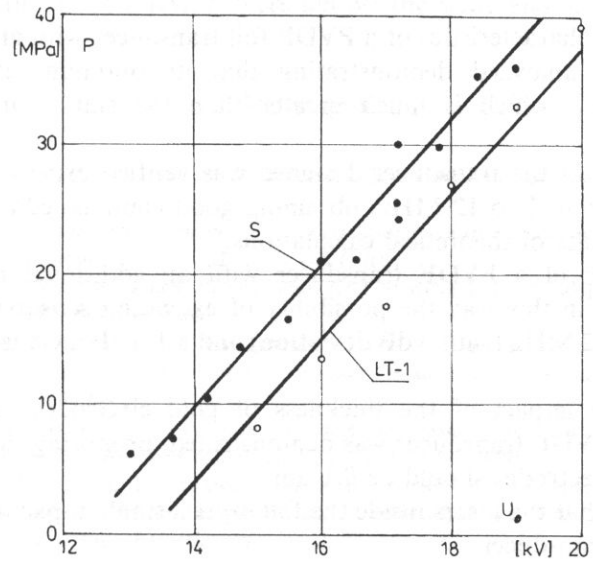


Fig. 12. The pressures of shock wave pulses measured using a capacitance transducer as a function of the supply voltage $U_0$ at the focus of the domestic lithotriptor (LT-1) and the foreign one from Siemens (S).

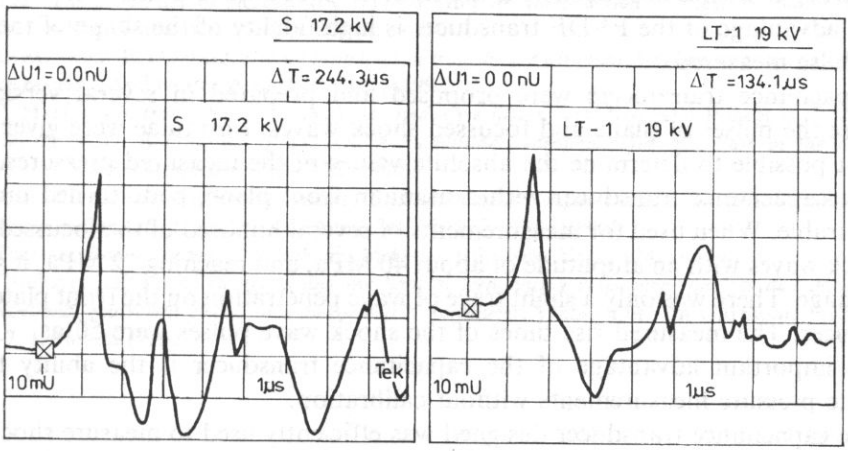


Fig. 13. The pressures pulses of the two lithotriptors in Fig. 12, determined using a capacitance transducer.

Then, Fig. 13 shows the shapes of pressure pulses detected for the two devices. In keeping with the properties of the capacitance transducer, for the two curves only the pressure curve was well reproduced over the range of about 2 μs, including the rise, the peak and the beginning of the falling slope of the shock wave pulse. The farther part of the course was distorted as a result of wave interference inside the front plate of the transducer.

## 5. Conclusions

The sensitivity characteristics of a PVDF foil transducer with an active diameter of 0.5 mm were analyzed demonstrating that its optimum electrical load is the capacitance $C_k$, which is much greater than the static capacitance of the transducer, $C_0$.

The sensitivity of the transducer designed was verified experimentally over the frequency range from 1 to 12 MHz, obtaining good compliance between measurements and the results of theoretical calculations.

A new version of a PVDF transducer with an additional plastic load was proposed, to gain in this way the possibility of extending sensitivity characteristic from 28 MHz to 42 MHz (with 3 dB deviation) and a 1.5 dB increase in sensitivity at low frequencies.

A quantitative impact of the thickness of gold electrodes on the frequency responses of the PVDF transducer was demonstrated, proposing that the maximum thickness of the electrodes should be 0.1 μm.

It was shown that the losses inside the foil exert a small impact on the frequency responses of the transducer.

The PVDF transducer prepared was used to measure the pressure and the shape of the shock wave pulse generated in water. It was found that this transducer is not durable for it was destroyed after a dozen or so shock wave pulses.

An advantage of the FVDF transducer is high fidelity of the shape of the shock wave pulse measured.

Capacitance transducers were proposed and prepared in several versions, to measure the pulses of plane and focussed shock waves. Formulae were given which make it possible to determine the absolute values of the measured pressures.

The capacitance transducer with a titanium front plane, plate turned out to be very durable. When used for measurements of several hundred of the focussed pulses of shock waves with an amplitude of about 40 MPa, and reaching 72 MPa, it showed no damage. There was only a slight trace of wave penetration on the front plate of the transducer. The measured rise times of the shock wave pulses were 50 ns.

An important advantage of the capacitance transducer is the ability to take absolute pressure measurements without calibration.

The capacitance transducer designed was efficiently used to measure shock wave pulses. It is simple, cheap and reliable and the results obtained show good

repeatibility. Its disadvantage is the limitation of its faithful reproduction of the pulse shape only to the rise, the peak and the first drop phase of pressure as a function of time.

The use of these transducers made it possible to compare the shock wave pulses generated by the one domestically designed and those for a foreign lithotriptor from Siemens. This comparison showed that there was an almost linear increase in the shock wave pressure with an increase in the supply voltage over the pressure range from 6 MPa to 40 MPa. But these pressures were the same in the two devices for a 10% higher supply voltage in the pressure range of 6–40 MPa. The rise times of the pulse measured for the two devices were almost the same and shorter than 0.5 μs.

## References


[1] J. Brown, D. Carlson, *Ultrasound transducer models for piezoelectric polymer films*. IEE Trans. on UFFC, **36**, 3 (1980).

[2] L. Filipczyński, *Absolute measurements of particle velocity, displacement or intensity of ultrasonic pulses in liquids and solids*. Acustica, **21**, 173–180 (1969).

[3] L. Filipczyński, *Ultrasound diagnostic methods*, [In:] Medical Ultrasound [Ed.] J. Keller, WKiŁ, Warszawa 1974, Table 6–1 [in Polish].

[4] L. Filipczyński, J. Etienne, A. Grabowska, T. Waszczuk, H. Kowalski, S. Gryziński, J. Stanisławski, *The experimental lithotripsy system for study of shock wave effects*, Archives of Acoustics, **14**, 11–27 (1989).

[5] L. Filipczyński, A. Grabowska, *Deviation of the acoustic pressure to particle velocity ratio from the ρc value in liquids and solids*, Archives of Acoustics, **14**, 173–179 (1989).

[6] L. Filipczyński, J. Etienne, T. Kujawska, *Attenuation of shock wave pulses in kidney tissues*, [In:] Ultrasound in Biomeasurements in Diagnostics and Theraphy [Eds.:] L. Filipczyński and A. Nowicki, International Center of Biocybernetics, Warsaw 1995, 45–49.

[7] L. Filipczyński, G. Łypacewicz, *Dependence between the Q-value of piezoelectric transducers loaded acoustically and the electromechanical coupling coefficient k*, Proc. Vibr. Problems, Warsaw, **10**, 213–229 (1969).

[8] R. Leć, *The properties of piezoelectric crystals*. [In:] *An Introduction to Piezoelectronics*. [Ed.] W. Soluch, WKiŁ, Warszawa, 1980, p. 269 [in Polish].

[9] G. Łypacewicz, E. Duriasz, *Design principles of transducers with matching layers based on admittance measurements*, Archives of Acoustics, **17**, 1, (1992).

[10] W.P. Mason, *Electromechanical transducers and wave filters*, Van Nostrand Princeton, 1948.

[11] K. Shotton, D. Bacon, R. Quilllian, *A membrane hydrophone for operation in the range 0.5 MHz–15 MHz*, Ultrasonics, 123–126 (1980).

[12] J. Somer, J. Corsel, H. Vandervoort, *Evaluation of a computer model for PVDF transducers of arbitrary configuration*, Archives of Acoustics, **13**, 127–135 (1988).

[13] F. Terman, *Radio engineer's Handbook*. McGraw-Hill, New York, 1943, p. 198.

[14] R. Thurston, *Effect of electrical and mechanical terminating resistances on loss and according to conventional equivalent circuit of a piezoelectric transducer*, Transactions on Ultrasonic Engineering, **UE-7**, 1, 16–25 (1960).

ARCHIVES OF ACOUSTICS
21, 1, 53–63 (1996)

# CRITICAL PROPERTIES OF ACOUSTIC WAVE ABSORPTION IN THE BENZONITRILE-ISOOCTANE SYSTEM

T. HORNOWSKI and M. ŁABOWSKI

Institute of Acoustics
A. Mickiewicz University
(61-679 Poznań, ul. Matejki 48/49)

Experimental results for the absorption of ultrasonic waves in critical benzonitrile+isooctane mixtures in the frequency range 5–21 MHz and at temperatures $0.15 \leqslant T - T_c \leqslant 20$ K are reported and confronted with the Shiwa-Kawasaki's mode-coupling theory. The theoretical scaling function was found to describe the experimental results correctly throughout the reduced frequency range $\omega^* < 50$. The values of certain thermodynamic parameters necessary for the determination of the reduced amplitude $A(\varepsilon)$ were calculated using the linear relation between $\alpha_c/f^2$ and $f^{-1.06}$ predicted by the Bhattacharjee–Ferell dynamic scaling theory.

## 1. Introduction

Acoustic investigations of critical mixtures are a source of valuable information concerning the dynamical properties of phase transitions [1–6]. In the first place, such systems exhibit a strong increase in acoustic wave absorption as they approach the critical point. This anomaly is attributed to the coupling between acoustic field and fluctuations in concentration [9]. Three theoretical models have been proposed for the description of the acoustic wave propagation in critical mixtures: the renormalization group theory [7], the dynamic scaling theory [8], and the mode-coupling theory [9–12]. The last one, in the three versions due respectively to KAWASAKI [9], MISTURA [10] and CHABAN [11], after initial success, came up against serious difficulties, in particular the expressions for the critical amplitude failed to describe the experimental data correctly. A drawback of the mode-coupling theory resided in the fact that it led to a scaling function that broke down at high reduced frequencies $\omega^* = \omega/\omega_D$ (where $\omega_D$ is a characteristic frequency of fluctuations of the order parameter). Recently several papers have been published aimed at the overcoming of these difficulties. A general expression for the critical amplitude was proposed [13, 14] that comprises the formulae of Kawasaki, Mistura and Chaban as special cases. Moreover, applying the four heat-mode approximation, a new expression for the scaling function was derived [12].

## 2. Theoretical background

Absorption of acoustic waves in critical mixtures is best represented in the form of the absorption coefficient per wavelength versus the reduced frequency

$$\omega^* = \omega/\omega_D, \tag{2.1}$$

where $\omega_D$ denotes the characteristic frequency of fluctuations in concentration. Since the characteristic frequency is a function of temperature, the description in terms of $\omega^*$ enables us to comprise in a single graph the results obtained under different experimental conditions of temperature and frequency. For critical mixtures, $\omega_D$ takes the form [3]

$$\omega_D = \frac{k_B T_c}{3\pi\eta_s \xi^3} = \frac{k_B T_c}{3\pi\eta_0 \xi_0^3} \epsilon^{(3+x_\eta)\nu} = \omega_0 \epsilon^{z\nu}, \tag{2.2}$$

where $k_B$ is the Boltzmann constant and $\epsilon = (T - T_c)/T_c$ the reduced temperature, providing a measure of the distance of the system from the critical point on the temperature scale. The correlation length $\xi$ and shear viscosity $\eta_s$ occurring in Eq. (2.2) fulfil the following exponential relations near the critical point: $\xi = \xi_0 \epsilon^{-\nu}$ and $\eta_s = \eta_0 \epsilon^{-x_\eta}$. The quantities $z = (3 + x_\eta) = 3.06$ and $\nu = 0.638$ are the so-called critical exponents.

The dynamic scaling hypothesis predicts the anomalous part of the acoustic wave absorption to be a function of the reduced frequency given by the following general expression:

$$\alpha_\lambda = \pi A(\epsilon) I(\omega^*), \tag{2.3}$$

where $A(\epsilon)$ is the critical amplitude and $I(\omega^*)$ the scaling function. Each version of the mode-coupling theory has its own expression for $A(\epsilon)$ [9–11]. However, none of them describes the experimental results satisfactorily. Lately, TANAKA *et al.* [13] as well as the present authors [14] have re-analyzed this aspect of the theory and obtained the following general formula for $A(\epsilon)$:

$$A(\epsilon) = \frac{k_B g^2 u^2 \nu^2}{\pi^2 \rho T_c c_p^2 \xi_0^3} \epsilon^{-\bar{\alpha}}, \tag{2.4}$$

which for particular cases reduced to the expressions of the different versions of the mode-coupling theory. In (2.4), $\rho$ is the density of the mixture, $u$ the velocity of the ultrasonic wave, $c_p$ the specific heat at constant pressure, and $\bar{\alpha} = 0.11$ the critical exponent for the specific heat. The dimensionless constant $g$ introduced by Bhattacharjee and Ferrel in their dynamic scaling theory has been shown [2] to remain unchanged as the system approaches the critical point. Once the values of all the thermodynamic parameters of the mixture are available, the constant $g$ can be determined from the following formula derived by Tanaka:

$$g = -T_c\alpha_{Pb} + \frac{T_c\alpha_{Pc}}{c_{Pc}} c_{Pb}, \tag{2.5}$$

whre, $\alpha_P$ the thermal expansion coefficient $\alpha_p$ and the specific heat can be expressed by the following exponential relations: $\alpha_P = \alpha_{Pc}\epsilon^{-\tilde{\alpha}} + \alpha_{Pb}$, $c_P = c_{Pc}\epsilon^{-\tilde{\alpha}} + c_{Pb}$. The quantities with the subscript $b$ denote the regular part (showing no critical anomaly) whereas those with subscript $c$ denote the amplitude of the critical part. The critical amplitude $A(\epsilon)$ given by Eq. (2.4) is a function only of the reduced temperature $\epsilon$. However as shown by TANAKA *et al.* [13], it should depend also on the frequency $\omega$. This circumstance, resulting from the frequency-dependence of the specific heat, results in the breakdown of the dynamic scaling hypothesis for the acoustical anomaly. Since this dependence is noticeable only at very high values of the reduced frequency, it can be neglected in the usually accessible range of frequencies.

The expression (2.3) states that all the values of the absorption coefficients (all the $\alpha$'s measured for different temperatures and frequencies and divided by the critical amplitude) scale along the single universal curve $I(\omega^*)$, referred to as the scaling function. This function depends on but one variable — the reduced frequency. Earlier versions of the mode-coupling theory applied a perturbation procedure taking into account only two heat-mode intermediate states. According to these approximations, the scaling function has the form [9]:

$$I^{(2)}(\omega^*) = \int_0^\infty dx [xy(x)]^2 \frac{\omega^* K(x)}{K^2(x) + \omega^{*2}}, \tag{2.6}$$

where $x$ is the product of the wave number $k$ and the correlation length $\xi$. The function $y(x)$, defined as the derivative of the logarithm of the correlation function of the order parameter $X(x)$ takes the form:

$$y(x) = 1 - \frac{\eta}{2} + x\frac{d}{dx}\ln X(x), \tag{2.7}$$

where $\eta = 0.041$ is the critical exponent introduced by FISHER [15]. The function $K(x)$ is defined in terms of the decay rate of fluctuations of the wave number $k$. The explicit form of $K$(x), as proposed by KAWASAKI [8], is

$$K(x) = \frac{3}{4}[1 + x^2 + (x^3 - 1/x)\arctan(x)]. \tag{2.8}$$

The scaling function in the two heat-mode approximation has been shown to be inadequate for the description of the experimental results, particularly for high reduced frequencies [16]. This led SHIWA and KAWASAKI [17] to extend a perturbation procedure to include the contributions of four heat-mode intermediate states to the bulk viscosity. They obtained the scaling function in the form of the sum $I^{(2)}(\omega^*) + I^{(4)}(\omega^*)$, with $I^{(4)}(\omega^*)$ given by

$$I^{(4)}(\omega^*)=\frac{1.42^2}{54\pi^3}\int_0^\infty dx_1\int_0^\infty dx_2\int_0^\infty dx_3\int_0^\pi d\theta_2\int_0^\pi d\theta_3\int_0^{2\pi} d\phi\,\times$$

$$\times(x_1x_2x_3)^2\cdot\sin\theta_2\sin\theta_3\cdot\omega^*\Re(x_1,x_2,x_3,\theta_2,\theta_3,\phi)\,. \tag{2.9}$$

The explicit form of $\Re(x_1,x_2,x_3,\theta_2,\theta_3,\phi)$ is to be found in ref. [17].

The key to the successful use of the mode-coupling theory resides in a proper choice of the correlation function of the order parameter fluctuations occurring in the formulae (2.8) and (2.9), since the expression for $I(\omega^*)$ is highly sensitive to the form of the correlation function $X(x)$ for high values of $x$, i.e. when $\omega^*$ is large. Earlier versions of the mode-coupling theory applied the Ornstein–Zernike formula [17]. However, the latter is well known to fail to account correctly for the long-range "tail". Thus the $X(x)$ for $x\gg 1$ has to be replaced by the Fisher-Langer expression [18]. Recently, BRAY [19] proposed an approximation of the correlation function ideally reproducing the shape of the Ornstein-Zernike and Fisher-Langer functions for small and large values of $x$, respectively.

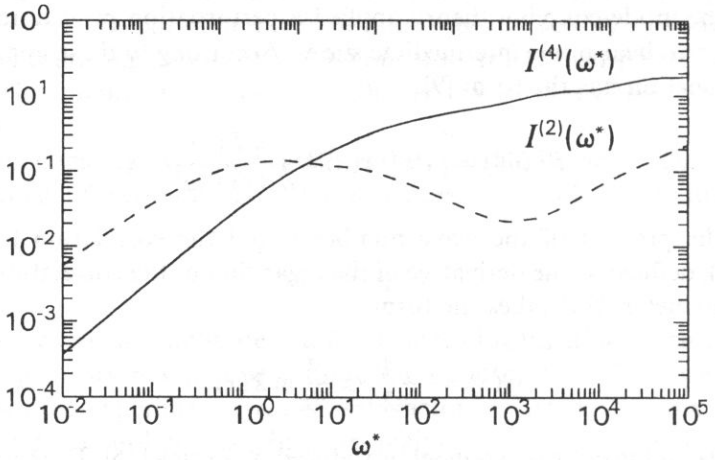


Fig. 1. $I^{(2)}(\omega^*)$ (dashed) line and $I^{(4)}(\omega^*)$ (solid line) calculated from the Bray's function.

The numerically determined values of $I^{(2)}(\omega^*)$ (dashed line) and $I^{(4)}(\omega^*)$ (solid line) are plotted in Fig. 1. In both cases, Bray's expression has been used for the correlation function.

With regard to the nature of the initial kinetic equations involved, the mode-coupling theory is unable to describe the absorption and dispersion of ultrasonic waves *versus* frequency at the critical point as such (the "critical region"). Ferrell and Bhattacharjee succeeded in deriving an expression of this kind that is owing to their highly ingenious use of the dynamic scaling hypothesis. They postulate that at the critical point the absorption coefficient $\alpha_c/f^2$ should depend linearly on $f^{-1.06}$:

$$\frac{\alpha_c}{f^2}=\left[\frac{\pi^2\bar{\alpha}g^2u_cc_{Pc}}{2zvT_cc_{Pb}^2}\left(\frac{\omega_0}{2\pi}\right)^{\bar{\alpha}/zv}\right]f^{-(1+\bar{\alpha}/zv)}+\frac{\alpha^b}{f^2}=Sf^{-1.06}+b\,, \tag{2.10}$$

with $\alpha^b/f^2$ — classical absorption. Eq. (2.10) has been confirmed repeatedly by experiment [3–6]; it has proved to be a highly useful tool permitting the determination of the coupling constant $g$. Whereas the counterpart of Eq. (2.3) in the dynamic scaling theory is given by the expression

$$\alpha_\lambda=\pi\,\frac{\pi\bar{\alpha}u^2g^2c_{Pc}\epsilon^{-\bar{\alpha}}}{2zvT_cc_{Pb}^2}\,\frac{(\omega^*)^{-\bar{\alpha}/zv}}{[1+(\omega^*)^{-1/2}]^2}=\pi A_{FB}(\epsilon)G(\omega^*)\,. \tag{2.11}$$

## 3. Experimental results

The measurements were carried out by the pulse-echo method using an experimental set-up developed by MATEC. The details of the measuring position as well as the evaluation of the accuracy achieved are given elsewhere [20, 21]. The critical mixture of benzonitrile+isooctane (2,2,4-trimethylpentane) exhibits an upper critical point, and the critical parameters of the separation curve are [22]: $T_c=18.71°C$ and $x_c=0.465$ (molar fraction of benzonitrile). Our measurements of the ultrasound velocity and absorption covered the temperature range $\Delta T=T-T_c=0.1$ K to 20.2 K for five frequencies of the ultrasonic wave: 5, 7, 10, 15 and 21 MHz.

The measurement started at 40°C and the temperature was then lowered gradually down to the critical one. The velocity of the ultrasound as function of temperature was found to be linear: $u=1205-3.5\,(T-T_c)$. To within the experimental error, no dispersion of the velocity was found throughout the frequency limits ranging from 5 to 25 MHz. Figure 2 shows the velocity as a function of temperature.

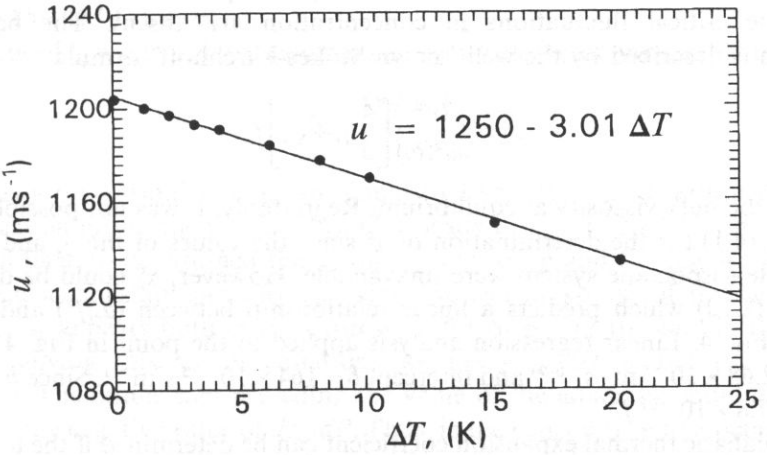


Fig. 2. Propagation velocity of ultrasonic waves versus $\Delta T$ in the critical benzonitrile+isooctane system.

In Fig. 3, the absorption per wavelength is plotted as a function of temperature. The graph is typical for critical mixtures: the absorption grows progressively as the system approaches the critical temperature, the quicker the lower is the frequency of the wave.

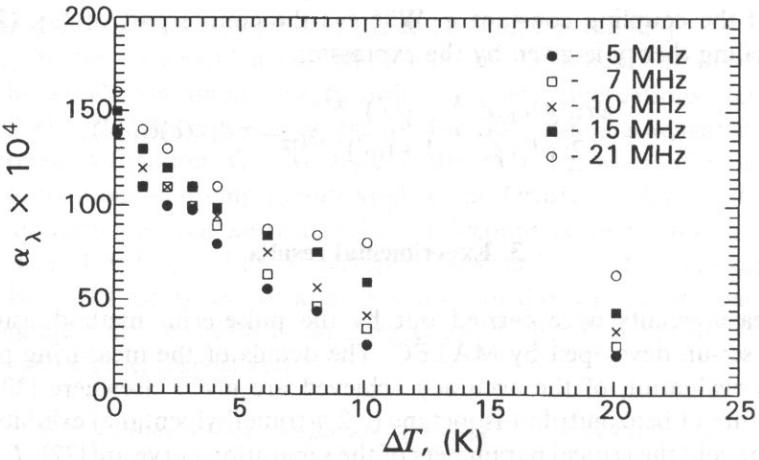


Fig. 3. Absorption coefficient per wavelength versus temperature for different frequencies of the ultrasonic wave.

## 4. Determination of the collateral thermodynamic parameters

The absorption coefficient measured in experiment is the sum of the critical absorption and the background (Navier-Stokes) absorption, the latter being present even if the critical fluctuations in concentration are absent. The background absorption is described by the well known Stokes-Kirchhoff formula

$$\alpha_\lambda^b \simeq \frac{2\pi^2}{\rho u^2(\omega)}\left[\frac{4}{3}\eta_s + \zeta_0\right] f, \tag{4.1}$$

where $\zeta$ is the bulk viscosity at equilibrium. Regrettably, it was not possible to make use of Eq. (4.1) for the determination of $\alpha_\lambda^b$ since the values of the $\eta_s$ and $\zeta_0$ for the benzonitrile+isooctane system were unavailable. However, $\alpha_\lambda^b$ could be determined from Eq. (2.10) which predicts a linear relationship between $(\alpha_c/f^2)$ and $f^{-1.06}$, as shown in Fig. 4. Linear regression analysis applied to the point in Fig. 4 led to the slope $S = 2.68 \times 10^{-5}\,\mathrm{m \cdot s^{-0.94}}$ and intercept $b = 164 \times 10^{-15}\,\mathrm{s^2 m^{-1}}$. Since $b = \alpha_\lambda^b / f_u$, we have $\alpha_\lambda^b = 7.8 \times 10^{-11} f$.

The adiabatic thermal expansion coefficient can be determined if the temperature dependence of the density is given in the form $\rho = C_1 + C_2\epsilon + C_3\epsilon^{1-\alpha}$. Exact measure-

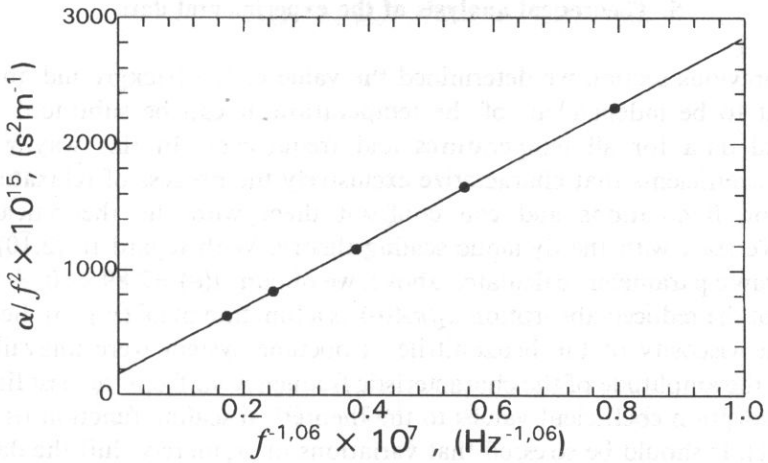


Fig. 4. $\alpha_c/f^2$ as a function of $f^{-1.06}$ for critical benzonitrile+isooctane mixture.

ments of the density of benzonitrile+isooctane mixtures have been performed by MILLER *et al.* [22] leading to $\rho\,(\mathrm{kg\cdot m^{-3}}) = 807.086 - 294\,\epsilon + 13\epsilon^{1-\bar{\alpha}}$. Together with the relations $\alpha_{Pc} = (\bar{\alpha}-1)C_3/\rho_c T_c$ and $\alpha_{Pb} = -C_2/\rho T_c$, this gives $\alpha_{Pc} = -0.49\times10^{-4}\ \mathrm{K^{-1}}$ and $\alpha_{Pb} = 12.48\times10^{-4}\ \mathrm{K^{-1}}$.

The critical part of the specific heat at constant pressure can be determined from the relation

$$\frac{dT_c}{dP} = \frac{T_c\alpha_{Pc}}{\rho_c c_{Pc}}. \tag{4.2}$$

Using the values $\rho_c = 807.086\ \mathrm{kg\cdot m^{-1}}$ and $dT_c/dP = -11.8\times10^{-8}\ \mathrm{K\cdot Pa^{-1}}$ [22], we got $c_{Pc} = 0.15\times10^3\ \mathrm{J\cdot kg^{-1}K^{-1}}$.

The value of $\xi_0$ was calculated assuming the two-scale factor universality that leads to

$$R_\xi = \frac{c_{Pc}\rho_c\bar{\alpha}\xi_0^3}{k_B}, \tag{4.3}$$

where $R_\xi$ is a dimensionless constant equal to $1.95\times10^{-2}$ as determined from the renormalization group theory [23]. Eq. (4.3) leads to $\xi_0 = 2.72\times10^{-10}\ \mathrm{m}$.

We still have to determined the coupling constant $g$ and the regular part of the specific heat at constant pressure $c_{Pb}$. Here we can make use of the fact that the quotient $g/c_{Pb}$ appears both in the expression for $S$ [Eq. (2.10)] and in the formula (2.5). On solving this set of equations we get $g = -0.678$ and $c_{Pb} = 3.29\times10^3$ $\mathrm{J\cdot kg^{-1}K^{-1}}$. The minus sign preceding the value of the adiabatic coupling constant comes from the negative value of $dT_c/dP$. Thus, in the benzonitrile+isooctane mixture the changes in the critical temperature are in opposite phase to the changes in the pressure.

## 5. Theoretical analysis of the experimental data

In the previous section we determined the value of the background absorption. Assuming it to be independent of the temperature, it can be subtraced from the experimental data for all temperatures and frequencies. In this way we obtain absorption coefficients that characterize exclusively the process of relaxation of the concentration fluctuations and can confront them with the theoretical scaling function. We start with the dynamic scaling theory. With regard to (2.10) and the thermodynamic parameters calculated above, we obtain $A(\epsilon)=2.89\times10^{-3}$. With this value we plot the reduced absorption $\alpha_\lambda/\pi A(\epsilon)$ as a function of $\omega^*$ (Fig. 5). Because the data for the viscosity of the benzonitrile+isooctane system were unavailable, we detemrined the amplitude of the characteristic frequency $\omega_0$ from the best fit between reduced absorption coefficient values to the theoretical scaling function $G(\omega^*)$ given by Eq. (2.11). It should be stressed that variations in $\omega_0$ merely shift the data to the right or left, whereas their displacement upwards or downwards is governed by the value of the critical amplitude. The least-squares method in the form of the CURFIT procedure [24] yielded a characteristic frequency of $\omega_0=3.89\times10^{10}\ \mathrm{s}^{-1}$.

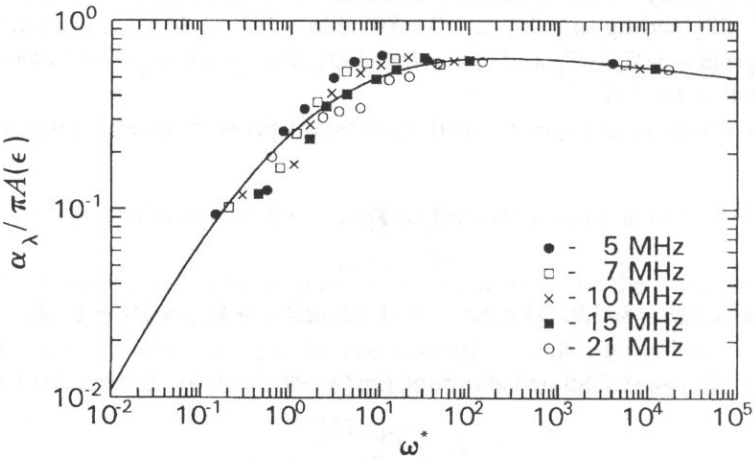


Fig. 5. $\alpha_\lambda/\pi A(\epsilon)$ versus the reduced frequency $\omega^*$ for the benzonitrile+isooctane mixture. The solid line represents the scaling function $G(\omega^*)$ given by Eq. (2.11).

Figure 5 shows good agreement between experimental results and the theoretical scaling function of Bhattacharjee and Ferrell within the whole range of the reduced frequencies.

Let us now pass on to the mode-coupling theory. We have got all the values of the thermodynamic parameters required for the detailed analysis of the critical amplitude $A(\epsilon)$. Fig. 6 shows the values of $A(\epsilon)$ determined from Eq. (2.4) *versus* $\epsilon$; $A(\epsilon)$ is found to diverge, but insiginificantly, from the exponential const $\epsilon^{-\alpha}$ (dashed line in Fig. 6). This is due to the circumstances that the critical part of the specific heat at constant

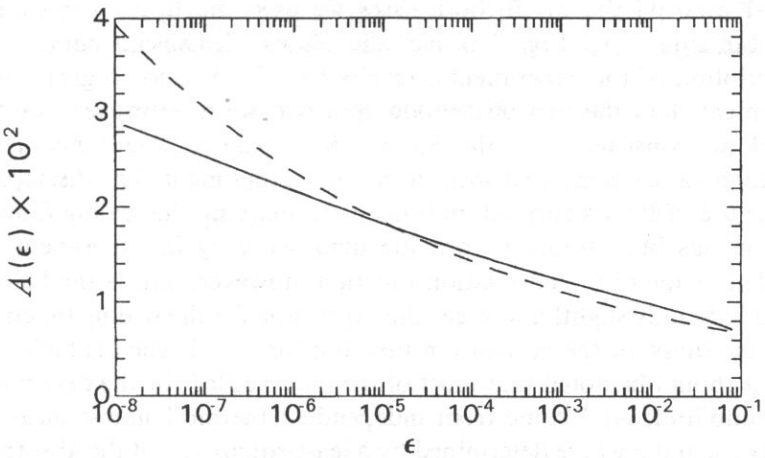


Fig. 6. $\alpha_\lambda/\pi A(\epsilon)$ *versus* the reduced temperature $\epsilon$ for the benzonitrile+isooctane mixture. The dashed line shows the dependence on const $\epsilon^{-\bar{\alpha}}$.

pressure $c_{Pc}$ of the benzonitrile+isooctane mixture is relatively small compared with the regular part $c_{Pb}$. In mixtures where $c_{Pc}$ and $c_{Pb}$ are similar in magnitude (e.g. aniline—cyclohexane [25]) the critical amplitude $A(c)$ remains practically constant because in Eq. (2.4) the quantities divergent to infinity — $c_P$ in the denominator, $\epsilon^{-\bar{\alpha}}$ in the numerator — cancel out mutually. The temperature dependence of the acoustic wave velocity affects the critical amplitude $A(c)$ but slightly.

Figure 7 represents the dependence of the expression $\alpha_\lambda/\pi A(c)$ on $\omega^*$. The dashed line gives the scaling function $I^{(2)}(\omega^*)$ proposed by Kawasaki in the approximation of two heat-mode contributions, whereas the solid line gives the sum $I^{(2)}(\omega^*)+I^{(4)}(\omega^*)$ of

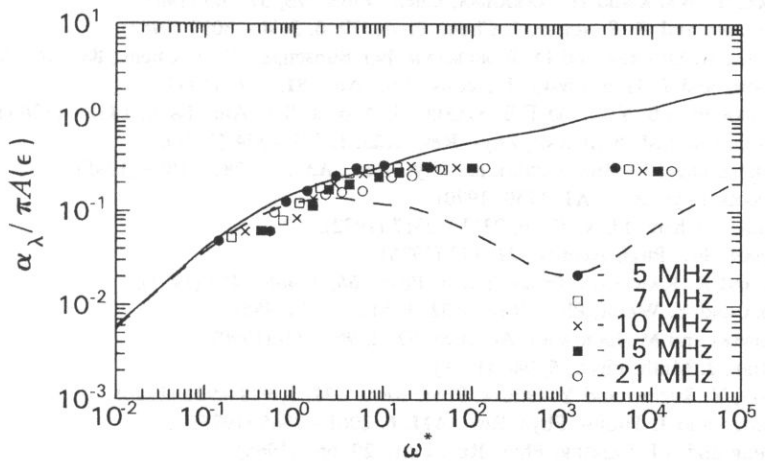


Fig. 7. $\alpha_\lambda/\pi A(\epsilon)$ *versus* the reduced frequency for the benzonitrile+isooctane mixture; dashed line — the scaling function $I^{(2)}(\omega^*)$, solid line — the sum $I^{(2)}(\omega^*)+I^{(4)}(\omega^*)$.

the Shiwa–Kawasaki theory. In both cases we used the Bray expression for the correlation function $X(x)$. Fig. 7 proves the Shiwa–Kawasaki curve to provide a good description of the experimental results for $\omega^* < 50$ and to give a somewhat better agreement than the two heat-mode approximation. However, for higher $\omega^*$ there is still no consistence — the Shiwa–Kawasaki scaling function leads to excessively high values compared with those from experiment. The discrepancy may be due to the use of Bray's correlation function in deriving the scaling function. The Bray function has been found to provide high accuracy in experiments on light scattering. The shape of the correlation function, however, affects the half-width of the scattered light only slightly, whereas the expression for the scaling function is very sensitive to the shape of the correlation function for $k\xi > 1$ when is high.

Finally, it should be noted that most of the data needed for the determination of the critical amplitude $A(\epsilon)$ come from independent thermodynamic measurements, whereas only $c_{Pb}$ and $g$ where determined by a least-squares fit of the absorption data to the linear relation between $\alpha_c/f^2$ and $f^{1.06}$ derived from the dynamic scaling theory. The fact that the critical amplitude determined in this way leads to a correct scaling of the absorption data for the low values of the $\omega^*$ points to the validity of new generalized expression for $A(\epsilon)$ given by Eq. (2.4). The discrepancy between the experimental results and the Shiwa–Kawasaki theory at high valeus of $\omega^*$, however, points to the necessity of searching for further modifications of the scaling function. Work in this direction is now under-way.

## References


[1] Y. HARADA, Y. SUZUKI and Y. ISHIDA, J. Phys. Soc. Jpn., **48**, 703 (1980).
[2] H. TANAKA, Y. WADA and H. NAKAJIMA, Chem. Phys., **75**, 37–43 (1983).
[3] C.W. GARLAND and G. SANCHEZ, J. Chem. Phys., **79**, 6, 3090–3099 (1983).
[4] G. JASCHULL, H. DUNKER and D. WOERMANN, Ber Bunsenges. Phys. Chem., **88**, 630–635 (1984).
[5] M. ŁABOWSKI and T. HORNOWSKI, J. Acoust. Soc. Am., **81**, 1421 (1987).
[6] I.R. ABDELRAZIQ, S.S. YUN and F.B. STUMPF, J. Acoust. Soc. Am., **88**, 4, 1831–1836 (1990).
[7] D.M. KROLL and J.M. RUHLAND, Phys. Rev., **A23**, 1, 371–374 (1981).
[8] R.A. FERRELL and J.K. BHATTACHARJEE, Phys. Rev., **A31**, 3, 1788–1809 (1985).
[9] K. KAWASAKI, Phys. Rev., **A1**, 1750 (1970).
[10] L. MISTURA, J. Chem. Phys., **57**, 6, 2311–2317 (1972).
[11] I.A. CHABAN, Sov. Phys. Acoust., **21**, 177 (1975).
[12] Y. SHIWA and K. KAWASAKI, Progr. Theor. Phys., **66**, 2, 406–419 (1981).
[13] H. TANAKA and Y. WADA, Phys. Rev., **A32**, 1, 512–524 (1985).
[14] T. HORNOWSKI and M. ŁABOWSKI, Acustica, **72**, 2, 96–100 (1990).
[15] M.E. FISHER, J. Math. Phys., **5**, 944 (1969).
[16] Y. HARADA, Y. SUZUKI and Y. ISHIDA, Phys. Rev., **A21**, 3, 928–931 (1980).
[17] P. TARTAGLIA and J. THOEN, Phys. Rev., **A11**, 6, 2061–2065 (1975).
[18] M.E. FISHER and S.J. LANGER, Phys. Rev. Lett., **20**, 665 (1968).
[19] A. BRAY, Phys. Rev., **B14**, 3, 1248–1270 (1976).
[20] T. HORNOWSKI and M. ŁABOWSKI, Acta Phys. Pol., **A79**, 5, 671–682 (1991).
[21] T. HORNOWSKI, Acta Phys. Pol., **A82**, 6, 961–966 (1992).

[22] B.C. MILLER, E.A. CLERKE and S.C. GREER, J. Phys. Chem., **87**, 6, 1063–1066 (1983).
[23] C. BERVILLIÈRE and C. GODRÈCHE, Phys. Rev., **B21**, 11, 5427–5431 (1980).
[24] P.R. BEVINGTON, *Data reduction and error analysis for the physical sciences*, McGraw-Hill, New York, 1969.
[25] H. TANAKA, Y. WADA and H. NAKAJIMA, Chem. Phys., **68**, 223 (1982).

ARCHIVES OF ACOUSTICS
21, 1, 65–73 (1996)

# EXPERIMENTAL INVESTIGATIONS OF SHOCK WAVE PROPAGATION IN THE POSTFOCAL REGION OF A FOCUSED SOUND FIELD

H. HOBAEK

Department of Physics
University of Bergen
Allégt. 55, N5007 Bergen, Norway

This paper reports some experimental results on the postfocal region of the sound field from a curved circular transducer at very high amplitude. It is found that along the axis the shock front seems to propagate with a speed different from the "background sound". This is explained by diffraction: The field may be separated into two main contributions, one from the edge of the source — arriving first and causing the "background sound" — and one from the main region of the source — causing the shock. After being formed the shock propagates with no change in shape, and with uniformly decreasing amplitude. The shock propagation speed seems to increase slightly with source amplitude.

## 1. Introduction

Focused ultrasound has many applications, as for example in medical diagnostics and therapy. The linear (small amplitude) field from focusing transducers is well known [1, 2], in particular if the parabolic wave equation is valid (i.e. if focusing angles $< 16°$). Also the large amplitude case has received much attention lately [3, 4]. In this paper results from an experiment investigating the waveform in the post focal region are reported, and some of the findings seem not to have been published previously. In particular, it is found that the shock front, after being formed close to the focus, propagate along the axis with almost unaltered form but varying amplitude throughout the field, superposed a "background field" which seems to propagate with a different velocity. This is seen by recording time series of the waveform (traces) at increasing distances along the sound axis, in such a way that the traces display sequences in retarded time. In fact, the shock seems to be overtaken by the "sinusoidal" background field. Moreover it is found that beyond the focal region the arrival time of the shock depends on the source amplitude, even if the sound pulse (burst) contains many periods. Such behaviour is expected from single sound pulses, or if there is significant asymmetry in the signal (positive sound pressure peak exceeds that of the negative).

## 2. Experiment

A layout of the experimental arrangement is shown in Fig. 1, and the experimental parameters presented in Table 1. The source transducer was a circular cross section of a piezoelectric shell, with a fundamental resonance frequency about 1 MHz. Its radius of curvature was measured with a curvature gauge to $99 \pm 2$ mm. It was powered by a ENI 210L power amplifier through an impedance matching transformer, resulting in a maximum voltage of 370 V peak-to-peak measured at its terminals. Signals were

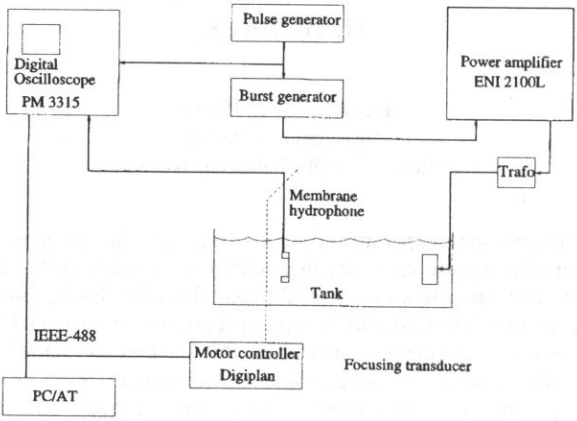


Fig. 1. Experimental arrangement.

**Table 1.** Experimental parameters

| | |
|---|---|
| Tank dmensions: | |
| Length: | 1.3 m |
| Width: | 0.3 m |
| Height: | 0.3 m |
| Contents: | Tap water, ca. 21°C |
| Sound speed: | 1485 m/s |
| Focusing source: | |
| Radius of curvature: | $99 \pm 2$ mm |
| Diameter: | 47.85 mm |
| Frequency: | 1.05 MHz |
| Wavelength: | 1.41 mm |
| ka: | 105.8 |
| Rayleigh distance: | 1.275 m |
| Length of near field: | 405 mm |
| Gain-factor: | 12.9 |
| Focusing angle: | 14° |
| Hydrophone: | |
| Diameter: | 10 cm |
| Active surface: | 1 mm diameter |
| Sensitivity (1 MHz): | 0.155 mV/Pa |

provided by a pulse generator delivering trigger signals to a burts generator and the digital sampling oscilloscope (DSO). A jitter of up to 0.02 μs from trace to trace was impossible to remove. The hydrophone was a bilaminar PVDF membrane type, with circular active area of 1 mm diameter. Its frequency response is reasonable flat to about 22 MHz. It was connected directly to the DSO through a 73 cm long 75 Ω cable. The DSO used for digitizing the signals was a PM 3315 (256 samples and up to 125 MHz sampling frequency with 8 bits resolution). The DSO and the positioning system was controlled by a PC/AT by IEEE-488 bus, and the records were transferred to the PC/AT for storage and further processing. The waveforms presented here (traces) are taken at the axis of the transducer, obtained by careful alignment of the source and hydrophone.

The burst used in this experiment were 125 μs long. At the longest ranges this may have caused some interference from surface reflections in the weak parts of the signal, but this is believed not to have influenced the shock regions. The single traces were recorded in the following manner: after positioning the hydrophone at a new axial range, the first arrival of the burst was searched for the first clearly visible zero crossing in the positive direction. This was easily identifiable in all cases, and was used as a reference time for the trigger. To this was added the fixed delay of 100 μs. Thus, the traces always start 100 μs after the first arrival of the burst.

## 3. Results

Figure 2 a–c show samples of traces taken at different ranges along the axis, with 370 V peak-to-peak driving voltage. Figure 2a shows three traces near the focal region. Note that there is no sign of a shock wave in the trace at 84 mm, which is just before the focus. The peak positive pressure of 2.08 V at 104 mm corresponds to 12.7 MPa, according to the nominal sensitivity of the hydrophone, while the peak negative pressure corresponds to −2.8 MPa. Already at 124 mm the shock front is seen to be retarded significantly. The fluctuations just behind the shock front was thought to be due to the limited bandwidth of the hydrophone.

Figure 2b shows traces near the first axial zero outside the focal region, which is located at 194 mm as shown in Fig. 4. It is clearly seen how the shock arrives later as range increases, with respect to the "sinusoidal" background signal which remains stationary in the retarded frame.

Figure 2c shows samples of traces at longer ranges, in 80 mm steps. The shock front continues to arrive at later times relative to the sinusoidal background signal, although more and more slowly with increasing range. Observe that the shape of the shock front remains almost unchanged over the whole range, even through the axial zero at 194 mm. The rise time increases from 0.06 μs to 0.08 μs from 104 mm to 464 mm — although the amplitude varies strongly.

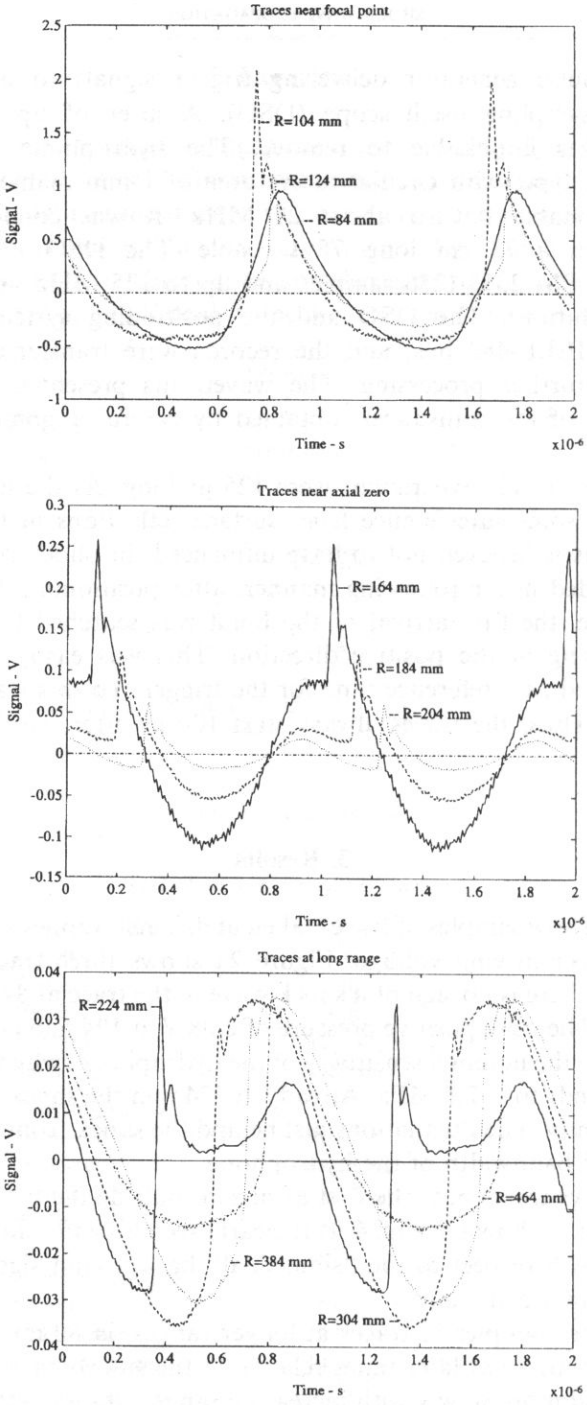


Fig. 2. Traces and different ranges.

Figure 3 shows amplitude variation with range, and the small amplitude simulations for this case (with arbitrary amplitude normalization). The shock amplitude is obtained by fitting a straight line to the shock front and taking the common part. It exceeds the positive peak amplitude when it starts below zero level, even in cases where the positive peak is higher than the peak of the shock. Where it is less than the positive peak the shock starts at a positive level. It is interesting to note that the negative peak amplitude has a minimum close to 200 mm, and another one about 470 mm, while that of the positive peak amplitude is at about 250 mm. The shock amplitude decreases uniformly with distance, although fastest within the first 100 mm

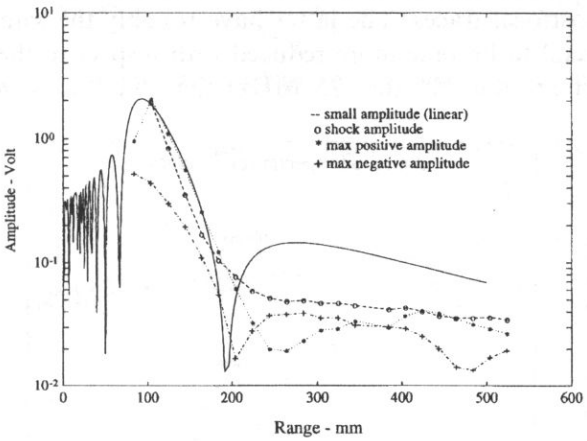


Fig. 3. Amplitude versus range.

front the focal region.

Figure 4 shows arrival times of the shock front and location of the positive and negative peak amplitudes, scaled in periods of the fundamental frequency. Also

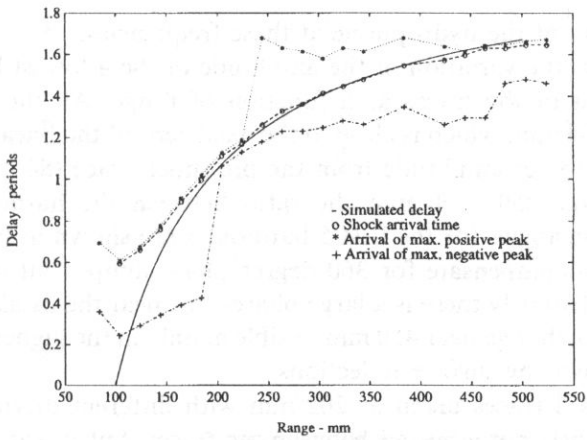


Fig. 4. Arrival times versus range.

shown is a curve representing the delay between arrivals of the wave from the edge of the source and that from the source center. The origin of the measured arrival times are adjusted so that the curve for the shock front coincides with the simulations at 384 mm. Jumps in the peak arrivals occur when the shock is overtaken by the background signal. Note that apart from these jumps the arrival times for the positive and negative peak amplitudes remain roughly constant (except where the positive peak coincides with the shock).

Figure 5 show amplitude spectra for the ranges 84–164 mm, up to the 26th harmonics. The amplitude at the fundamental frequency has been normalized to 1 in all the curves. There is, as expected, a major difference between the spectra of the prefocal and the postfocal traces. The latter have roughly the same shape, but the higher harmonics tend to become more reduced with respect to the fundamental as range increases. Above the 24th (i.e. 25 MHz) the amplitudes decay due to the

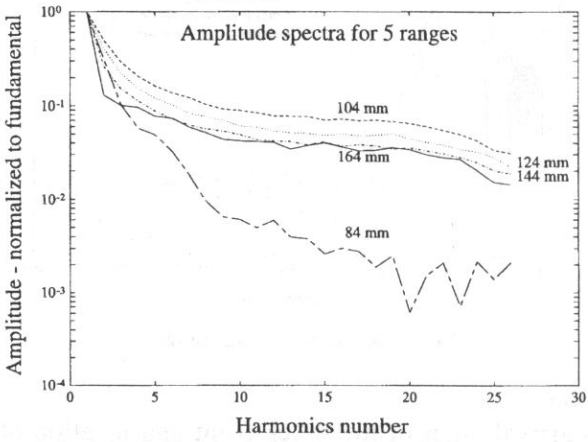


Fig. 5. Amplitude spectra for the ranges 84–164 mm, in 20 mm steps.

vanishing sensitivity of the hydrophone at these frequencies.

Figure 6a shows the variation of the amplitude of the 4 lowest harmonics in the frequency spectrum of the traces as a function of range. All the harmonics have a minimum near 204 mm, which is close to the axial zero of the linear field. Also note the change in harmonics amplitude from the pre-shock trace (84 mm) to the shock region. In the range 250–450 mm the ratio between the harmonics is roughly constant. The phase angles for the first 5 harmonics are shown in Fig. 6b. Attempts have been made to compensate for 360 degree phase jumps, but ambiguity in this respect remains. Obviously there is a large phase-shift near the axial zero at 194 mm, and another smaller change near 450 mm, visible mainly in the higher harmonics. The latter could be caused by surface reflections.

Figure 7 shows 3 traces taken at 202 mm with different driving voltages. The oscilloscope delay was not adjusted between the traces, but it was slightly different from the traces above. No shock exists in the trace at 138 V, and it is visible but not

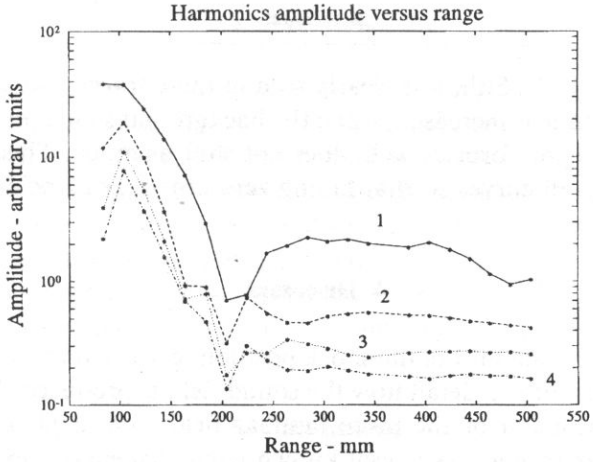


Fig. 6a. Variation of the amplitude of 1 – 4 harmonics with range.

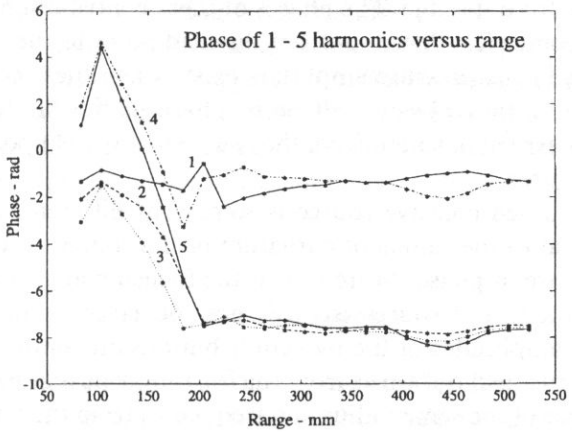


Fig. 6b. Variation of the phase angle of 1 – 5 harmonics with range.

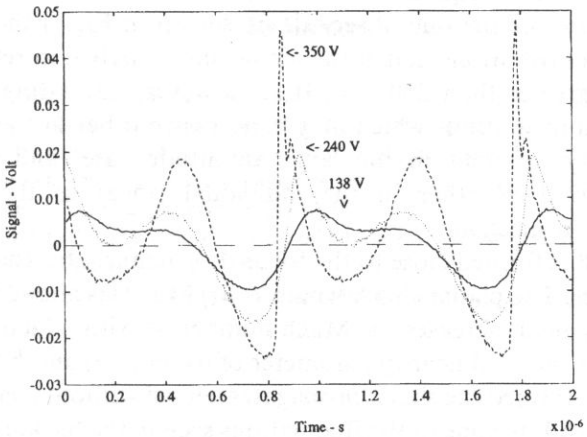


Fig. 7. Traces at 202 mm with different source amplitudes.

fully developed at 240 V. Still, it is clearly seen in these traces that the shock arrives earlier as the amplitude is increased, while the background signal, although not quite stationary and changing form as well, does not shift as much. This can be seen for example by shifting all curves so that falling zero crossings coincide.

## 4. Discussion

In order to explain the shift of the shock position relative to the background signal it is necessary to examine in detail how the sound field is produced. Here it is helpful to start with a discussion of the more familiar field from a plane circular piston source, in the linear regime. As is well known from elementary textbooks the axial field consists of two contributions of equal amplitude, namely one from the center of the source, and one from its edge. The phases of these contributions are proportional to the respective geometrical distances from the field point to these source points. In the near field zeros in the pressure amplitude exists when these contributions are in opposite phase, while they always will be in phase in the far field (on the axis). Obviously, the first arrival of sound from the source to any field point has its origin at the center of the source.

The field of a curved concave source is somewhat different. At the focal point — i.e. at range equal to the radius of curvature of the source — the central and the edge contributions are in phase. Moreover, if the focusing angle (angle between axis and line through focus and source edge) is not too large — in practice less than approx. 16° — the amplitudes of the two contributions are almost equal [5]. (It may also be shown that the field outwards from the focus may be mapped to the field from a plane piston source of the same radius and frequency, from the far field and inwards [6]). Outside the focus the first arrival of the signal will come from the edge of the source. Thus, if the shock originates from the central region of the source one should expect a retardation like the one observed. As shown in Fig. 4 the simulated delay between the two contributions match the actual shock arrival in retarded time quite nicely for ranges greater than 230 mm. It is, however, interesting to note that the central and edge contributions which may cancel each other in the small amplitude case, becomes very different in the large amplitude case, and actually may be distinguished from each other in the individual traces as the shock and the background signal respectively.

The shock itself is formed close to the focus. It is remarkable that it is not formed nearer to the source: The planar shock length $L=(\beta \mathrm{Mk})^{-1}$ is about 14 cm in this case, but the converging field increases the Mach number M with a factor of almost 13 at the focus. Here $\beta$ is the nonlinearity parameter of water (3.5) and $k$ the wave number. However, after it is formed the shock propagates almost without change in shape. The shock amplitude exhibits none of the fluctuations seen in the background field, and in the harmonics. This is especially surprising with regard to the region around the axial zero (linear), where in the linear case a phase reversal takes place. The change in shock

arrival time with amplitude is explained by a well known result from weak shock theory, which is that the shock speed is the arithmetic mean of the speed just in front of the shock front, and the speed just behind it. Thus, if the waveform is highly asymmetric, as in the present investigation, the speed of the shock front is different from the small amplitude sound speed, and will depend on the amount of asymmetry. This asymmetry must be amplitude dependent (it appears only at high amplitudes) and has been seen by many previous investigators. The crucial question then remains: What is the physical explanation for this asymmetry?

## 5. Conclusions

The observed shock retardation with range is largely explained by accounting for the first arrival of sound as coming from the edge of the source. The shape of the shock itself remains remarkably stable throughout the post-focal zone, and its amplitude decays uniformly with range without fluctuations and phase reversal. It is, however, superimposed a background field originating from the source edge which is largely of the same amplitude, but contains no shocks. The shock seems to propagate with a speed which depends on the source amplitude. This is in accordance with weak shock theory.

## Acknowledgments

The experiments were conducted during my sabbatical term visiting at School of Physics, University of Bath, England, whose hospitality is greatly acknowledged.

## References

[1] H.T. O'Neil, J. Acoust. Soc. Am., **21**, 516 (1949).
[2] B.G. Lucas and T.G. Muir, J. Acoust. Soc. Am., **72**, 1289 (1982).
[3] A.C. Baker, V.F. Humphrey and K. Anastasiadis, J. Acoust. Soc. Am., **84**, 1483 (1988).
[4] S. Nachef, *Generateur piezoelectrique d'ondes de choc a focalisation electronique*, Doctoral thesis, Institut national des sciences appliquées de Lyon 1992.
[5] J. Naze Tjotta and S. Tjotta, [in:] Frontiers of Nonlinear Acoustics [Ed.] M. Hamilton and D.T. Blackstock, Elsevier, London 1990, pp. 80.
[6] H. Hobaek, [in:] Ultrasonics International Conference Proceedings, 1981, pp. 123.

ARCHIVES OF ACOUSTICS
21, 1, 75–84 (1996)

# ACOUSTICAL MODELLING OF THE SURFACE SOURCES — IV INTERPOLATION MODEL, AXISYMMETRIC PROBLEM

A. BRAŃSKI

Institute of Technology
Pedagogical College
(35-310 Rzeszów, Reytana 16)

In the paper, the quadratic shape function were applied to construct an interpolation model of a plane axisymmetric source. Optimizing the least squares distance between the exact directivity function and directivity of the model, an optimal interpolation model was found. The optimal model was considered as a function of the shape of the vibration velocity, wave number and the place of the driving surface in the baffle. An optimal model was compared to other interpolation models, namely regular and irregular ones.

## 1. Introduction

An exact solution of the radiation acoustic problem of a complicated shape source and arbitrary vibration velocity can be obtained by numerical methods only. This problem is solved applying the boundary element method (BEM). The first step of BEM is discretization of the geometry of the source and the vibration velocity.

In the classical BEM the surface of the source is replaced by planar elements. In addition, the vibration velocity is represented by piecewise constant values on these elements. Then the elements vibrate as pistons. In this way a piston model of the source (PM) is obtained [15]. This model well approximates the source if it contain a lot of elements.

BEM was improved applying quadratic shape functions (interpolating functions) [1, 14]. Because the same shape functions are usually used to approximate both the geometry of the source and the vibration velocity [9, 13, 15–18, 21], then the source is replaced by an array of isoparametric elements. This array is called interpolation model (IM). The IM model yields more accurate result than PM model for the same number of surface elements. If the IM model is solved numerically [7, 10, 12], the disadvantage is arisen namely it is necessity to calculate double singular integrals. However, in the case of PM, double integrals can be converted analytically to single integrals [9].

Recently, an excellent computer program called BEMAP [19] was worked out to solve the acoustic field of the IM of an arbitrary source.

In Refs. [2, 3, 11], a PM of rectangular membranes was taken into account where the constant vibration velocity was assumed on each element. In paper [2], only the first mode of the membrane was analyzed but in [11] higher modes were dealt with. General rules of modelling plane rectangular sources with an infinite and rigid baffle were given in [3]. Axisymmetric sources with an infinite and rigid baffle were considered in [8].

It has been shown in references that the primary discretization (gives primary elements) is imposed by the singularities of geometry (edges and corners) and singularities of vibration velocity (nodal lines and extremum). Such obtained model did not give sufficient results. Then, in all the above mentioned works, more refined regular discretization (secondary discretization giving secondary elements) of primary elements was applied. But, as mentioned above, such a model (i.e. PM) consists of too many element or, during numerical calculations for IM, singular double integrals appear.

As pointed out in [4, 5, 6], the number of surface elements in PM may be reduced applying irregular secondary discretization. In particular an optimal piston model ($PM_o$) may be obtained. This model approximates most accurately the source for a fixed number of elements and fixed method for calculation of the vibration velocities on elements.

This paper discusses the application of irregular secondary discretization for constructing an optimal interpolation model ($IM_o$). As an example, an axisymmetric

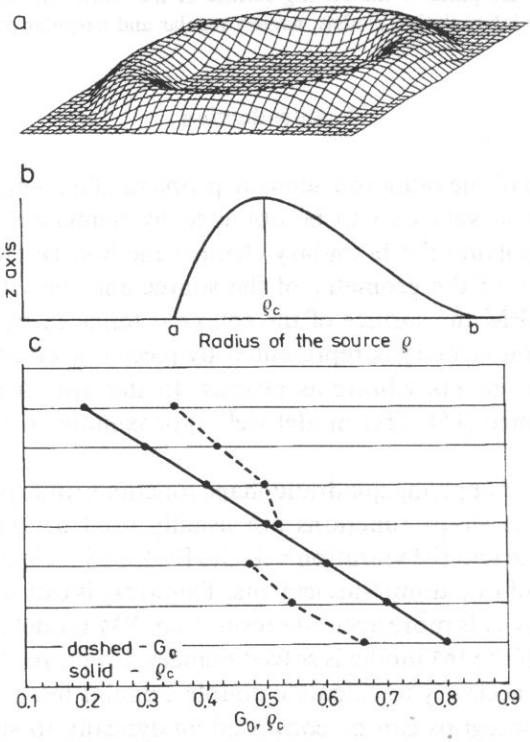


Fig. 1. (a) Picture of the driving surface, (b) Cross-section of the driving surface, (c) Places $\rho_c$ of the maximum of vibration velocity and boundary $G_o$ of the optimal interpolation model.

source with a plane infinite baffle was considered. Due to a symmetry with regard to z-axis, only the cross-section line of vibration velocity needs to be discretized. However, it is assumed that this line is asymmetrical with regard to its nodal points (see Fig. 1).

The problem of optimal model was analyzed depend on asymmetry of the line of vibration velocity, wave number (frequency of vibration) and the place of the driving surface in the baffle. Searching of $IM_o$ quite similar as in Ref. [6], a least squares distance between exact directivity function and of the model was optimalized. In the paper, it will not put any emphasis on mathematical aspects of optimalization problem. Rather, the numerical problems are presented with some details.

## 1. Directivity function of axisymmetric source

The acoustic field of a circular driving surface set in an infinite and rigid baffle is considered. Assuming axisymmetric (AS) vibration velocity, an axially symmetric field is obtained. The acoustic potential of this acoustic field is given by Helmholtz–Rayleigh integral [5]. The directivity function of such field normalized by the field of point source placed in an origin of coordinates is given by [6]:

$$Q_{ON}(\gamma) = \int_{\rho} v_{ON}(\rho)\, J_o(k\rho \sin\gamma)\, \rho d\rho\,, \tag{1.1}$$

where $J_o(x)$ — Bessel function of first kind and zero order, $k$ — wave number, $\rho$, $\phi$ — polar coordinates, $\gamma$ — azimuthal angle in spherical coordinates, $v_{ON}(\rho)$ — vibration velocity function, given explicite by

$$v_{ON}(\rho) = C_1 \sin\left(\pi \frac{\rho - a}{b - a}\right) \exp\left(-C_2 \frac{\rho - a}{b - a}\right). \tag{1.2}$$

The coefficients $C_1$, $C_2$ have been chosen to attain the assumed asymmetry of $v_{ON}(\rho)$. The Eq. (1.1) has been described extensively in Refs. [4, 5].

## 2. Directivity function of the model

After discretization of the driving surface, the vibration velocity of arbitrary $j$-element can be expressed in terms of its nodal values which are chosen in $i$-points as follow [1]:

$$v_j(\rho) \cong \sum_{i=1}^{I} N_i(\rho)\, v_j(\rho_i)\,, \tag{2.1}$$

where $N_i(\rho)$ — shape functions.

Equation (2.1) presents interpolation of function $v_j(\rho)$. From the properties of this interpolation it follows that the right hand side equals the left hand one only at $i$-points. In general, except $i$-points, the sign of equality cannot be placed in Eq. (2.1). An absolute error, as an effect of equality in Eq. (2.1) can be calculated analytically. But it will be an error of vibration velocity which, in acoustic, has no useful physical meaning.

The error brought about by Eq. (2.1) was evaluated indirectly analysing the convergence of both the exact directivity function and the model. The vibration velocity of this model was expressed by the right hand side of Eq. (2.1). The least squares distance was assumed as the measure of convergence of directivity functions [5]. Its value may be interpreted as an interpolation model error (IME). Substituting (2.1) into (1.1) we obtain

$$Q_{ON}(\gamma)=\sum_{j=1}^{J}\sum_{i=1}^{I} v_j(\rho_i)\int_{\rho_j} N_i(\rho)\,J_o(k\rho\sin\gamma)\,\rho d\rho. \tag{2.2}$$

Using formula (2.2) in numerical calculation is somewhat difficult because of the boundaries of each $j$-element change. To overcome this difficulty the shape function, coordinate $\rho$ and vibration velocity are expressed in nondimensional coordinates. In literature e.g. [14, 20], quadratic shape functions are recommended to interpolate a function of lower order

$$\begin{aligned} N_1(\xi)&=\xi(\xi-1)/2,\\ N_2(\xi)&=1-\xi^2,\\ N_3(\xi)&=\xi(\xi+1)/2, \end{aligned} \tag{2.3}$$

where $\xi\in\langle -1,1\rangle$.
In nondimensional coordinates the coordinate $\rho$ is given by

$$\rho(\xi)=\sum_{i=1}^{3} N_i(\xi)\,\rho_i, \tag{2.4}$$

Substituting (5) into (6) and assuming

$$\rho_1=G_1,\qquad \rho_2=\frac{1}{2}(G_1+G_2),\qquad \rho_3=G_2, \tag{2.5}$$

leads to

$$\rho(\xi)=\frac{1}{2}[\xi(G_2-G_1)+G_2+G_1]. \tag{2.6}$$

In Eq. (2.5) $G_1$ and $G_2$ are boundaries of $j$-element. These boundaries are consequence of discretization.

Now the values of $\rho_i$ can be calculated from Eq. (2.6) for $\xi=\xi_i$ where $\xi_1=-1$, $\xi=0$, $\xi_3=1$.

In Eq. (2.2), it is advisable to express also $v_j(\rho_i)$ as a function of $\xi_i$. Using Eq. (2.4) we obtain

$$v_j(\rho_i)=v_j[\rho(\xi_i)]\,. \tag{2.7}$$

Because the integration is to do with respect $\xi$ instead of $\rho$ than the Jacobian $J_B$ of the transformation (2.4) is

$$J_B=\frac{\partial\rho}{\partial\xi}=\frac{1}{2}(G_2-G_1)\,. \tag{2.8}$$

Making use of Eqs. (2.3), (2.4), (2.7) and (2.8) in Eq. (2.2) gives

$$Q_{ON}(\gamma)=\sum_{j=1}^{J}\sum_{i=1}^{3} v_j[\rho(\xi_i)]\int_{-1}^{1} N_i(\xi)\,J_o[k\rho(\xi)\sin\gamma]\,\rho(\xi)\,J_B(\xi)\mathrm{d}\xi\,. \tag{2.9}$$

Equation (2.9) presents the directivity function of the interpolation model and together with (1.1) constitutes the basis of numerical calculations.

## 3. Numerical calculations

In the numerical calculations a vibration velocity function without internal points is applied. Furthermore, its maximum is not half distance between nodal points [5, 6], it reaches its maximum value at $\rho_c$ ($\rho_c\in\langle a,\ b\rangle$). Outer and inner radius of the driving surface are marked by $a$ and $b$ respectively, $b=a+1$ (Fig. 1).

The numerical calculations are performed for three two-element models, i.e. $J=2$, obtained as a result of:

1 — regular discretization leading to the regular interpolation model ($IM_r$),

2 — irregular discretization leading to the irregular interpolation model ($IM_i$) where the discretization passes on $\rho_c$, i.e. the maximum of the vibration velocity,

3 — optimization of least squares distance between exact directivity function and the directivity function of optimal interpolation model ($IM_o$).

The boundary between the elements of the over determined models was denoted as $G_r=G_{0.5}=0.5$, $G_i=\rho_c$ and $G_o$ respectively. The models were compared with one another based on the analysis of the least squares distance among the exact directivity functions exact and of the models.

This comparison is made in relation to:

A — shape of vibration velocity function given by $\rho_c$

B — wave number $k$,

C — position of driving surface in the baffle given by $a$.

Here, least squares distance is a measure of the error of each of the interpolation models (IME) [6]. This error depends on both the discretization (number of elements and boundaries among them) and the number of $i$-points chosen on the element.

I. In first part of the numerical calculations, the influence of the shape vibration velocity on the construction of the model and on their directivity functions was searched; it was assumed that $k=2.5$, $a=0$. Boundary $G_o$ if $IM_o$ (dashed line) and the place $\rho_c$ of maximum vibration velocity (solid line) were shown in Fig. 1c. An examination of this figure indicates that boundary $G_o$ does not coincide with maximum $\rho_c$. Only for $\rho_c=.5$ boundary $G_o$ is quite close to this value i.e. $G_o=.52$.

The errors of the models as a function of shape vibration velocity are presented in Fig. 2. It can be seen from this figure that $IM_o$ assures the least error $IM_oE$. Furthermore, in the range $\rho_c \in \langle .2, .6 \rangle$ this error is almost constant. All models give a good convergence only for $\rho_c \cong .5$.

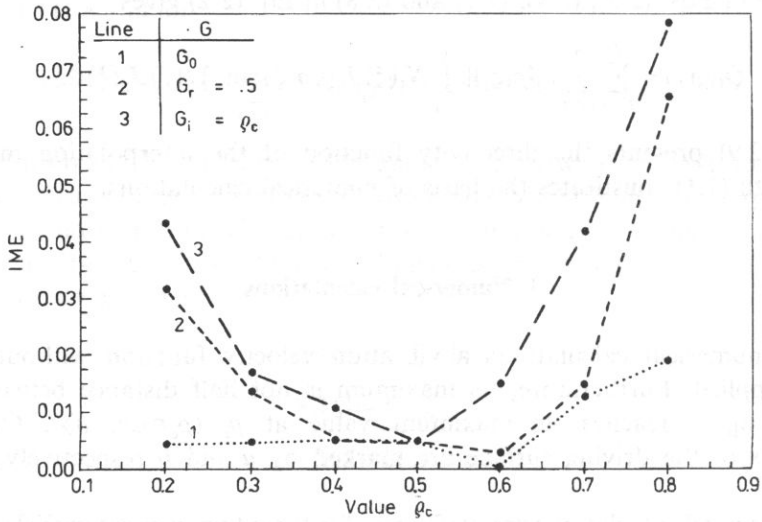


Fig. 2. Interpolating model error in the shape of the vibration velocity; $k=2.5$, $a=0$.

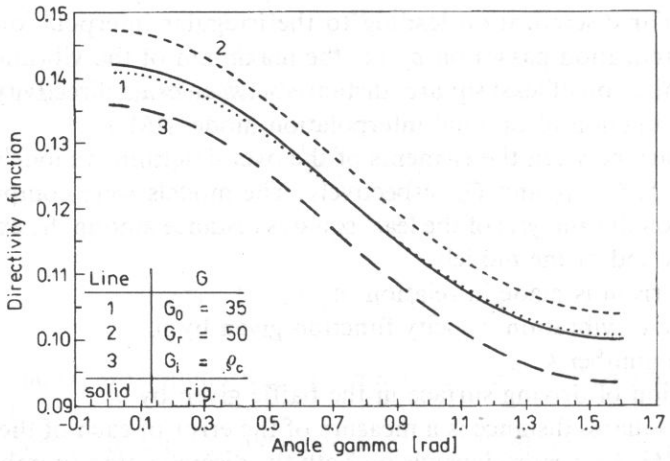


Fig. 3. Directivity functions of the models; $k=2.5$, $\rho_c=.2$, $a=0$.

To check the convergence of exact directivity function and of the model, expressed by IME, the directivities of each of the models, for $\rho_c = .2$, were depicted in Fig. 3. Of course, the best agreement of the directivities is for $IM_o$. While examining Fig. 3 it is interesting to note that, for $\rho_c = .2$, $IM_oE = .004439$ and it is about 10 times less than $IM_iE = .043190$, but about 7 times less than $IM_{0.5}E = .031444$.

II. In the second part of the numerical calculations the influence of the wave number $k$ on the models is investigated. The numerical calculations are run only for one shape of the vibration velocity function i.e. $\rho_c = .2$ and $a = 0$ is assumed. Values of $G_o$, for separate $k$, are given in Table 1.

**Table 1.**

| $k$ | 1 | 2 | 3 | 4 | 5 | 6 | 7 | 8 | 9 | 10 | 20 |
|---|---|---|---|---|---|---|---|---|---|---|---|
| $G_o$ | .37 | .36 | .35 | .34 | .34 | .34 | .34 | .34 | .33 | .33 | .32 |

As can be seen from Table 1, boundary $G_o$ does not significantly change for $k \in \langle 1, 20 \rangle$, particularly for its higher values. Figure 4 presents the values of the model errors as a function of $k$. This figure shows that the error $IM_oE$ is the least and its changeability is not large.

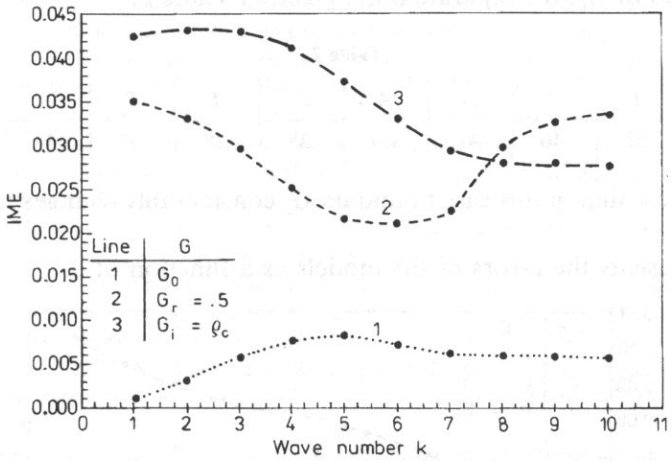


Fig. 4. Interpolating model error in the wave number $k$; $\rho_c = .2$, $a = 0$.

The discrepancy between the exact directivity function and that of the model, for $k = 10$, i.e. such directivity functions which have sharp minimum, is given in Fig. 5. Numerical calculations performed in detail pointed out that the sharp minimum of exact directivity function and of the models $IM_o$, $IM_r$, $IM_i$ are in space described by angle $\gamma$ equal 0.8, 0.8, 0.73 and 0.83 respectively. The discrepancy between directivity functions presented above reflects the errors given in Fig. 4 for $k = 10$; $IM_oE = .005568$ and it is about 5 times less than $IM_iE = 0.0276395$ and about 6 times less than $IM_rE = 0.3342$.

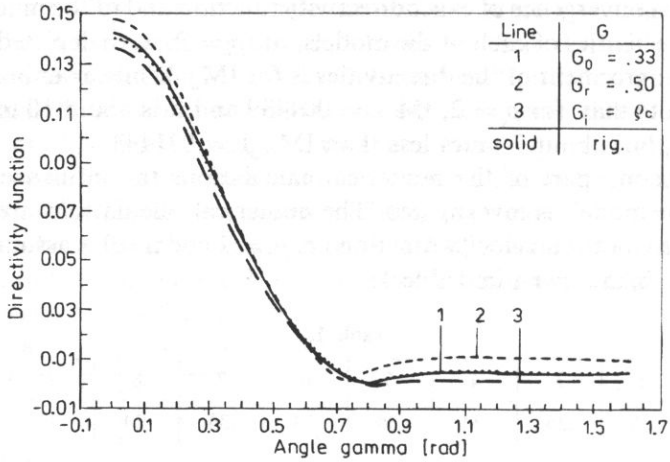


Fig. 5. Directivity functions of the models; $k=10$, $\rho_c=.2$, $a=0$.

III. In the last part of numerical calculations, the influence of the place of driving surface described by value $a$ on the models is considered; $\rho_c=0.2$ and $k=2.5$ are assumed. Values of $G_o$, for separate $a$ are given in Table 2.

**Table 2.**

| $a$ | 0. | .1 | .2 | .3 | .4 | .5 | .6 | .7 | .8 | .9 | 1. |
|---|---|---|---|---|---|---|---|---|---|---|---|
| $G_o$ | .35 | .37 | .40 | .41 | .40 | .38 | .38 | .37 | .37 | .37 | .37 |

The data show that in this case boundary $G_o$ considerably changes for little values $a$ only.

Figure 6 presents the errors of the models as a function of $a$.

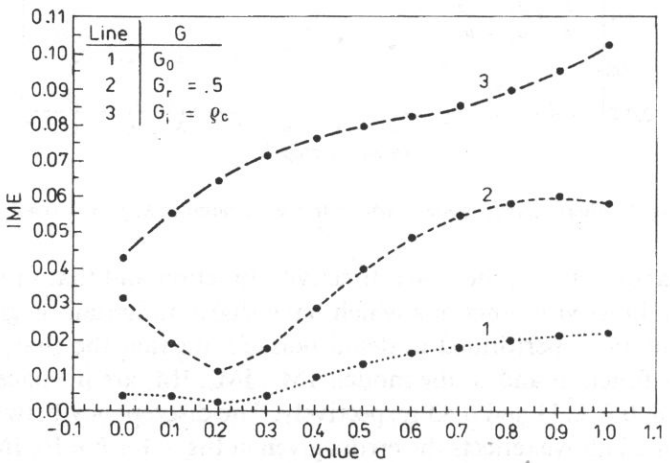


Fig. 6. Inteprolating model error in the place of driving surface in the baffle; $k=2.5$, $\rho_c=.2$.

## 4. Conclusions

The numerical analysis performed in this paper results in noticeable conclusions:

1 — directivity function of optimal interpolation model is more convergent to exact directivity than the directivity of a regular model and irregular model if the discretization passes on the maximum of vibration velocity,

2 — the best convergence directivity function of $IM_0$ and exact directivity is noted for:

- vibration velocity symmetric to its nodal points,
- low values of wave number,
- the place of the vibrating surface near the axis of the source.

3 — the place of $G_0$ depends a low degree on the wave number $k$.

## References


[1] J.K. BATHE, E.L. WILSON, *Numerical methods in finite element analysis*, Prentice Hall, Englewood Cliffs 1976.

[2] A. BRAŃSKI, R. PANUSZKA, M. ZABAWA, *Sound radiation by a rectangular plate represented by a model in form of a system of rectangular pistons*, Proceedings Noise Control'79, Vol. II, 53–56, Warszawa 1979.

[3] A. BRAŃSKI, *Acoustical model of the plates* (in Polish), WSP, Rzeszów 1991.

[4] A. BRAŃSKI, *Acoustical modelling of the surface sources — I. Piston model, discretizating error, axisymmetric problem*, Archives of Acoustics, **20**, 4, 311–326 (1995).

[5] A. BRAŃSKI, *Acoustical modelling of the surface sources — II. Piston model, symmetrical vibration velocity, discretizating error, axisymmetric problem*, Archives of Acoustics, **20**, 4, 327–345 (1995).

[6] A. BRAŃSKI, *Acoustical modelling of the surface sources — III. Piston model, model error, axisymmetric problem*, Archives of Acoustics, **20**, 4, 347–359 (1995).

[7] C.C. CHIEN, H. RAJIYAH, S.N. ATLURI, *An effective method or solving the hypersingular integral equations in 3-D acoustic*, J.A.S.A., **88**, 2, 918–937 (1990).

[8] A. DOBRUCKI, *Modelling of the Acoustical Systems* (in Polish), Raport nr I-28 (s-54) 90, Wrocław 1990.

[9] Y. FURUE, *Calculation of sound diffraction by means of the integral equation*. The second Joint Meeting of ASA and ASJ, (1988), private communication.

[10] G. KRISHNASAMY, L.W. SCHMERR, T.J. RUDOLPHI, F.J. RIZZO, *Hypersingular boundary integral equations: some applications in acoustic and elastic wave scattering*, Trans. ASME J. Appl. Mech., **57**, 404–414 (1990).

[11] L. LENIOWSKA, A. BRAŃSKI, *The directivity function of the model rectangular plate vibrating with the higher modes*, Proceedings Noise Control'88, Vol. I, 263–266, Cracow 1988.

[12] P. LINZ, *On the approximate computation of certain strongly singular integrals*, Computing 35, 345–353 (1985).

[13] W.L. MEYER, W.A. BELL, B.T. ZINN, *Boundary integral soluton of three dimensional acoustic radiation problems*, J. Sound Vib., **59**, 2, 245–262 (1978).

[14] A. RALSON, *A first course in numerical analysis* (in Polish), PWN, Warszawa, 1983.

[15] A.F. SEYBERT, B. SOENARKO, F.J. RIZZO, D.J. SHIPPY, *Application of the BIE method to sound radiation problems using an isoparametric element*, ASME Trans., **106**, 414–420 (1984).

[16] A.F. SEYBERT, B. SOENARKO, F.J. RIZZO, D.J. SHIPPY, *An advanced computational method for radiation and scattering of acoustic waves in three dimensions*, J.A.S.A., **77**, 2, 362–368 (1985).

[17] A.F. SEYBERT, B. SOENARKO, *Radiation and scattering of acoustic waves from bodies of arbitrary shape in a three-dimensional half space*, ASME Trans., J. Vib. Acoust. Stress Rel. Dsgn., **110**, 112–117 (1988).

[18] A.F. SEYBERT, T.W. WU, *Modified Helmholtz integral equation for bodies sitting on the infinite plane*, J.A.S.A., **85**, 1, 19–23 (1989).

[19] A.F. SEYBERT, T.W. WU, G.C. WAN, *BEMAP-Computer Program* Spectronics, INC., 2100 Elgin Place, Lexington, KY 40515, private communication.

[20] A.F. SEYBERT, Z.H. JIA, T.W. WU, *Solving knife-edge scattering problems using singular boundary elements*, J.A.S.A., **91**, (3), 1278–1283 (1992).

[21] T. TERAI, *On calculation of sound fields around three dimensional object by integral equation methods*, J.S.V., **69**, 1, 71–100 (1980).

ARCHIVES OF ACOUSTICS
21, 1, 85–88 (1996)

# OPTIMAL CONDITIONS FOR THE GENERATION SYSTEM OF A SAW GAS SENSOR

M. URBAŃCZYK and W. JAKUBIK

Institute of Physics, Silesian Technical University
44-100 Gliwice

The present paper describes the optimal conditions for generating a Surface Acoustic Wave (SAW) for a gas sensor system. For achieving stable operation it is necessary to assure the largest possible distance between the frequency modes. In order to attain this condition, the length between transducers should be decreased accordingly.

## 1. Introduction

The basic system for SAW gas sensors is a generator in which an acoustic delay line works in the positive feedback loop of the amplifier. The acoustic delay line assures the phase condition for generation whilst the amplifier assures the amplitude condition. The amplifier gain should be higher than delay — line insertion losses.

The SAW can be excited with the use of the interdigital transducers, one being a transmitter and the other one a receiver. The acoustic path of the delay line is usually covered in a vacuum by a thin chemical layer. This layer has some selective absorbing properties and can interact with gas molecules from the ambient atmosphere. Such layers are, for instance, macromolecular compounds, such as organic polymers [1] and phthalocyanines [2].

A change in the physical properties of these layers affects the SAW propagation in an acoustic delay line. Particularly, as a result of the change of mass and electrical conductivity of the layer, the velocity of a SAW undergoes a change. Consequently, as a result of the velocity change, the phase conditions undergoes a disturbance and a new frequency is generated depending on the gas concentration monitored in the ambient atmosphere [3].

## 2. The frequency and modal characteristic of a SAW generator

Taking into account the work of the SAW generator it is important to distinguish two essential parts which form the frequency characteristic of the generation system:

a. the system: transmitter – receiver,
b. the delay line system.

The interdigital Rayleigh wave transducers have a frequency characteristic of the $|\sin(x)/x|$ type [4], shown in Fig. 1, where:

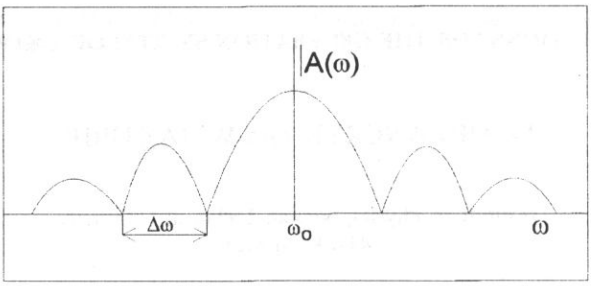


Fig. 1. Frequency response for an interdigital Rayleigh wave transducer.

$$x=\frac{N\pi(\omega-\omega_0)}{\omega_0}, \tag{2.1}$$

$N$ — is the number of finger pairs in the transducer, $\omega_0$ — is the fundamental resonant frequency.

The fundamental resonant frequency $\omega_0$ is specified by the geometric dimensions of the transducer, that is, by the electrode width and the SAW velocity in a waveguide medium:

$$\omega_0=\frac{2\pi v_0}{4p}, \tag{2.2}$$

where: $v_0$ — is the propagation velocity of SAW, $p$— is the finger width (equal to the spacing between electrodes).

The zeros of the frequency characteristic will be for $\omega_n$ given by the equation

$$\omega_n=\omega_0\pm n\frac{\omega_0}{N}, \tag{2.3}$$

when $n=1, 2, 3,...$
and the distance between them, $\Delta\omega$ is

$$\Delta\omega=\frac{\omega_0}{N}. \tag{2.4}$$

The acoustic line system specifies the frequencies when the generator oscillation is possible. The modal characteristic is specified by the following formula [5]:

$$\frac{\omega L}{v_0}+\Phi_T+\Phi_A=2\pi n, \tag{2.5}$$

where: $\Phi_T$, $\Phi_A$ — are the phase shifts in the transducers and amplifier, respectively, $L$ — is the length of the delay line (distance between the middle point of the transducers), $\omega$ — is the generation frequency.

If the length, $L$, is sufficiently large, the phase shifts in the transducers and amplifier can be neglected. So, the frequency modes of the generator are equal:

$$\omega_n = n\frac{2\pi v_0}{L}, \tag{2.6}$$

where: $n=1, 2, 3,...$
with the distance between them:

$$\delta\omega = \frac{2\pi v_0}{L}. \tag{2.7}$$

In the fundamental resonant frequency range of the transducers system a certain number of mode frequencies can appear for which the amplitude condition of the generation will be fulfilled. The amplifier gain will be larger than the signal attentuation in this case (Fig. 2).

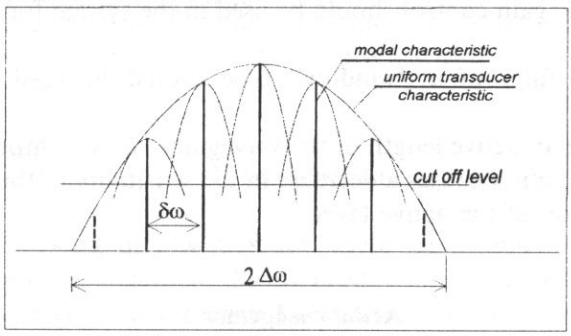


Fig. 2. The modal characteristic of the generation system.

An interaction between the gas and the active layer causes a change in the SAW propagation velocity and, consequently, in the general frequency. If the frequency change is too large, we observe a "jump" to the next frequency mode. For achieving a stable work of the generation system of the SAW sensor it is necessary to assure a possibly large distance, $\delta\omega$, between the frequency modes. In this case a large frequency range of the sensor work will be achieved.

In the case of the dual-delay line configuration there is a possibility to working at the fundamental frequency $\omega_0$. In this case, the following condition must be fulfilled:

$$\delta\omega = \Delta\omega. \tag{2.8}$$

The generator mode frequencies, except $\omega_0$, covers the "zeros" of the transducers frequency characteristic in this case.

Formulas (2.2), (2.4) and (2.7) imply that the condition (2.8) will be fulfilled when the distance between the transducers, $L$, will be equal to the length of one of them $L_p$, i.e.

$$L=4pN=L_p. \tag{2.9}$$

The second transducer is a wideband with a small number of electrodes.

In practical the fulfilment of the condition (2.8) and (2.9) is rather difficult to achieve. The distance between the transducers has become so small that the active layer square placed between them is not sufficient for obtaining an adequate sensor sensitivity.

## 3. Conclusions

The main conclusion concerning optimal conditions for the generation system of the SAW sensor are:

1. The length between the transducers, $L$, should be decreased properly in order to fit the necessary generation frequency range change.
2. An automatic gain control should be used in the system for a wider frequency generation range.
3. A bandpass filter of a "window" type should be used with a bandwith equal to $2\Delta\omega$.

When matching an active length of the waveguide, $L$, it is important to take into account that its reduction causes a decrease in the sensitivity of the sensor as a result of the area limitation of the active layer.

## Acknowledgements

The work was sponsored by the Polish State Committee for Scientific Research within grant 16.8T10C03608.

## References

[1] H. WOHLTJEN, *Mechanism of operation and design considerations for Surface Acoustic Wave device vapour sensor*, Sensors and Actuators, 5, 307–325 (1984).

[2] A.J. RICCO, S.J. MARTIN, T.E. ZIPPERIAN, *SAW gas sensor based on film conductivity changes*, Sensors and Actuators, **8**, 319–333 (1985).

[3] M. URBAŃCZYK, W. JAKUBIK and S. KOCHOWSKI, *Sensor properties investigation of copper phtalocyanine with use of SAW*, Sensors and Actuators, **B, 22**, 2, 133–137 (1994).

[4] H. MATTHEWS, *Surface wave filters. Design, construction and use*, John Wiley and Sons, New York–London–Sidney–Toronto 1977.

[5] M.F. LEWIS, *Surface acoustic wave devices and applications*, Ultrasonics, 115–123 (1974).

ARCHIVES OF ACOUSTICS
21, 1, 89–98 (1996)

# THE APPLICATION OF A NEURAL NETWORK TO CLASSIFY THE ACOUSTIC EMISSION WAVEFORMS EMITTED BY THE CONCRETE UNDER THERMAL STRESS

Z. RANACHOWSKI

Institute of Fundamental Technological Research
Polish Academy of Sciences
(00-049 Warszawa, ul. Świętokrzyska 21)

In this article Acoustic Emission (AE) measurement results for five different compositions differing in compression strength are presented. Thermal stresses occuring in concrete samples during their cooling after heating up to 150°C in controlled conditions have been the source of AE signals. The influence of structure of frequency spectra of recorded AE signals is described. An automatic recognition procedure of the recorded AE waveforms using neural network is discussed and the details of the learning process of the neural network are shown.

## 1. Introduction

The thermal working in low-pressure steam environment is in Poland wide introduced technological treatment during production of prefabricated elements [1]. The heating period may usual vary from single to several hours while the hydratation processes in concrete matrix are improving and the presence of hardened regions in the material are formed. The internal stresses occurring in the fast hardening material are the drawback of the described technology, caused by the local temperature gradients and different volume changes of the concrete ingredients. For example the linear thermal expanding rate of the gravel aggregates may be five times smaller than the same parameter of the concrete matrix. The increasing stress concentration in the structure under thermal processing may result in some internal defects as microcracks and porosity increase.

In the following paper the correlation between frequency spectra of the AE signals registered during thermal stress relaxation processes and the compression strength of the different concrete compositions is discussed. The occurrence of the maxima on the spectral pattern of the registered AE waveforms have been used to characterise the certain concrete composition and to determine its strength to be fed into automatic recognition procedure, the spectral patterns were digitised as it is shown in the further sections of this work.

## 2. Experimental materials and methods

Five concrete compositions, similar to used in [2], are indicated in Table 1. The cement of Grade "35" was used. The specimen were 140 millimeters long, 40

**Table 1.** Physical and structural parameters of the compositions used for the investigation

| Set number | seeming density [$Tm^{-3}$] | specific density [$Tm^{-3}$] | porosity [%] | water to cement ratio | aggregate to cement ratio | sand to cement ratio | compressive strength [MPa] |
|---|---|---|---|---|---|---|---|
| 0 | 1.20 | 1.67 | 34.2 | 0.4 | 0 | 0 | 48.0 |
| I | 2.129 | 2.559 | 16.8 | 0.4 | 0.45 | 2.2 | 43.0 |
| II | 2.096 | 2.560 | 18.12 | 0.5 | 0.33 | 3.0 | 37.5 |
| III | 2.075 | 2.564 | 19.07 | 0.6 | 0.23 | 4.3 | 23.0 |
| IV | 2.054 | 2.565 | 19.92 | 0.65 | 0.20 | 5.0 | 21.8 |

millimeters wide and 40 millimeters thick. The set labelled "0" was made of mortar while the other sets were made of standard, medium plasticity concrete. All the samples were heated in the oven with controlled temperature gradient. They were left in the temperature 150°C for two hours. Then, after removing from the oven the sample were cooled with use of a fan. The first 20 minutes of the cooling process were used to register the AE signals. Then the inner temperature of the samples came to the ambient value. The temperature sensor was fixed to the sample 50 millimeters from its colder end and 30 millimeters from the same end the wideband AE sensor was mounted. The sensor, type WD SN954 made in Physical Acoustic Corporation performs flat (+/−20 dB) response to the AE signals within the frequency band 50 − 800 kHz when matched to the block of concrete. The AE signals were amplified and high-pass-filtered (over 25 kHz) with the use of EA200 Acoustic Emission Processor, made in Institute of Fundamental Technological Research. The IWATSU DS 6612C storage oscilloscope was connected to the output of AE processor to capture the AE waveforms. When the amplitude of the AE signal (after 80 dB amplification) was greater than 100 mV, the trigger of the oscilloscope enabled the capturing of 500 microsecond of the AE signal at a sampling rate of 2 MHz. Several hundreds of such waveforms caused by the thermal stresses in the concrete samples under test were stored in the disk of logged — in PC computer with the application of the procedure described above.

## 3. Spectral characteristic of measured concrete samples

The averaging of 100 AE waveforms for each of 5 tested sets of samples, differing in compression strength was made for the purpose of further processing using neural network. The examples of averaged spectra calculated for the sets labelled as "0", "II" and "IV" are presented in Fig. 1 − 3. The distinct patterns of presented spectra

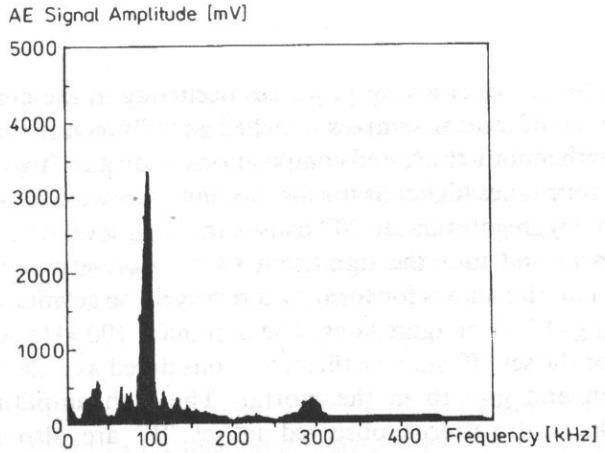


Fig. 1. Averaged spectrum of concrete composition "0", constructed in linear scale. The amplitude of the AE signals was measured after 40 dB amplification.

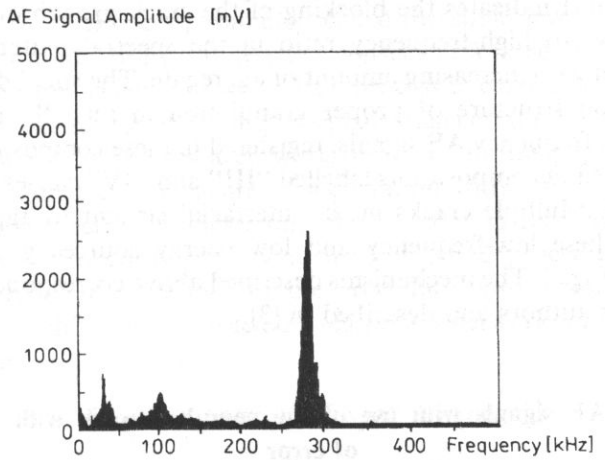


Fig. 2. Averaged spectrum of concrete composition "II", constructed in linear scale. The amplitude of the AE signals was measured after 40 dB amplification.

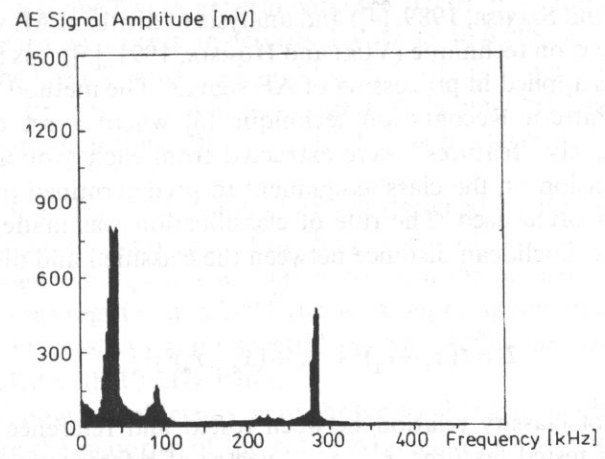


Fig. 3. Averaged spectrum of concrete composition "IV", constructed in linear scale. The amplitude of the AE signals was measured after 40 dB amplification.

are related to the nature of cracking processes occurring in the compositions under investigation. The set of mortar samples (labelled as "0") having the highest value of compressive strength among the tested compositions, indicated high — amplitude EA pulses — approx. four times higher as for the mechanically weakest set, labelled "IV". The absence of the aggregates in set "0" causes the high level of contraction during fabrication processes and thus the significant (34%) porosity of the material. The structure of such material allows for forming a relatively large microcracks due to the lack of the blocking effects of aggregates. The dominant 100 kHz components of the spectral pattern for the set "0" may be therefore considered as reflecting the processes of crack initiation and growth in the mortar. The high amplitudes of 100 kHz components of spectral patterns observed in set "I" are also related with the mechanism described for the pure mortar. The low contents of aggregates for this set let us suppose that the dominant effects here are appears in the spectral pattern of set "I". The latter effect indicates the blocking of the crack growth due to aggregates. The different low- to high-frequency ratio in the spectral patterns is present in samples composed with increasing amount of aggregate. The small dimensions of the cracks, blocked on structure of proper granulation in sets "I" and "II" enable generation of high frequency AE signals, registered in these compositions. More sand and aggregates used in compositions labelled "III" and "IV" causes the compression strength decrease. Multiple cracks in the interfacial cement to aggregate zone are observed here. These low-frequency and low energy sources produce a spectral pattern shown in Fig. 3. The mechanisms described above correspond with the results obtained by other authors and described in [3].

## 4. Processing of AE signals with use of the neural network with backpropagation of error

Since an identification of artificial AE sources with use of neural associative memory (GRABEC and SACHSE, 1989, [4]) and analysis of artificial AE waveforms using neural backpropagation technique (YUKI and HOMMA, 1991, [5]) was made, the neural network analysis is applied in processing of AE signals. The method has replaced the previously used Pattern Recognition technique [6] where a set of characteristic measurements, namely "features" were extracted from each grouping of measured data. To make decision on the class assignment to predetermined pattern the linear classifier was most often used. The rule of classification was made on the basis of finding the minimal Euclidean distance between the classified and different reference sets of features:

$$D=((x_1-r_1)^2+ \ldots +(x_n-r_n)^2)^{1/2}. \tag{4.1}$$

Here: $D$ distance of classify relation between tested and reference set of features, $x_1 \ldots x_n$ — vector of tested features, $r_1 \ldots r_n$ — vector of reference features.

The described above linear classifier seemed to be insufficient to determine within the class of *linear non separable vectors* (MINSKY and PAPPERT, 1969 [7]). The non-linear neural backpropagation algorithm is able to solve the problem. Neural networks are computer models of circuits composed of multi-input vs. angle output elements (neurons) connected in serveral chains called layers. Each neuron output (except the output layer) is connected with all the neurons, consisting the next layer. The relation between element input and output signal can be expressed as:

$$y_j(t+1)=\theta(\Sigma_j w_{ij} x_j(t)-\mu_i). \tag{4.2}$$

Here: $y_i(t+1)$ — neuron output signal after signal processing cycle, $\theta$ — one of the neural activation functions [in this paper assumed as $1/(1+\exp(-x))$], $w_{ij}$ — called a weighting coefficient a synaptic weight which expresses the bonding strength, between connected neurons labelled $j$ and $i$, $x_j(t)$ — neuron input signal before signal processing cycle, $\mu_i$ — process parameter, called threshold level.

The computer model of neural network consists of a table of weight coefficients, being modified in the *learning process*. This process is carried out to vary synaptic weights to obtain desired network output signal when certain signal is fed to input of the network. The aim of the research work presented in this paper was to form the network output signal as a measure of association with one of the five averaged acoustic emission spectra characterising the tested concrete compositions. Each weight was changed according to wide used iterative procedure called "backpropagation of error" [8]. The idea of the procedure is to make a weight changes proportional to the difference between the temporary network output and the desired (optimal) output:

$$\Delta w_{ij}^{(k)}=\eta_1(d\theta(E_i)/dE)\, x_j\, \delta_i^{(k)}+\eta_2 m_{ij}^{(k+1)}. \tag{4.3}$$

Here: $\theta$ — activation function, $\Delta w_{ij}^{(k)}$ — weighting coefficient between neuron labelled $i$ in the layer $k$ and neuron $j$ in the layer $(k-1)$, $\eta_1$ — parameter called learning rate, in described work experimental set to 0.01, $\eta_2$ — momentum, parameter optimising the learning process, in described work set to 0.008, $E_i$ — total excitation of $j$-th neuron in the layer $k$, equal to $\Sigma_j w_{ij}^{(k)} x_j$, $z_i$ — desired signal at $i$-th output of the network, $y_i$ — temporary signal at $i$-th output of the network, $m_{ij}$ — weight change used in the previous iteration, $\delta_i^{(k)}-z_i-y_i$ for the output layer or $\Sigma_1 w_{1i}^{(k)} \delta_1^{(k+1)}$ for the other layers.

Algorithm, described as formula (3.3) was designed by P.J. Werbos in 1974 but was wider practised ten years ago. For the purpose of the research work described here, the following assumptions was taken to form the data processing procedure:

- AE waveforms registered in 200 bytes with sampling rate of 2 MHz were used in averaging process to obtain spectral power coefficients while each coefficient corresponded with 10 kHz band,
- 31 spectral power coefficients were chosen to characterise the range of 30–310 kHz, where the majority of the entire AE signal power is included,

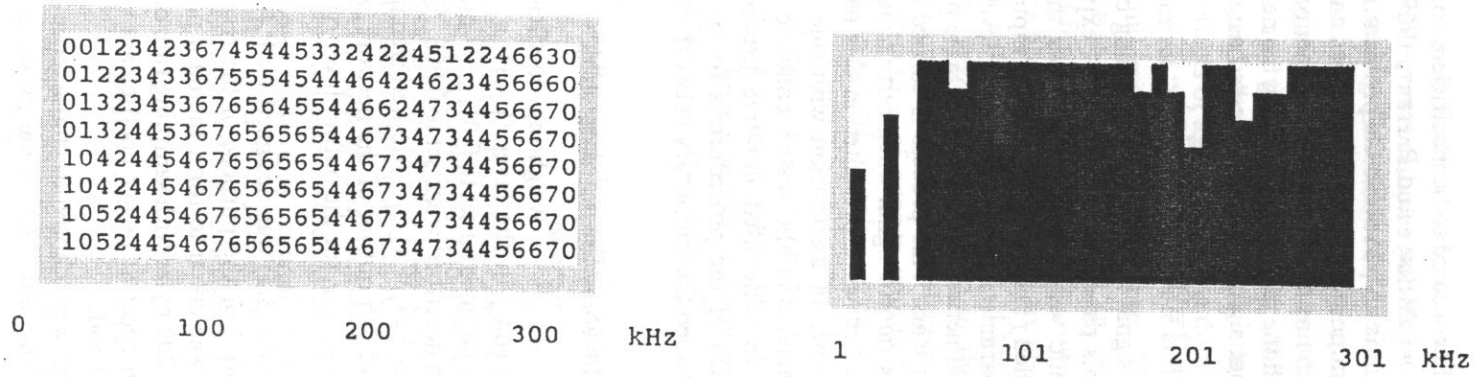


Fig. 4. Number of the occurrences of certain patterns elements for waveforms registered in composition labelled "0" (left). The averaged pattern for these waveforms (right).

- the used neural network was able to analyze 8 signal levels of the values of discretized spectral power coefficients (the discretization was set up every 6 dB of the signal level),
- this spectral modelling scheme required 31 times 8 binary inputs to the network, connected to 62 neural units used in the first layer,
- the second layer consisted of five neurons to generate five output signals due to association between the input signals and five learned patterns.

The following procedure was used to prepare the five spectral patterns representative for five tested concrete compositions. Seven most typical AE waveforms were chosen for each composition and their discrete spectral patterns were combined at one graph. The left side of the Fig. 4 presents the numbers proportional to the occurrences of certain pattern elements in seven waveforms registered for composition labelled "0". The pattern element was used in the learning process if it was present in not less than in three waveforms used to compare. The averaged pattern for composition labelled "0" is shown at the right side of Fig. 4. The Fig. 5 and 6 present the averaged patterns obtained for the compositions labelled "II" and "IV".

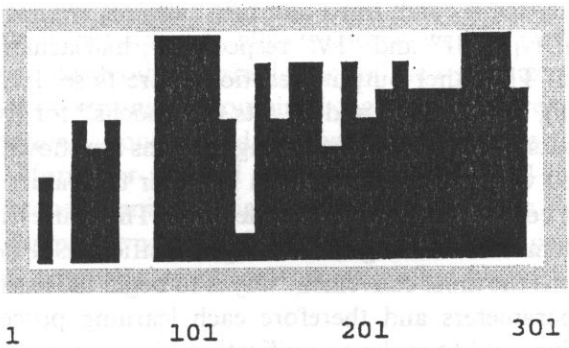


Fig. 5. The averaged pattern constructed for the waveforms registered in composition labelled "II".

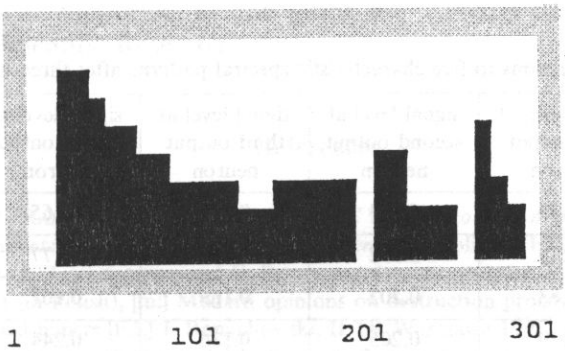


Fig. 6. The averaged pattern constructed for the waveforms registered in composition labelled "IV".

## 5. Process of learning the neural network

The main shortcoming of the backpropagation method of learning the network is longer period of the iterative process when comparing to other methods. The advantage of backpropagation is its algorithm — simple and therefore easy to modify the size of processed binary pattern. The important point is that time required for the single iteration step is proportional to the number of the network interconnections. Such iteration step called "epoch" lasted aporox. 0.3 s for the network configuration described in Section 3 when executed on PC 486 DX/40 MHz computer. 800 sets of repetitions had to be run to complete the learning process. The operation of comparing the learned pattern and test signal took approx. 1 s. The procedure of learning the network consisted of several steps. Five spectral patterns, corresponding to five concrete compositions were presented in controlled order to overcome the effect of gradual disappearing of previously formed associations when the new associations were formed. After the three series of learning steps (400, 300 and 50 sets of "epochs" for each pattern) the network was able to produce the signals at its outputs as it is shown in Table 2. The values presented in five consecutive rows of the table correspond with the network reactions to presentation of five characteristic spectral patterns. Only the second, third and fifth outputs, trained to be associated with compositions of type "II" and "IV" respectively, had achieved the ability of proper determination. The other outputs reactions were false. In the next part the three series of learning steps (25, 20 and 15 sets of "epochs" for five patterns) were performed. The outputs obtained for five testing patterns are shown in Table 3. Each output was associated with the proper pattern however the values generated as the reaction for different compositions were not identical. The cause of this effect is the influence of the random initial setting of the weight coefficients. For large sets of the neural interconnections the most convenient way is to begin the learning process with randomised initial parameters and therefore each learning process comes to the unique final equilibrium and to make an unification of output signals the additional signal processing is required.

**Table 2.** Network reactions to five characteristic spectral patterns after three series of learning

| pattern symbol | signal level at first output neuron | signal level at second output neuron | signal level at third output neuron | signal level at fourth output neuron | signal level at fifth output neuron |
|---|---|---|---|---|---|
| 0 | 0.179 | 0.184 | 0.140 | 0.165 | 0.114 |
| I | 0.179 | 0.212 | 0.154 | 0.177 | 0.125 |
| II | 0.183 | 0.202 | 0.169 | 0.167 | 0.126 |
| III | 0.179 | 0.205 | 0.136 | 0.244 | 0.135 |
| IV | 0.175 | 0.200 | 0.137 | 0.224 | 0.139 |

**Table 3.** Network reactions to five characteristic spectral patterns after six series of learning

| pattern symbol | signal level at first output neuron | signal level at second output neuron | signal level at third output neuron | signal level at fourth output neuron | signal level at fifth output neuron |
|---|---|---|---|---|---|
| 0 | 0.195 | 0.236 | 0.263 | 0.119 | 0.211 |
| I | 0.186 | 0.277 | 0.275 | 0.130 | 0.223 |
| II | 0.192 | 0.259 | 0.311 | 0.120 | 0.220 |
| III | 0.182 | 0.202 | 0.161 | 0.219 | 0.221 |
| IV | 0.174 | 0.238 | 0.210 | 0.216 | 0.254 |

## 6. Conclusions

After completion of learning process where the averaged spectral patterns were used, reactions of the network for real signal patterns presentation were tested. The proper outputs for the patterns of type "III" was observed in 67% of all cases however for other types approx. 60% patterns were classified right. It can be explained with the considerable dissimilarities of the real patterns and the occurrence of sample signals representing the combined character of more than one spectral type. Considering these limitations the adaptative algorithm able to determine different categories of waveforms or spectral patterns may be useful in practise to examine large records of acoustic emission signals. The collected sets of data concerning the different standard concrete compositions can be used to compare with tested samples during the routine compression strength investigation.

## Acknowledgement

This work was supported by the grant no. 7 T07B 020 08 of Polish State Committee for Scientific Research.

## References

[1] J. Hoła and Z. Ranachowski, *Application of AE method to determination of technological and exploatation parameters to destruction process in concrete* (in Polish), IFTR Reports 37 (1992).

[2] A. Jaroszewska, J. Ranachowski and F. Rejmund, *Acoustic emission in concrete under thermal and mechanical stress* (in Polish), [in:] Modern opinions on destruction processes of bones, ceramics and concrete, Collected papers [Ed.] J. Ranachowski, IFTR Warszawa 1995.

[3] J.-M. Berthelot, M. Ben Souda and J.L. Robert, *Frequency analysis of acoustic emission signals in concrete*, Journal of Acoustic Emission, **11**, 1, 11–18 (1993).

[4] I. GRABEC and W. SACHSE, *Application of an intelligent signal processing system to acoustic emission analysis*, J. Acoust. Soc. Am., **85**, 3, 1226–1234 (1989).

[5] H, JUKI and K. HOMMA, *Analysis of artificial acoustic emission waveforms using a neural network*, J. of Acoustic Emission, **10**, 3/4, 35–40 (1992).

[6] M. OHTSU and K. ONO, *Pattern recognition of magnetomechanical acoustic signals*, Journal of Acoustic Emission, **3**, 2, 69–78 (1984).

[7] J. HERTZ, A. KROGH and R. PALMER, *Introduction to the theory of neural computation*, Addison-Wiley Publ. Company, Reading, Mass., 1991.

[8] M. WEIGL, *Neural networks and fuzzy logic deduction systems in approximation problems* [in Polish], D. Sc. Thesis, IFTR, Warszawa (1995).

ARCHIVES OF ACOUSTICS
21, 1, 99–107 (1996)

# PIEZOELECTRIC INTERFACIAL WAVES IN LANGASITE AND DILITHIUM TETRABORATE

E. DANICKI and W. LAPRUS

Polish Academy of Sciences
Institute of Fundamental Technological Research
(00-049 Warszawa, ul. Świętokrzyska 21)

Waves propagating along a perfectly conducting plane embedded in a piezoelectric medium are investigated. Numerical analysis of trigonal langasite (LGS) and cubic dilithium tetraborate (LBO) crystals shows that such waves exist for many orientations of the conducting plane with respect to the crystallographic axes, and for many directions of propagation. The wave velocity is close to that of the slowest shear wave for the same direction, and the piezoelectric coupling coefficient can be as high as 1.65% for LBO and 0.25% for LGS. The conditions of existence, and the properties of the most interesting waves are presented. Expected applications are discussed.

## 1. Introduction

SAW devices must be encapsulated to protect the free substrate surface (required for SAW to propagate) against the adverse environmental influence. Otherwise, contamination would cause ageing effects. The encapsulation, in turn, creates problems of its own: the case and the crystal have different thermal expansion coefficients; the difference causes stress in the crystal (all-quartz encapsulation has been devised to avoid this problem). Some interesting crystals cannot be used because of their high sensitivity to the environment.

The piezoelectric interfacial wave (PIW), which has been proposed in [1] as an alternative to SAW, is immune to these problems. PIW propagates inside the piezoelectric crystal, and is guided by the conducting plane embedded in it. The wave energy density is high in the immediate vicinity of the plane, and decreases exponentially with the distance from the plane.

From the practical point of view, one can cut the crystal into two pieces, put metal on the faces, and attach the pieces together with perfect mechanical contact (the metal diffusion technique can be used for that purpose). The metallization need not be full, there can be periodic metal strips instead, and still PIW will exist. The periodic metal strips can be further employed to form interdigital transducers, like these applied to

SAW. Another possibility is the application of a fragile sheet of high-temperature superconductor [2].

PIW can be easily excited and detected in both langasite and dilithium tetraborate due to high piezoelectric coupling. Although the highest coupling is accompanied by rather high beam steering (27° for LBO and 12° for LGS), there exist waves with high coupling (1% for LBO and 0.2% for LGS) and zero beam steering.

The wave polarization at the conducting plane depends on the orientation of the plane, and can be almost aribtrary. This opens certain interesting possibilities of application of PIW in acousto-optical devices like Bragg cells.

## 2. Eigenvalue problem

The system of coordinates $(x, y, z)$ is chosen so that the perfectly conducting plane is described by the equation $z=0$, and is an interface between two half-spaces (for $z>0$ and $z<0$) of a homogeneous piezoelectric medium. It is assumed that the field is independent of $y$, and that the time dependence is given by the factor $\exp(j\omega t)$.

The electro-mechanical field satisfies the equations

$$T_{ij,j} = -\omega^2 \rho u_i , \tag{2.1}$$

$$D_{k,k} = 0 , \tag{2.2}$$

complemented with the constitutive relations

$$T_{ij} = c_{ijkl} u_{k,l} + e_{kij} \phi_{,k} , \tag{2.3}$$

$$D_k = e_{kij} u_{i,j} - \varepsilon_{ki} \phi_{,i} , \tag{2.4}$$

where $i, j, k, l = 1, 2, 3$ ($x_1 = x$, $x_2 = y$, $x_3 = z$). The medium is described by the following constants: elastic tensor $c_{ijkl}$, piezoelectric tensor $e_{kij}$, dielectric tensor $\varepsilon_{ki}$, and mass density $\rho$. The field variables are: displacement $u_i$, electric potential $\phi$, stress tensor $T_{ij}$, electric induction $D_k$.

If we eliminated $T_{ij}$ and $D_k$ from Eqs. (2.1)–(2.4), we would get the conventional system of four second-order partial differential equations for the four functions $u_i$ and $\phi$. Instead, we introduce the four additional field variables $T_i$ and $D_3$, where $T_i = T_{3i}$ (cf. [3]). Then we assume that the field depends on $x$ and $z$ through the factor $\exp(-j\omega r x - j\omega s z)$. We obtain the system of eight linear algebraic equations

$$H_{KL}(r) F_L = q F_K , \tag{2.5}$$

where $q = s/r$, $(F_K) = (j\omega u_i, j\omega r\phi, T_i, D_3)$, and $K, L = 1,\ldots,8$. The matrix $H_{KL}$, which is real and non-symmetric for real $r$, depends on material constants.

After solving the eigenvalue problem defined by Eq. (2.5) we get eight eigenvectors $\tilde{F}_K^{(J)}(r)$ corresponding to eight eigenvalues $q^{(J)}(r)$ for $J = 1,\ldots,8$. Each eigenwave

has the form $F_K^{(J)} = \tilde{F}_K^{(J)} \exp(j\omega t - j\omega r(x + q^{(J)} z))$, and the solution of Eqs. (2.1)–(2.4) is a linear combination of these waves.

We are interested in solutions for real $r$ such that no eigenvalue is real (this is true for $r > r_s$ where $1/r_s$ is the phase velocity of the slowest shear wave). Therefore, the solution in the upper half-space, $F_K^+$, and the solution in the lower half-space, $F_K^-$, should consist of the eigenwaves that are decaying for $z \to \infty$ and $z \to -\infty$, respectively.

At the plane $z = 0$, the complex amplitudes of the two solutions are

$$\tilde{F}_K^{\pm} = \pm \sum_J^{\pm} C_J \tilde{F}_K^{(J)}, \tag{2.6}$$

where the summation is performed over $J$ such that $\operatorname{Im} q^{(J)} < 0$ (for $\tilde{F}_K^+$) and $\operatorname{Im} q^{(J)} > 0$ (for $\tilde{F}_K^-$); $C_J$ are constant coefficients. The boundary conditions imply that all the field variables are continuous across the plane $z = 0$ except $D_3$. The amplitude $\tilde{D}_3$ suffers a jump $\Delta\tilde{D}_3$ (assumed to be real). Thus $\Delta\tilde{F}_K = \tilde{F}_K^+ - \tilde{F}_K^- = 0$ for $K = 1,...,7$, and $\Delta\tilde{F}_8 = \Delta\tilde{D}_3$. Using these equalities and Eq. (2.6) we can find the coefficients $C_J$, and then the amplitudes $\tilde{F}_K^+$ and $\tilde{F}_K^-$ for $K = 1,...,8$. In particular, for $K = 4$,

$$j\omega r\tilde{\phi} = Z(r)\Delta\tilde{D}_3, \tag{2.7}$$

where $Z(r)$ is a complex-valued function determined by the set of eigenvectors for the given $r$.

It can be shown that the function $Z(r)$ is purely imaginary for $r > r_s$, and that $\operatorname{Im} Z(r)$ tends to a positive value as $r \to \infty$. PIW exists if the dispersive equation $Z(r) = 0$ is satisfied for a particular value of $r$, say $r_p$. Then $\tilde{\phi} = 0$ (i.e. $\phi$ satisfies the boundary condition for $z = 0$), and $1/r_p$ is the phase velocity of PIW.

## 3. Calculations

The dispersive equation gives different solutions for different triplets of Euler angles. These triplets may be represented as points in a three-dimensional space. We scan the space at discrete points so that the angles change in steps of 2°. The symmetry of the piezoelectric crystal suggests that it is sufficient to scan the following ranges: 0° – 45°, 0° – 180°, 0° – 180° for LBO, and 0° – 30°, 0° – 180°, 0° – 180° for LGS.

At each chosen point in the angle space, the eigenvalue problem is solved numerically (using EisPack routines [4]) for several values of $r$ in search of $r_s$, and then in search of $r_p$ in a small neighbourhood of $r_s$, just above $r_s$ (simple zero-finding routines).

If PIW exists then its parameters are calculated: $\delta = (r_p - r_s)/r_s$, $v_p = 1/r_p$, beam steering angle $\psi$, effective permittivity $\varepsilon_{\text{eff}}$, piezoelectric coupling coefficient $\kappa$ (see [1]), and normalized complex amplitudes (with respect to the time average of the total energy flux of the wave) for $z = 0$, i.e., $\tilde{D}_3^+$, $\tilde{u}_k$ and $\tilde{T}_k$. The calculations are performed for $\omega = 10^6\ \text{s}^{-1}$. The material constants for LBO and LGS are from [5].

## 4. Conclusion

PIW exists for a high percentage of points in the angle space (93% for LBO and 60% for LGS), although many of these points are not very interesting in view of applications (low piezoelectric coupling).

The most important features of PIW are illustrated in Figure 1 and Figure 2. Table 1 and Table 2 give PIW parameters for eight points in the angle space (representative of eight groups of points), selected from over 120 thousand points where PIW exists.

**Table 1.** PIW parameters for LBO

| Euler angles | $\delta$ | $v_p$ | $\psi$ | $\varepsilon_{eff}$ | $\kappa$ | $\tilde{D}_3^+$ | $\tilde{u}_1$ | $\tilde{u}_2$ | $\tilde{u}_3$ | $\tilde{T}_1$ | $\tilde{T}_2$ | $\tilde{T}_3$ |
|---|---|---|---|---|---|---|---|---|---|---|---|---|
| deg | % | m/s | deg | – | % | $\frac{nC/m^2}{P^{1/2}}$ | $\frac{pm}{P^{1/2}}$ | $\frac{pm}{P^{1/2}}$ | $\frac{pm}{P^{1/2}}$ | $\frac{N/m^2}{P^{1/2}}$ | $\frac{N/m^2}{P^{1/2}}$ | $\frac{N/m^2}{P^{1/2}}$ |
| 42 90 70 | 1.18 | 3628 | −27 | 18.8 | 1.65 | $13.4\angle 0°$ | −60.7 | 77.2 | −0.15 | $-j3.33$ | $-j2.40$ | $j118.$ |
| 0 90 90 | 0.50 | 3905 | 0 | 18.9 | 1.00 | $9.50\angle 0°$ | −63.2 | 0.00 | −0.05 | $j0.28$ | $j0.00$ | $-j365.$ |
| 30 90 90 | 0.45 | 3807 | 0 | 18.9 | 0.80 | $9.27\angle 0°$ | −62.8 | 0.00 | 0.01 | $-j0.06$ | $-j33.2$ | $-j348.$ |
| 45 90 30 | 0.05 | 3818 | 37 | 18.6 | 0.10 | $2.84\angle 0°$ | 0.02 | 32.2 | 0.00 | $j0.00$ | $j0.00$ | $j37.7$ |

NOTES. Row 1: maximum $\kappa$. Row 2: $\kappa \geq 1\%$, $\psi = 0$, Row 3: $\kappa \geq 0.4\%$, $\psi = 0$, Row 4: maximum $|\psi|$. P = 1 mW/m.

**Table 2.** PIW parameters for LGS

| Euler angles | $\delta$ | $v_p$ | $\psi$ | $\varepsilon_{eff}$ | $\kappa$ | $\tilde{D}_3^+$ | $\tilde{u}_1$ | $\tilde{u}_2$ | $\tilde{u}_3$ | $\tilde{T}_1$ | $\tilde{T}_2$ | $\tilde{T}_3$ |
|---|---|---|---|---|---|---|---|---|---|---|---|---|
| deg | % | m/s | deg | – | % | $\frac{nC/m^2}{P^{1/2}}$ | $\frac{pm}{P^{1/2}}$ | $\frac{pm}{P^{1/2}}$ | $\frac{pm}{P^{1/2}}$ | $\frac{N/m^2}{P^{1/2}}$ | $\frac{N/m^2}{P^{1/2}}$ | $\frac{N/m^2}{P^{1/2}}$ |
| 0 146 26 | 0.17 | 2851 | −12 | 57.5 | 0.25 | $12.2\angle -3°$ | 7.34 | 49.5 | 24.9 | $-j379.$ | $j36.6$ | $j43.5$ |
| 7 144 35 | 0.13 | 2936 | 0 | 57.9 | 0.20 | $10.9\angle -2°$ | 11.5 | 42.1 | 28.8 | $-j433.$ | $j48.7$ | $j105.$ |
| 0 14 90 | 0.08 | 2816 | 0 | 62.7 | 0.15 | $10.1\angle -6°$ | 0.00 | −40.4 | 0.00 | $j0.00$ | $j1.14$ | $j0.00$ |
| 0 132 18 | 0.00 | 2681 | −31 | 51.9 | 0.00 | $2.59\angle -50°$ | −0.87 | 15.6 | 5.47 | $-j84.2$ | $-j11.4$ | $j18.8$ |

NOTES. Row 1: maximum $\kappa$. Row 2: $\kappa \geq 0.2\%$, $\psi = 0$, Row 3: $\kappa \geq 0.1\%$, $\psi = 0$, Row 4: maximum $|\psi|$. P = 1 mW/m.

Some asymmetry seen in the figures, especially at the boundary of PIW existence, is an effect of the finite precision of calculation.

PIW exists in many other piezoelectric crystals, including well known bismuth germanium oxide (BGO) and quartz (SIO). Figure 3 and Figure 4 illustrate PIW existence and features for these two media.

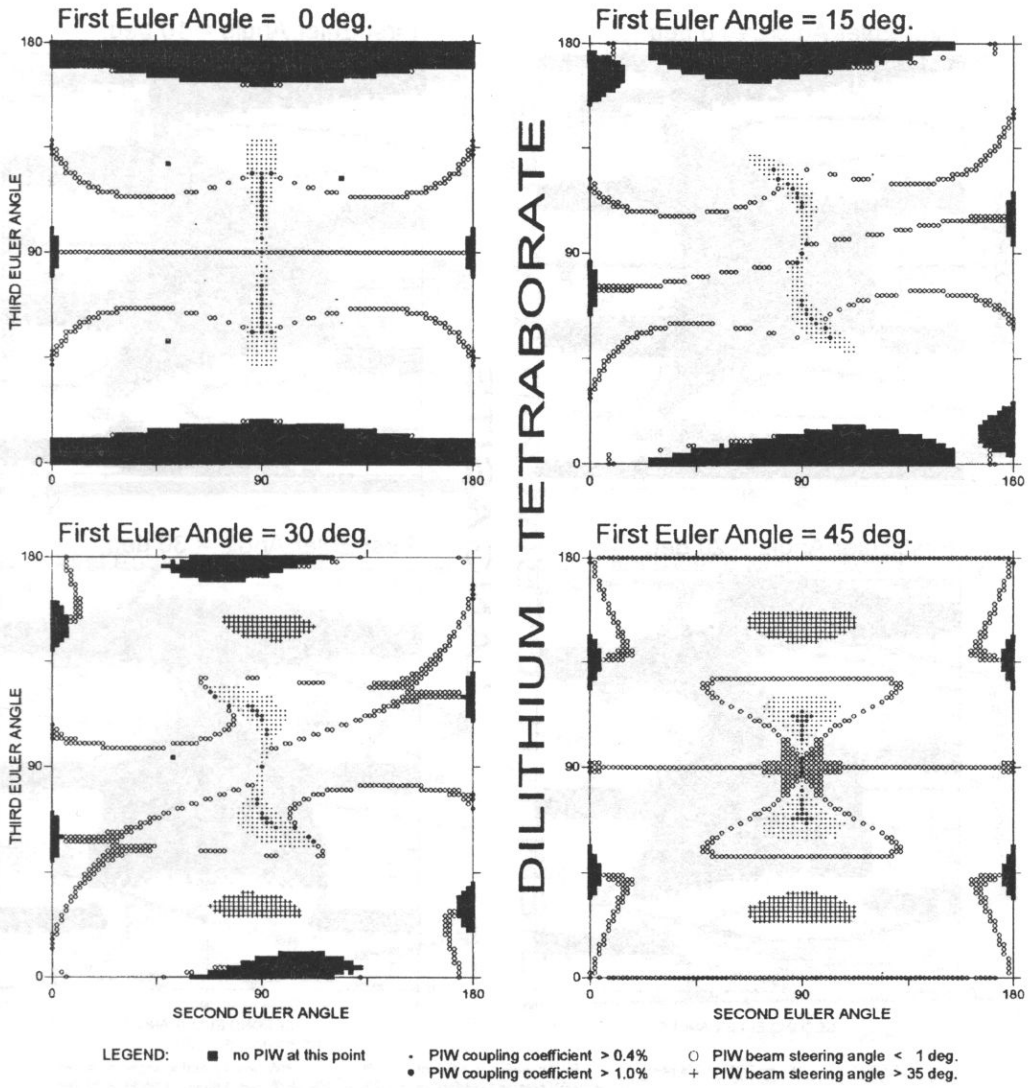


Fig. 1. Maps of PIW properties for LBO.

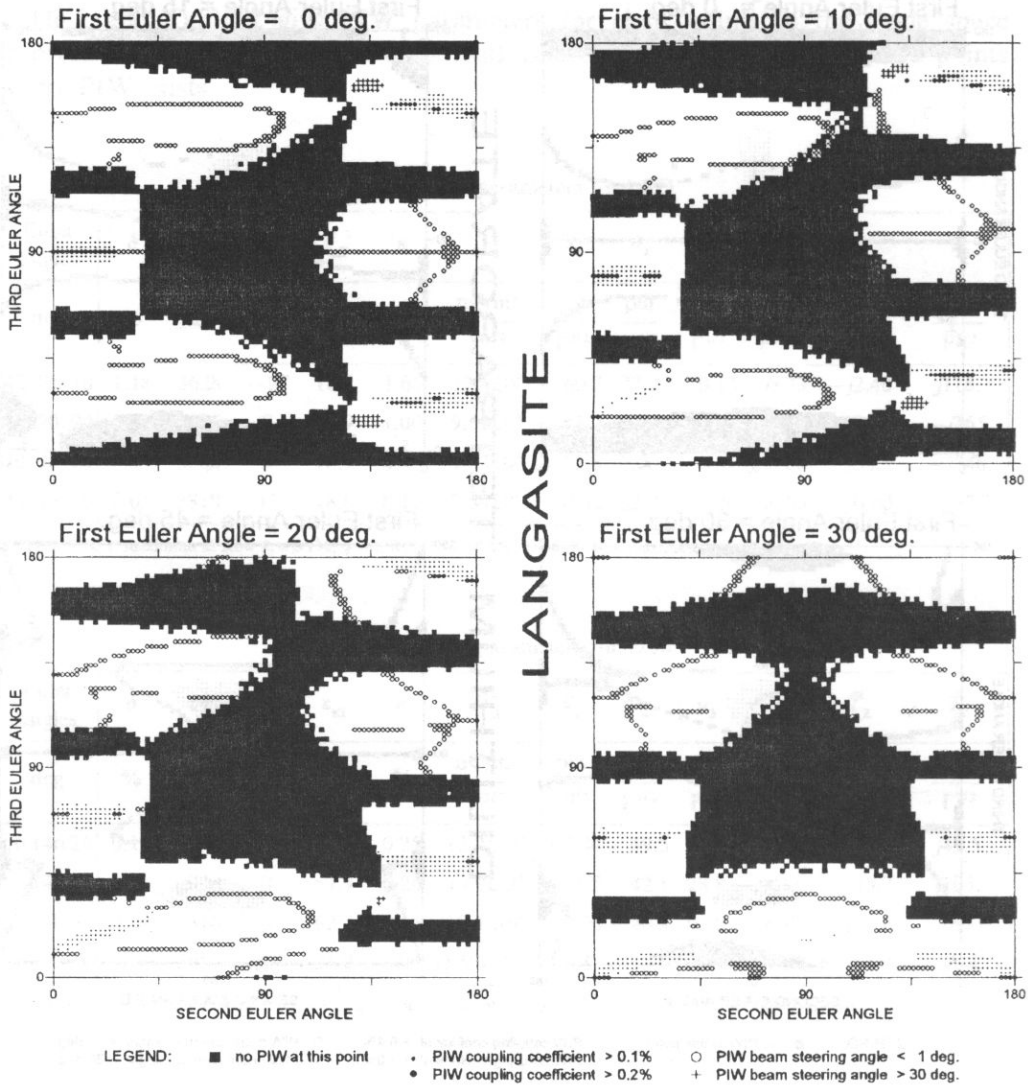


Fig. 2. Maps of PIW properties for LGS.

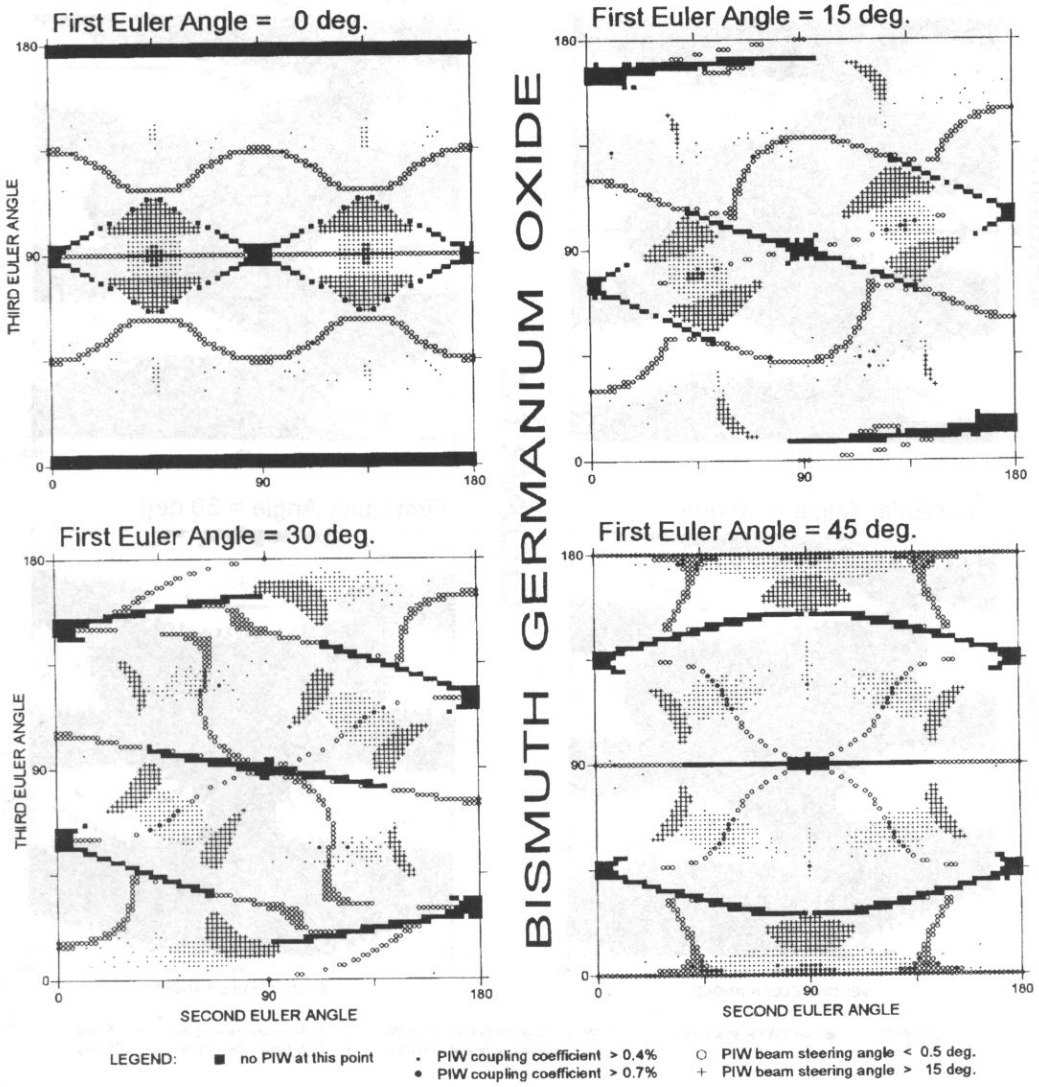


Fig. 3. Maps of PIW properties for BGO.

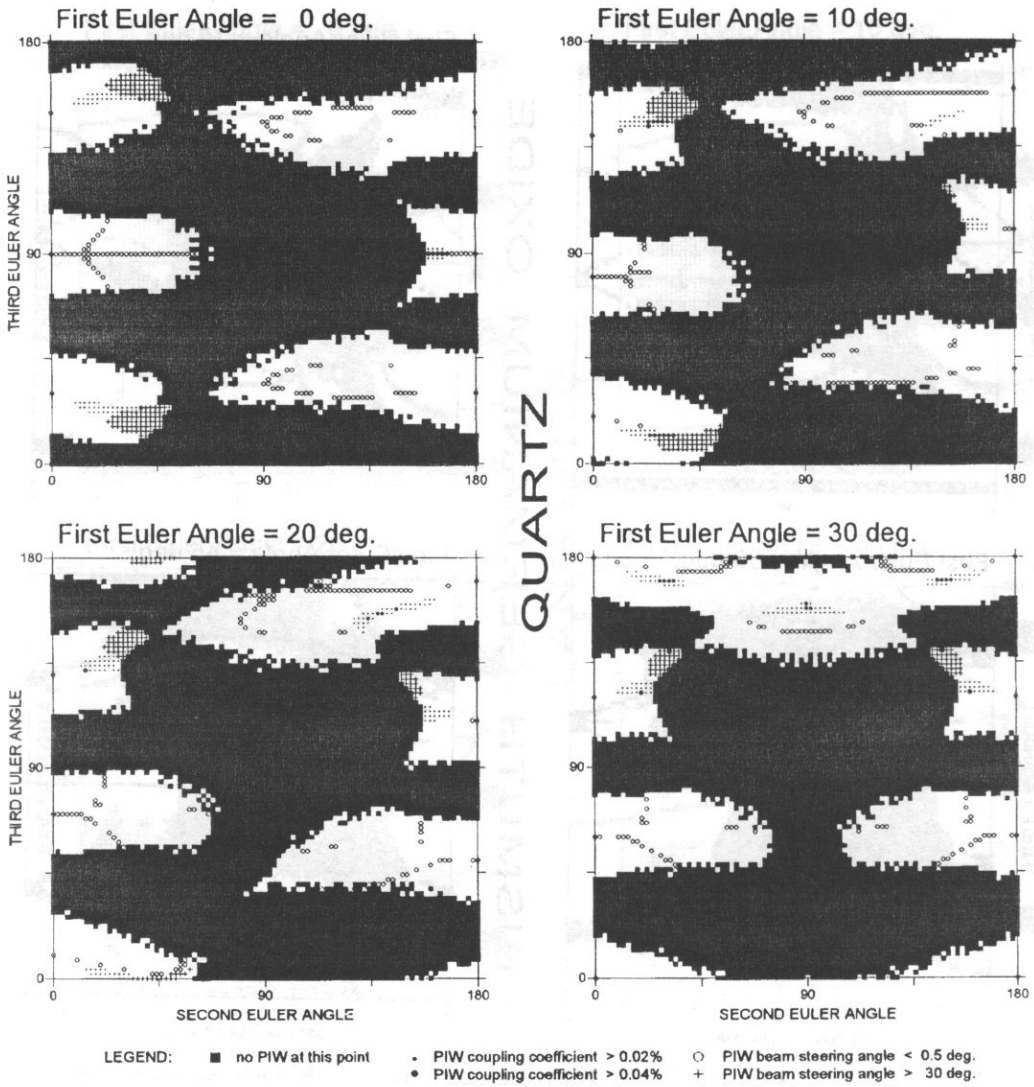


Fig. 4. Maps of PIW properties for SIO.

## References

[1] E. DANICKI, Appl. Phys. Lett., **66**, 3439–40 (1995).
[2] J. FELLER. M. LEVY, B.K. SARMA, 1994 IEEE Ultrasonic Symp. Proc., pp. 825–828.
[3] E.L. ADLER, IEEE Trans. UFFC, **41**, 699–705 (1994).
[4] B.T. SMITH *et al.*, Lecture Notes in Computer Science, Vol. 6, Springer-Verlag 1974.
[5] J.G. GUALTIERI, J.K. KOSIŃSKI and A. BALLATO, IEEE Trans. UFFC, **41**, 53–59 (1994).

ARCHIVES OF ACOUSTICS
21, 1, 109–113 (1996)

# C H R O N I C L E

## 6-th INTERNATIONAL SPRING SCHOOL ON ACOUSTO-OPTICS AND APPLICATIONS GDAŃSK–JURATA, 22–25 MAY 1995

At the same place as the 5-th School in 1992* at Jurata situated on the Hel Peninsula 70 km from Gdańsk the 6th International Spring School on Acousto-optics was organized by the Institute of the Experimental Physics of the University of Gdańsk in cooperation with the Polish Acoustical Society, Committee of Acoustics of the Polish Academy of Sciences and co-sponsored by the Polish Committee for Scientific Research and by the Polilsh Chapter of SPIE (the International Society for Optical Engineering).

The Scientific Committee included: Prof. L. Adler, Ohio State University, USA; Prof. A. Alippi, Instituto di Acustica, ITALY; Prof. P. Banerjee, University of Alabama, USA; Dr. E. Blomme, V.H. Techn. Inform., Kortrijk, BELGIUM; Prof. M.A. Breazeale, University of Mississippi, USA; Dr R.C. Chivers, University of Surrey, U.K.; Prof. I. Gabrielli, University of Trieste, ITALY; Prof. H.W. Jones, University of Swansea, U.K.; Prof. Z. Kleszczewski, Silesian Techn. Univ., POLAND; Prof. A. Korpel, Dept. Electr. & Comp. Eng., USA; Prof. S.V. Kulakov, Inst. Aviat. Instr., St. Petersburg, RUSSIA; Prof. O. Leroy, Kath. Univ., Leuven–Kortrijk, BELGIUM; Prof. N.B. Lezhnev, Acad. of Sc. of Turkm., TURKMENISTAN; Prof. M. Łabowski, A. Mickiewicz University, POLAND; Prof. I. Malecki, Polish Acad. of Sc., POLAND; Prof. W. Mayer, Georgetown University, USA; Prof. R. Mertens, Roy. Belg. Acad. Sci., BELGIUM; Prof. A. Opilski, Silesian Techn. Univ., POLAND; Prof. V. Parygin, Moscow State University, RUSSIA; Prof. M. Pluta, President of the Polish Chapter of SPIE/PL; Prof. T.C. Poon, Polyt. Inst.

---

* The international spring meetings on Acousto-optics and Applications are organized every three years since 1980. The previous took place:

1-st School, Gdańsk–Wieżyca, 1980, May 26–30 proceedings issued by the University of Gdańsk; a report published in Arch. Acoust., 6, 85 (1981) and in Ultrasonics, 19, 44 (1981).

2-nd School, Gdańsk–Wieżyca, 1983, May 24–29 proceedings issued by the University of Gdańsk; a report published in Arch. Acoust., 9, 381 (1984) and Ultrasonics 22, 15 (1984).

3-rd School, Gdańsk–Wieżyca, 1986, May 26–31 proceedings issued by the University of Gdańsk; a report published in Ultrasonics, 25, 182 (1987).

4-th School, Gdańsk–Sobieszewo, 1989, May 23–27 proceedings published by World Scientific, Singapore–New Jersey–London–Hong Kong, 1990.

5-th School, Gdańsk–Jurata, 1992, May 25–29 proceedings published by Proc. SPIE, Bellingham, USA, 1992.

State Univ., Virginia, USA; Prof. V. Proklov, Acad. Sci., Moscow, RUSSIA; Prof. J. Ranachowski, Polish Acad. of Sc., POLAND; Prof. R. Reibold, Phys. Tech. Bund., Braunschweig, GERMANY; Prof. J. Sapriel, Centr. Nat. d'Etudes Tel., Paris, FRANCE; Prof. M. Szustakowski, Military Acad. of Tech., Warszawa, POLAND; Prof. B.R. Tittmann, The Pennsylvania State University, USA; Prof. Chen Tsai, University of California, Irvine, USA; Prof. A. Zarembowitch, Dep. Rech. Phys., Paris, FRANCE.

The Organizing Committee consisted of Prof. A. Śliwiński, president, Prof. P. Kwiek, vice president, Dr M. Kosmol, secretary and members: Prof. C. Lewa, Dr M. Borysewicz, Mgr G. Gondek, Dr B. Linde, Dr A. Markiewicz, Dr A. Sikorska, Dr J. Szurkowski.

The School brought together 71 participants, above 60 specialists and students from the following countries: Belgium (1), Brazil (1), Bulgaria (1), Denmark (1), France (1), Germany (6), Italy (3), Lithuania (1), Poland (39), Russia (7), Switzerland (1), United Kingdom (1), United States of America (8) and Poland. 17 invited lecturers, 25 papers and 15 posters were presented.

The Programme of the School included:

## General invited papers

1. Ultrasound field mapping by light diffraction tomography — a review.
   *R. Reibold, P. Kwiek*
2. Nearfields of ultrasonic transducers.
   *B.D. Cook*
3. Strong acousto-optic interaction during collinear diffraction.
   *V. Parygin*
4. Image propagation through acousto-optic devices.
   *P. Banerjee*
5. Acoustically induced light polarization effects in isotropic media.
   *E. Blomme*
6. The wavelet transforms: fundamentals and acousto-optic implementation.
   *P. Das, C. DeCusatis, J. Koay, D.M. Lityński*
7. Sensors for material process monitoring and control.
   *B.R. Tittmann*
8. Integrated optical Mach-Zehnder interferometer (technology, structure, functioning).
   *A. Opilski, R. Rogoziński*
9. Acousto-optics without Bessel functions and Bessel functions by acousto-optics.
   *I. Gabrielli*
10. Quantum wells as a future acousto-optic materials.
    *V. Proklov*
11. New developments of resonant acousto-optics in semiconductors.
    *J. Sarpiel*

12. Acousto-optic studies of planar optical waveguides: velocity and attenuation of SAW in proton-exchanged $LiNbO_3$.
*D. Ciplys*

13. A short history of acoustical imaging.
*H.W. Jones*

14. The scanning acoustic microscopy and confocal laser scanning microscopy — foundations and applications on human bones.
*H.-J. Hein*

15. Nonlinear acoustics and its impacts on nondestructive evaluation with acousto-optic technique.
*L. Adler*

16. Investigation of acousto-optic interaction in dense flint glass and tellurium dioxide.
*V. Voloshinov*

## Oral contribution papers

1. Light diffraction by ultrasound: near field investigation.
*G. Gondek, T. Katkowski, P. Kwiek*

2. Collinear acousto-optic tunable filter using $CaMoO_4$ single crystal for processing of nonpolarized radiation.
*V.Ya. Molchanov*

3. Numerical and experimental comparison of polarization effects in ultrasonic light diffraction in the intermediate range in isotropic $SiO_2$.
*E. Blomme, P. Kwiek, O. Leroy, A. Śliwiński*

4. Use of acousto-optic image correlators for wavelet transforms.
*D.M. Lityński, C. DeCusatis, J. Koay, P. Das*

5. CAD techniques for electronic and optoelectronic devices and circuits.
*M.N. Armenise, M.N. Passaro*

6. Polarization effects at acousto-optic interaction in anisotropic medium.
*V. Balakshy, G. Gondek, T. Katkowski, I. Kryłov, P. Kwiek, A. Śliwiński*

7. Construction and properties of the multielement filters for matching piezoelectric transducer.
*I. Merta*

8. Photoluminescence temperature sensor.
*T. Pustelny*

9. Integrated optical amplitude refractometer.
*P. Karasiński*

10. Optimisation of heterodyne signal in acousto-optical experiment.
*K. Abramski*

11. Bonded Silicon Wafers as a test object for the resolution power of subsurface voids.
*K. Kosbi*

12. Using of acousto-optical resonant conditions in GaAs and InP for the creation of high efficiency 2 GHz bandwidth Bragg cells.
*V. Petrov, B. Gur'ev, V. Kolosov, S. Kuryshov, J. Sapriel*

13. Acousto-optical Bragg interaction in isotropic media under uniaxial stress condition.
*R. Bukowski, A. Dziechciarczyk*

14. Method of analysis of acousto-optic interaction by used Kotelnikov-Shannon's distribution on sample function.
*W. Rysakow, M. Stoń*

15. Investigation of acousto-electronic gain piezosemiconductor by method of light diffraction.
*W. Rysakow*

16. Nanoscale acoustics: detection of ultrasound using an atomic force microscope (AFM).
*A.J. Kulik, N.A. Burnham, G. Gremand, F. Oulevey, P.-J. Gallo*

17. Influence of an excentric transducer on V(z) measurement.
*U. Scheer*

18. Investigation of tooth tissue — photoacoustics versus other spectroscopic methods..
*A. Christ, U. Cobet, T. Siebert, K. Giese, N. Harendt*

19. Combined acousto- and electro-optic effects study and applications.
*G. Mendes Pacheco*

20. Acousto-optical investigation of the phase transitions in the olygoethertmetacrylates.
*R. Mervinskij, J. Kityk, M. Makowska-Janusik, J. Filipecki, J. Straube, J. Yatczyszyn*

21. Modified polyvinile alcohol photopolymer modulators and deflectors.
*V. Kravchuk, J. Kityk, M. Makowska-Janusik, D. Korolev, M. Yasinskij, B. Holan*

22. Multifunctional processors of acousto-optic signal processing.
*M. Szusztakowski*

23. Photothermal measurements for plates.
*J. Bodzenta*

24. Preliminary investigation of the degradation of motor oil by photoacoustic spectroscopy.
*J. Motylewski, J. Szurkowski, B. Wiślicki, T. Zmierczak*

25. Precision measurements of elasticity modulus by improvement of Schaefer-Bergmann method.
*E. Kotlicka, I. Gronowska, G. Hendor, A. Latuszek*

## Poster form papers

1. Nonradiative processes in CdS:Cu system doped by diffusion as studied by microphone-gas coupled photoacoustic spectroscopy.
*M. Grus, A. Sikorska*

2. Propagation of acoustic waves in randomly inhomogeneous media.
*E. Soczkiewicz*

3. Is it possible to determine times of thermal deactivation excitation energy of molecules placed in thin films?
*J. Szurkowski*

4. Light diffraction by two spatially separated ultrasonic beams — Intermediate region of investigation. The case of $v \ll Q$.
*T. Katkowski*

5. Acoustic investigations of liquids ($C_8F_{16}$, $C_9F_{18}$) at various termodynamic conditions.
*T.V. Burlachenko, N.B. Lezhnev*

6. Acoustic spectroscopy of simple liquids at high pressure.
*U.M. Esanov*

7. Ultrasound studies of critical micellar concentrations of ionic surfactants.
*A.Jumaev, N. Lezhnev, B. Ovlyakuliev, K. Amanov*

8. Influence of pressure on acoustic and reologic parameters in water solution of lauril sodium sulphate.
*B.T. Khamidov, N.B. Lezhnev*

9. Kinetics of micelle formation of carboxymathylated surfactant in aqueous solution.
*N. Pirmedova, N.B. Lezhnev, B. Ovlyakuliev*

10. Temperature-pressure hysteresis of the acoustic parameters of the supercooled liquids.
*A.V. Rudin*

11. Mathematical processing of Mandelshtam-Brillouin spectra.
*G.P. Stanev*

12. Correlation of acoustic distribution of the relaxation times and anti-water properties of lubricant liquids.
*V.M. Troitsky*

The sessions involved numerous debates. In addition a final round table discussion under Professor B.D. Cook's moderatorship summarized achievements of the School. The two and a half hour of mutual exchange of information and ideas on the role of acousto-optics, its development and perspectives was very alive and fruitful.

An excursion by boat from Hel to Gdańsk, the short visit to the acousto-optical laboratory at the Institute of Experimental Physics of the University of Gdańsk (demonstrations by P. Kwiek) and sightseeing of the Gdańsk Downtown were included.

The proceedings of the School are published by SPIE (International Society of Optical Engineering) (Acousto-Optics and Applications II, A. Śliwiński, P. Kwiek, B. Linde, A. Markiewicz [Eds.] Proc. SPIE 2643, 1–394).

The next 7-th International Spring School on Acousto-optics and Applications will be organized in May 1998.

*A.S. Śliwiński*

ARCHIVES OF ACOUSTICS
21, 1, 115–117 (1996)

# B O O K R E V I E W

*Acoustic Emission: Sources, Methods and Applications* (in Polish), I. MALECKI and J. RANACHOWSKI [Eds.], Institute of Fundamental Technological Research, Warszawa 1994, 492 pp.

Acoustic emission (AE) is a phenomenon and a method as well. The investigations of this phenomenon, its sources, signals interpretation and their connections with the source character constitute a currently developing subject for research studies. The applications of AE as an investigation method are being developed faster. Ranachowski and Malecki's book introduces both aspects of AE. The book is set of twenty one articles written by different authors, arranged into seven parts.

The description of the phenomenon and its physics, signals and sources classifications are introduced in the first part. The following part of the monograph structure is based on a sequence introducing AE in terms of its application as a study of method. The chapters from second to sixth concentrate respectively on the applications of the AE method for ceramic materials, metals, metallic elements, concrete, wood, composites, and geological materials. The AE metod is used principally in pit-coal mines for "in situ" studies and also in the chemical technologies. The monograph introduces a very wide range of practical applications of the AE phenomenon.

The second part introduces one of the most important applications of AE, namely the possibility to estimate the strength and operating parameters of ceramic materials in the brittle crack process on the basis of AE signals. Also, studies of superconducting ceramics by the AE method are presented in this part.

The third part is devoted to the AE phenomena in metals. The main sources of AE in metals are dislocation migrations. The mechanism of these migrations is different for single crystals and polycrystals, and that is why both material groups are introduced separately. Since the metallic parts of the technical devices often work in chemically active surroundings, utilization of the AE method for studies of stress corrosion is especially effective.

The application of AE method for the investigations of heterogeneous materials is discussed in the fourth part. The AE application for studies of the multiple cracking process in these materials is described. The investigation of AE phenomena in geological materials is considered to be one of the first investigations of that kind.

The fifth part of the monograph introduces very interesting and not much investigated applications in building grounds, agriculture soils and geological

materials, particularly in pit-coals. It is worth while mentioning that both laboratory studies and the results of "in situ" investigations are introduced. Possibilities of applications to crumps forecasting in the pit-coal mines are described, along with ones in chemical processes, particularly in audiology. The studies of the AE method in respect to ears has proved successful, which gives unique information applicable in otolaryngology.

The sixth part describes AE applications for diagnostics of electrical power engineering devices. Such types of applications could be especially serviceable if optical waveguide transducers are used as AE signal receivers. The last part introduces a Polish apparatus for AE applications, its various modifications for specific applications, and standard sources of acoustic emission.

In summary, in the monograph the authors present the development of the application prospects of the AE method. They also suggested new research problems concerning both the applications of the method and the development of the methodology and apparatus. This variety of the introduced AE applications is a conspicuous feature of *Acoustic Emission: Sources, Methods, and Applications*. Each article is written by an expert on a specific problem and includes both a survey of the world literature, and especially the achievements of Polish researchers.

*Aleksander Opilski*

K.U. INGARD, *Notes on Sound Absorption Technology*, Noise Control Foundation, Poughkeepsie, NY 12603 USA

We obtained new book "Notes on Sound Absorption Technology". This book has been written by Professor K.U. Ingard.

Professor K. Uno Ingard was educated at the Chalmers University of Technology in Gothenburg, Sweden and at the Massachusetts Institute of Technology in Cambridge, Massachusetts, USA.

He received the Ph.D. degree in physics from MIT in 1950 and joined the MIT physics department as an assistant professor in 1952, having previously served as the Director of the Chalmers Acoustics Laboratory. He became an associate professor at MIT in 1956, a professor in 1966, and in 1971, he was appointed to a dual professorship in the department of aeronautics and astronautics. He taught acoustics and noise control engineering in the aeronautics department and has research interests ranging from aeroacoustics and nonlinear acoustics to structural vibrations and flow-induced instabilities.

He has worked on a wide variety of problems in acoustics and noise control engineering for more 45 years as a consultant to various industries. He is the author of several books, among them "Theoretical Acoustics", "Fundamentals of Waves and Vibrations", "Linear Acoustic theory", "Introduction to Mechanics", "Matter and Waves". He has authored more than 100 papers related to acoustics and the physics of fluids.

The book has two parts. Part I covers sound absorption technology, part II gives many examples of the use of the computer programs.

The essential problems of book are:

— Fundamentals of sound and acoustics.
— The acoustical properties of flow-resistive screens.
— The effects of viscosity and heat conduction on sound propagation.
— Design of multi-layer sound absorbers, including non-uniform absorber spacing.
— The properties of flexible porous sound absorbers, including open and closed cell materials.
— Attenuation in lined ducts, including both locally reacting and nonlocally reacting liners.
— Resonator design, including scattering and absorption cross-section.
— Sound absorption in wind tunnels.
— Interactions between shock waves and flexible porous layers.
— Characteristics of sound absorptive materials, including a new apparatus for measurement of flow resistance.
— Measurement of complex compressibility.
— The theory of transmission matrices.

The text in sound absorption technology is accompanied by three high-density floppy disks. The disks contain 38 executable DOS programs for IBM-compatible computer which, with the text, allow the user to make a wide variety of calculations of the properties of structures which contain acoustical materials. I think, with the text and software provided a user is able to:

— calculate the acoustical performance of materials
— calculate the performance of acoustic-resonator
— calculate the absorption coefficient of flow-resistive screens
— determine the acoustical performance of multi-layer porous absorbers, the acoustical performance of perforated and wire screen layers.

I have only one minor criticisms. In book Professor Ingard does not present references. Two years ago J.F. Allard published a book "Propagation of Sound in Porous Media: modelling sound absorbing materials" (Chapman Hall, London). Professor Ingard's book is there for second publication connected with the acoustical properties of porous absorbing materials.

Text of this book is an important and exciting one and should be required reading for researchers, graduate students, consultants and designers interested in subject sound absorption technology.

*Zbigniew Engel*

**inter · noise**
**97**

THE 1997 INTERNATIONAL
CONFERENCE ON NOISE
CONTROL ENGINEERING
BUDAPEST – HUNGARY
1997 AUGUST 25 – 27

ORGANIZED BY

THE ACOUSTICAL COMMISSION
OF THE HUNGARIAN
ACADEMY OF SCIENCES

THE SCIENTIFIC SOCIETY
FOR OPTICS, ACOUSTICS
MOTION PICTURES
AND THEATRE TECHNOLOGY
(OPAKFI)

## FIRST ANNOUNCEMENT

INTER-NOISE 97, the 1997 International Congress on Noise Control Engineering, will be held at the Technical University of Budapest, in the capital of Hungary from 1997 August 25 to 27. The Congress is sponsored by the International Institute of Noise Control Engineering, and is being organized by the Acoustical Commission of the Hungarian Academy of Sciences and the Hungarian Scientific Society for Optics, Acoustics, Motion Pictures and Theatre Technology.

INTER-NOISE 97 will be the twenty-sixth in a series international congresses on noise control engineering that have been held all over the world since 1972. The theme of INTER-NOISE 97 is: HELP QUIET THE WORLD FOR A HIGHER QUALITY LIFE.
Technical papers in all areas of noise control engineering will be considered for presentation at the congress and for publication in the Congress Proceedings.

An Announcement and Call for Papers will be issued; copies will be available from the Conference Secretariat at the address given below.

A major acoustical equipment, materials and instrument exhibition will be held in conjunction with INTER-NOISE 97. The exhibition wiill include materials and devices for noise control as well as instruments such as sound level meters, acoustical signal processing systems, and equipment for active noise control.

Programs for "accompanying persons" and social activities for all delegates will be organized.

Further information on the Congress and the Exhibition may be obtained from the INTER-NOISE Conference Secretariat.

**The next numbers Archives of Acoustics will contain the following papers**

**E. Hojan** and H. Fastl, Intelligibiillity of Polish and German speech for the Polish audience in the presence of noise

**A. Czyżewski, B. Kostek** and **S. Zieliński**, Synthesis of organ pipe sound based on simplified physical models

**U. Jorasz** and **G. J. Doley**, The perceptibility of the frequency drop caused by the Doppler effect for simulated sound source motion in the median plane

**L. Rutkowski**, Room response to frequency change and its relation to the pitch changes

**R. M. Lec**, Acoustic wavesensors

**J. Hola**, Effect of oiling up on the failure of concrete determined by acoustic emission